XIANYU LI

RICE UNIVERSITY

Properties and Applications of Bottlebrush Polymers

by

XIANYU LI

A thesis submitted in partial fulfillment of the requirements for the degree of

Doctor of Philosophy

APPROVED, THESIS COMMITTEE

Rafael Verduzco, Chair
Louis Owen Assistant Professor of
Chemical and Biomolecular Engineering

Walter G. Chapman
William W. Akers Professor of
Chemical and Biomolecular Engineering

Qilin Li
Associate Professor of
Civil and Enviromental Engineering

HOUSTON, TEXAS

[April 16, 2014]

ABSTRACT

Properties and Applications of Bottlebrush Polymers

by

XIANYU LI

This work presented in this dissertation aims to understand physical and chemical properties of bottlebrush polymers and determine their potential for applications including for anti-fouling surfaces and for reduction in oil-water interfacial tension. This dissertation focus on the following four parts: the synthesis of well-defined bottlebrush polymers and investigation of stimuli-responsive film properties; analysis of the solution phase behaviors and conformation of bottlebrush polymers with thermally-responsive side chains; the behavior of bottlebrush polymers in blends with linear polymers; and the development of bottlebrush polymers for antifouling surfaces and for reducing the oil-water interfacial tension.

In chapter 1, we provide an introduction to bottlebrush polymers. Details on the synthesis, conformation, phase behavior, potential applications, and recent work with bottlebrush polymers are discussed. Chapter 2 describes the preparation of stimuli-responsive bottlebrush thin films with hydrophobic polystyrene (PS) and hydrophilic poly(ethylene oxide) (PEO) amphiphilic side-chains. We find that due to the conformational flexibility of the polymeric side-chains, bottlebrush polymer films

exhibit a processing dependent contact angle. This behavior is analogous to that observed for polymer brush films and enables a more scalable approach to responsive, brushy polymer films.

In Chapter 3, we explore the solution phase behavior of bottlebrush polymers with thermoresponsive poly(N-isopropylacrylamide) (PNIPAAM) side-chains. PNIPAAM is a water-soluble polymer that exhibits a lower critical solution temperature (LCST). Due to the unique structure of bottlebrush polymers, PNIPAAM bottlebrush polymers exhibit very different solution phase behavior compared with linear PNIPAAM. We show that the LCST depends on the side-chain length and side-chain endgroup, and the bottlebrush polymer side-chains collapse on approaching the LCST. PNIPAAM bottlebrush polymers form lyotropic liquid crystal phases for sufficiently long PNIPAAM side-chains.

In Chapter 4 we explore the properties of bottlebrush polymers in blends with linear polymers. This work is aimed at investigating the potential of bottlebrush polymers to be used as additives for modifying polymer thin films. We show that bottlebrush polymers are interfacially active and spontaneously segregate to the film-substrate and film-air interface. The interfacial segregation of bottlebrush polymer additives was systematically studied for varying lengths of linear polymers and bottlebrush polymer side-chains through secondary ion mass spectrometry (SIMS), neutron reflectivity and optical microscopy. These results demonstrate that relatively small amounts of bottlebrush polymer additives can be used to tailor interfaces.

Chapter 5 presents preliminary results on the antifouling properties and oil-water interfacial properties of bottlebrush polymers. Stable films were prepared by introducing

cross-linker into the bottlebrush side-chains, and we demonstrate that PNIPAAM bottlebrush thin films have comparable cell resistance to that PEO polymer brushes. To study bottlebrush polymers at the oil-water interface, both pure bottlebrush polymers and a mixture of surfactant 4,5-orthoxylene sulfonate (OXS) were used as additives in water-chloroform blends. Experimental measurement of the interfacial tension show that the presence of bottlebrush polymer can reduce the interfacial tension significantly, larger than that for commercial surfactant. Although more work is needed, preliminary results are promising for bottlebrush polymers as interfacial tension reducer and anti-fouling surface materials.

Acknowledgments

This thesis work was accomplished at the Department of Chemical and Biomolecular engineering, Rice University, Houston, Texas from August 2009 to May 2014. During my Ph.D studies at Rice University, I worked with a lot great researchers. I would like to show my deepest gratitude for the help and support from them.

First and most, I would like to express my sincere and great thanks to my advisor: Dr. Rafael Verduzco. Throughout my graduate school career, he is an excellent research advisor for his great ideas, scientific guidance, supervision, patience and encouragement.

I would like to express my gratitude to Dr. Boualem Hammouda at national institute of standards and technology for his immense help in the filed of small angle neutron scattering, acquisition and fitting scattering data, various scientific discussions, and constructive comments on my paper of "Thermoresponsive PNIPAAM bottlebrush polymer with tailored side-chain length and end-group structure."

I would also like to thank prof. Gila Stein and her graduate student Indranil Mitra from Department of Chemical and Biomolecular Engineering, University of Houston, Texas. Thanks for their cooperation with the work of thin film phase behavior in athermal blends of branched and linear polymers. Thanks to neutron beam scientists at Oak Ridge National lab: John Ankner, Bradley S. Lokitz, and David Uhrig for proving deuterated linear polystyrene, and their technical advice and help on the neutron reflectivity experiments.

Special recognitions also must be given to professors who served as my committee members: Prof. Walter Chapman and prof. Qilin Li, I appreciate their help and critical suggestions while serving in my defense committee.

It is lucky for me to meet all my great colleagues, Stacy Pesek, Aditya Agrawal, Kendall Smith, Yen-Hao Lin, Luqing Qi, Jorge Mok, Hadi ShamsiJazeyi and Qiqi Xiang. Thanks all for their kind cooperation, assistance, encouragement, successful discussions, technical help and friendly and pleasant working atmosphere during the period of my PhD.

I also want to express my appreciation to Dr. Yan Xia from Stanford University for his help on the synthesis of bottlebrushes polymers. And finally, to my loved families, my boyfriend Zhibin, thanks a lot for supporting or accompanying me through the wonderful time.

This thesis proposal could not have been possible without their assistance. Last and not least, I want to share a poem I like very much by Emily Dickinson:

We never know how high we are

Til we are called to rise

And then, if we are true to plan

Our statures touch the skies

The heroism we recite

Would be a normal thing

Did not ourselves the Cubits warp

For fear to be a King

Table of Contents

List of Tables

List of Figures

1 BACKGROUND

1.1 Introduction

Bottlebrush polymers, also named as molecular brushes, are macromolecules with polymeric side-chains on each repeat unit (Figure 1.1). The dense grafting of polymeric side-chains results in both backbone and side-chain extension,[1-3] giving rise to large, highly extended macromolecules with individual molecules exceeding 100 nm in backbone length in some cases.[4] This worm-like or cylinder structure and diverse side-chains make bottlebrush polymers exhibit diverse functional properties, and can be used in numerous potential applications, ranging from rheological modifiers[5] to polymeric photonics[6] and from nanoparticles for drug-delivery[7 8] to anti-fouling materials[9] et al.

An attractive and challenging aspect of bottle polymers is the number of different variables that determine their structure. The conformation and size of these polymers is determined by the grafting density, side chain length, backbone length, side chain stiffness as well as other structural parameters. Depending on the flexibility of the backbone and side chains, brush polymers can assume a variety of conformations including hairy rods, flexibly brushes, and stiff bristles. Based on the backbone types and side-chain architecture, bottlebrush polymers can be classified into the following categories (Figure 1.2): Linear bottlebrush; dendronized bottlebrush[10,11] and cyclic bottlebrush[12]. According to side-chain types and the way the side-chain attached, bottlebrush polymers can be classified

into the following types: double brush bottlebrush, brush random bottlebrush, brush blocky bottlebrush, blocky brush bottlebrush, and random brush bottlebrush.

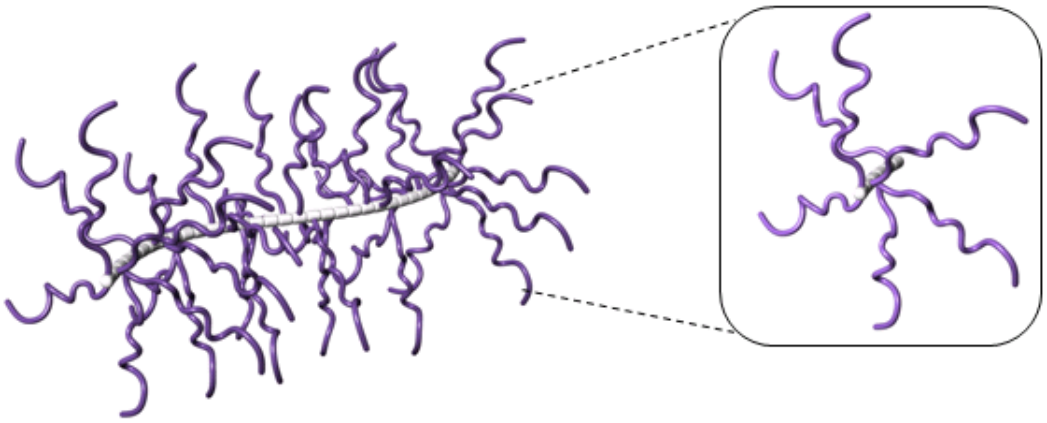

Figure 1.1 Schematic of bottlebrush polymer.

Every repeat unit on the polymer backbone has a polymeric side-chain attached, and steric interactions between the side-chains results in backbone and side-chain stretching.

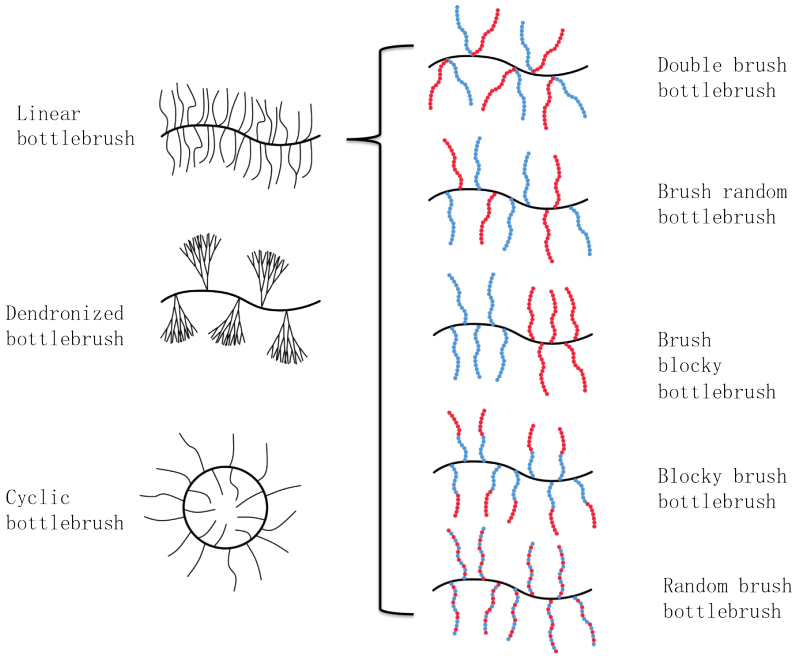

Figure 1.2 Types of bottlebrush polymers

The steric interaction between the side-chains is analogous to those in polymer brush layers, which are made up of polymers end-grafted to a flat or sphere surface. Polymer brushes have been shown to be useful for biological applications, surfactant as well as the preparation of surfaces with tunable properties[9,13-15]. The properties of bottlebrush polymers are determined by the side-chains, and understanding the conformation of the side-chains may be useful for a number of applications.

1.2 Synthesis of bottlebrush polymers

The synthesis of bottlebrush polymers is particularly challenging due to the large degree of steric interaction between the side-chains and the various parameters that need to be controlled (grafting density, degree of polymerization of both the backbone and side-chains, composition of the side-chains, length and polydispersity). The attachment methods of side chains to backbone polymers of bottlebrush materials are usually prepared through the three methods: "grafting from" [16-20], "grafting to" [21-23], and "grafting through" [18,24-37], shown in Figure 1.3. Each method has distinct advantages and limitations.

Within each method, various techniques, such as atom transfer radical polymerization (ATRP), reversible addition-fragmentation chain transfer (RAFT), ring-opening metathesis polymerization (ROMP), various coupling reactions (click chemistry), et al, can be employed.

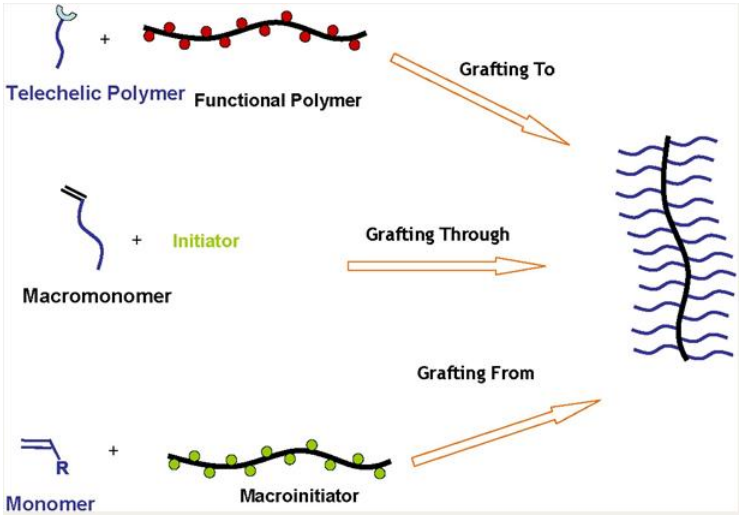

Figure 1.3 Three main techniques for prepare bottlebrush polymers: grafting from, grafting to, and grafting through[13]

.

In the "grafting from" approach, side chains are grown from the initiating sites of functionalized polymeric backbone (macroinitiator). This synthetic method allows for good control over the molecular weight and polydispersity index of the final bottlebrush polymer. Furthermore, the macroinitiator determines the brush structure, grafting density, and the overall size. Therefore, long and well defined backbone molecular brushes with high grafting density have been prepared[6,17,38-40]. However, precise control over the side-chain properties is more challenging, and this method does not guarantee that a polymer chain is attached to every repeat unit in the polymer [41].

In the "grafting to" method, the side-chains and backbone are prepared separately and then coupled together to form a bottlebrush (Figure 1.3). One main advantage for this method is that the backbone and the side chains are synthesized independently, and it is possible to characterize both backbone polymer and side chains before coupling.

However, the efficiency of "grafting to" method depends strongly on the size of side chains. For shorter and slimmer side chains, such as short PEO, the initiation can achieve to about 90%, but for longer or fatter side chains, like polystyrene (PS) or poly(butyl acrylate), the efficiency decreases a lot [13]. Another major limitation associated with this method is the poor control of the grafting density due to steric repulsion between bulky side chains.

The "grafting through" technique for the synthesis of polymer brushes involves the polymerization of well-defined monofunctional macromonomers (MMs); i.e. the side-chains are synthesized first and then polymerized to make bottlebrush polymers. The advantage of this method is that it guarantees that each repeat unit has a side chain attached. Additionally, the side chains are prepared independently, and can be characterized prior to the polymerization. Therefore "grafting through" allows for good control over the length of both the backbone chain and side chains. On the other hand, the synthesis of polymacromonomers (polyMMs) with a high degree of polymerization is typically challenging due to the large size of the side-chains as well as steric hindrance between the side-chains during polymerization.

The development of ring opening metathesis polymerization (ROMP) solved the problems of "grafting through" method as we mentioned above. ROMP was included in olefin metathesis reaction, it converts cyclic olefin monomers into linear polymers with unsaturated backbones. The most commonly used monomers are cyclic olefins having high-strain, such as norbornene, cyclobutene, cyclopentene.[42] Recently, an efficient method for synthesizing bottlebrush polymers using a "grafting-through" technique has been reported [7,43-46]. The synthesis involves a ring-opening polymerization of a

norbornene moiety. Norbornene is a bridged six-membered ring with a double bond on one side, and is soluble in many common solvents. The bridged ring puts extra strain on the double bond, making it highly reactive in ring-opening reactions.

To obtain the narrowly dispersed, polyMMs through ROMP with high conversion, catalyst plays a very important role. Early transition metals, such as molybdenum, have been used to produce narrowly dispersed polyMMs. However, the DP of the backbone of these polyMMs is just about 5-20 typically [47-49]. In addition, the limited functional group tolerance and air and moisture sensitivity of these catalysts narrow their applications. More recently, Ruthenium-based catalyst, Grubbs' catalyst, first generation, was applied in the ROMP of MMs (Figure 1.4 (b)). Although narrowly dispersed graft polymers were obtained, the DP of these graft polymers is still low, due to the relatively low reactivity of the first generation catalyst[50]. Compared to the Grubbs' first generation catalyst, Grubbs' second generation catalyst (Figure 1.4 (c)) shows greatly increased reactivity, but the slow initiation leads to poor PDI. As an example, the ROMP of a polylactide norbornenyl MM using Ru-based first generation catalyst, in their report, high Mw was obtained [51]. Recently a more efficient Grubbs' catalyst (the third generation, Figure 1.4 (d)) was reported, which exhibits fast initiation, high functional group tolerance, and high reactivity [52,53]. Dr. Wooley's group reported that polymerization with catalyst 3 can even be conducted in the presence of oxygen, without the need for purging with inert gases[46]. Grubbs' third generation catalyst was synthesized (Figure 1.4, (d)) in 2003, [54] this pyridine containing catalyst can initiate the ROMP fast and also has high activity, and therefore obtain well-controlled polymers with low PDI. ATRP, RAFT, "click chemistry" EDC/DMAP coupling have been employed into the synthesis of macromonomers, these

techniques make it possible to attach diverse side-chain polymers to the norbornene end group. All above advantages make ROMP based "grafting through" method is one of the most important reactions to synthesis a wide variety of useful product with unique architectures. The polymerization of dendronized polymers using the third generation catalyst was also reported[55]. The fast initiation, the high reactivity, and high functional group tolerance make the third generation Grubbs' catalyst an ideal catalyst for the polymerization of macromonomers.

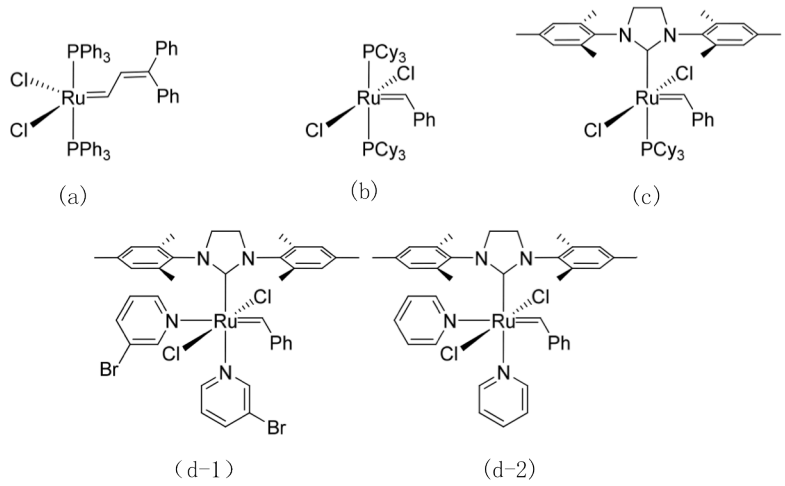

Figure 1.4 The structure of Ru-based metathesis catalyst [43].

In conclusion, there are three main grafting methods to prepare bottlebrushes: "grafting from", "grafting to", and "grafting through". The "grafting from" has been widely used to brush polymers, the previous reported brush polymers were synthesized by this grafting methods [6,39,56,57]. However, the poor control of the side chains and the high initiation density sites from the backbone limit the efficiency of the initiation [12-16]. The "grating to" allows well preparation of both backbone polymer and side chains, but

its disadvantage is also significant: grafting becomes more difficult as the conversion increases [17-19]. The "grafting through" method is the only one that can guarantee completed grafting (each macromonomer is consist of side chain polymers and backbone repeat unit), and both the backbone length and side chain length can be well controlled. The use of norbornene-based monomers and the development of an efficient catalyst system make the "grating through" approach a powerful method for synthesizing bottlebrush polymers with tailored properties.

In this dissertation, we will synthesize bottlebrush polymers using a "grafting-through" scheme based on ROMP techniques. We are particularly interested in studying the properties of the bottlebrush polymer side-chains, and the "grafting-through" scheme provides the best control over side-chain grafting density and properties.

1.3 Conformation and phase behavior of bottlebrush polymers

The cylinder bottlebrush polymers are attractive because of the expectation of their unusual properties arise from their unique structures. Compared to the corresponding same molecular weight linear polymers, bottlebrush polymers have the following characteristics: first, bottle-brushes have the extended cylinder conformation due to strong repulsion between densely grafted side chains, and this well-defined shape and large size enable accurate characterization by visualization of single molecules; second, bottle-brushes have a small and compact molecular dimension, which allow significant advancement in the visualization observations; third, for each molecule, the functional groups on the end of side chains can promote orderings along the relative stiffness of the backbone, and this makes the almost functional groups effective. The overcrowding stiff

side chains force the main chains into a stretched conformation, which means the significant reduced degree of freedom. The lyrotropic phenomena of bottlebrush polymers with rigid side chains are also expected like other polymers with stiff side chains. The former researches involve the properties of bottlebrushes in solution, surface and in bulk.

Bottlebrush structures have been observed as spheres and "worm-like" and "rod-like" cylinders. Theory predicts a correlation of backbone persistence length (l_p) and brush diameter D. Fredrickson presented a scaling analysis[1] which predicts that the persistence length increases faster than the brush diameter with increasing degree of polymerization. The predicted relationship between l_p/D and the length of side chains is $l_p/D \sim N^{9/8}$, where N is the degree of polymerization of side chains. A different analysis by Birhstein[58] predicts that the ratio between l_p and D is constant and that both will increase at a similar rate with the length of side chains. Experimentally, the results on the subject are contradictory [2,3,59] For the case of bottlebrush polymers with rigid side chains, the ration between l_p and D is predicted to be linear[60], potentially resulting in highly extended bottlebrush polymers which exhibit lyotropic behavior in solution. The properties of bottlebrush polymers with rigid side-chains have not been experimentally investigated.

Although bottlebrush polymers are gaining attention in synthetic and characterization reports, there exists a fundamental knowledge between the chemical composition and polymer chain lengths to the ultimate macromolecular size and shape.

1.4 Potential applications of bottlebrush polymers

1.4.1 Biological application

As stated above, the development of ROMP provides a facile method to obtain highly functional bottlebrush polymers with well-controlled molecular weight and low PDI.[44,61] And besides, former research showed the norbornene backbone in nontoxic, and can provide bio-compatible ability.[62,63] Especially, the worm-like structures are very common in nature, like proteoglycans.[64] Therefore, brush-like polymers with highly grafted functional groups have diverse applications in the filed of biology. Like anti-biofouling; drug-delivery; tissue engineering et al.

As the similar brush-like structure, bottlebrushes also have similar applications like polymer brushes, in the filed of anti-fouling. Our former research results show that the side-chains of bottlebrush polymers have enough flexibility, which makes bottlebrush polymers a possible candidate replacement for polymer brushes.[65] Bottlebrush polymers with cell resistance homo side-chains, like PEG have been reported. And besides, Tew's group reported on the non-fouling films of Amphiphilic Polybetaines bottlebrushes and the backbone structure effect on the anti-fouling abilities.[9,66,67] RGD peptide was proven to be mediate extracellular proteins bind to cell surface. [68] Cell adhesion inhibition by peptides functionalized bottlebrush polymers also reported. [69,70]

1.4.2 Optical and electronic application

Conductive polymers have diverse potential applications, like photovoltaic, electron-active materials, and photonics. [71] Well-defined nano-structured and multifunctional polymers have been regarded as essential in exploring the electric performance. Precisely-controlled ROMP provides a possible route to obtain conductive polymers with ideal nanoscopic phase separation.

An Enhanced Host–Guest Electro-Optical (EO) Polymer System Using Poly(norbornene-dicarboximides) via ROMP, has the potential application in high-speed broadenband devices. [72] In this report, the influence of molecular weight and trans–cis microstructure of bottlebrush as host materials on the EO activity was investigated and optimized. Bottlebrush polymer with ambipolar Nitronyl nitroxide (NN) side-chains were synthesized as organic secondary batteries Electron-active materials.[73] Grubbs catalysts have both high activity and broad functional group tolerance to achieve the polymerization of radical monomers. And besides, the high swelling properties of norbornene backbone would improve electrode performance. The improved charging/discharging capacity indicates such bottlebrush polymers might be potential efficient electric materials.

Among all conductive/semiconductive polymers, P3HT was considered as one of the most effective and most widely studied materials in organic photovoltaic. The phase separation between donor and acceptor is very important for the performance. In practice, the excitation formed after light is harvested and the separated charges could only travel less than 20 nm before recombination in organic–inorganic hybrid solar cells. [74] Several efforts to improve the efficiency and morphology of conjugated polymer films have been made. For example, by introducing TiO_2 nanotube array to induce the proper nanoscale phase separation,[75] and synthesizing star-shape polymers coated with oligo(thiophene) exhibits unique emission properties due to intramolecular energy transfer. [76] Recently, bottlebrush polymers with poly(3-thiopheneacetic acid) side-chains were synthesized and applied to modified TiO_2 nanowires and the CdS nanocrystal was also introduced to the above conductive polymer hybrid nanocomposite materials. [77] Since this methods can

make poly(3-thiopheneacetic acid bottlebrushes tailor the size and afford nanoscale interfacial contact with CdS nanocrystal, higher charge separation and transfer with minimal carrier recombination were expected.

Also, the types of bottlebrush polymers with donor-acceptor side-chains on the charge transfer band were investigated. [78] In the above studies, the bottlebrush polymers with homopolymer side-chains, random copolymer side-chains, blocky side-chains, and alternating side-chains were synthesized. And the noncovalent interactions between donor-acceptor pair along the side-chains can lead to aggregates and potentially secondary structures. And UV/Vis characterizations indicate that the intra chain not the interchain determines the charge transfer band. Therefore, the bottlebrush synthesis route can control over the secondary structure for further functional materials.

Compared to linear polymers, bottlebrush analogy side-chains have reduced entanglement due to high grating density. Therefore rapid self-assembly for blocky bottlebrush polymers might be employed in the field of photonics crystals. Bottlebrush polymers with PLA and PS blocky side-chains with different molecular weight were synthesized. Controlled evaporation and thermal annealing was applied to induce different nano scale self-assembly of bottlebrush blocky polymers, and enables a facile method to obtain photonic crystals with tailored band gap. [79] Besides, PLA and PS based macromonomers, helical isocyanate based macromonomers were also introduced to obtain photonic crystals. The domain size can be controlled by molecular weight directly. And the wavelength can be turned form UV to near IR. [80] And by blending blocky bottlebrush polymers with different molecular weight patched another way to turn band gaps without complex annealing procedure. [81]

1.4.3 Surfactant and additives application

As we mentioned earlier in this dissertation, bottlebrush polymers have structural similarities with polymer-coated nanoparticles. Polymer-coated nanoparticles (brushy nanoparticles) are versatile nanomaterials with controlled shape, size, and surface chemistry. Ideally, the nanoparticle core determines the size and shape of the particle and a dense polymer brush layer dictates surface properties and mediates interactions with the environment (e.g., solvent, other particles). In practice, achieving polymer-coated nanoparticles with controlled molecular characteristics is limited by low coupling efficiencies of polymers to nanoparticles,[82-84] poor displacement of solubilizing ligands from nanoparticle surfaces[85] and poor control over polymerization reactions mediated by chain transfer agents (CTAs) at the nanoparticle surfaces.[86] Recently, a report of bottlebrush polymers with amphiphilic alternating side-chains were reported as surfactant in the filed of stabilizing the interfaces. [87] Bottlebrush polymers can be an ideal candidate for polymer-coated nanoparticles in the field of surfactant and additives.

1.5 Objectives

Our research objective is to understand the conformation and flexibility of the bottlebrush polymer side-chains, study the unique physical properties of bottlebrush polymers and explore potential application of these novel materials. In this dissertation, we present a systematic investigation of bottlebrush polymers that incorporates the synthesis of well-defined macromolecules as well as the structural characterization of the bottlebrush polymers in thin films, in solution and in polymer matrix. In chapter 2, we took advantage of a "grafting-through" synthetic scheme to rationally design bottlebrush

with different length amphiphilic side-chains. Systematic studies on the relationship of surface properties (wetting and adhesion abilities) of bottlebrushes polymers with different side chains, different side chain lengths, and ratio of copolymer side-chains were carried out. Stimuli-responsive behaviors of bottlebrush polymer side-chains were illustrated. In chapter 3, conformational properties and phase behaviors of bottlebrush polymers in solutions were studied by neutron scattering method.

1.6 Bibliography

(1) Fredrickson, G. H. *Macromolecules* **1993**, *26*, 2825.

(2) Rathgeber, S.; Pakula, T.; Wilk, A.; Matyjaszewski, K.; Beers, K. *J. Chem. Phys.* **2005**, *122*, 124904/1.

(3) Zhang, B.; Gröhn, F.; Pedersen, J. S.; Fischer, K.; Schmidt, M. *Macromolecules* **2006**, *39*, 8440.

(4) Sheiko, S. S.; Möller, M. *Chem. Rev.* **2001**, *101*, 4099.

(5) Lee, S.; Spencer, N. D. *Science* **2008**, *319*, 575.

(6) Runge, M. B.; Bowden, N. B. *J. Am. Chem. Soc.* **2007**, *129*, 10551.

(7) Johnson, J. A.; Lu, Y. Y.; Burts, A. O.; Xia, Y.; Durrell, A. C.; Tirrell, D. A.; Grubbs, R. H. *Macromolecules* **2010**, *43*, 10326.

(8) Johnson, J. A.; Lu, Y. Y.; Burts, A. O.; Lim, Y.-H.; Finn, M. G.; Koberstein, J. T.; Turro, N. J.; Tirrell, D. A.; Grubbs, R. H. *J. Am. Chem. Soc.* **2010**, *133*, 559.

(9) Olanya, G.; Thormann, E.; Varga, I.; Makuska, R.; Claesson, P. M. *J. Colloid Interface Sci.* **2010**, *349*, 265.

(10) Chen, Y.; Xiong, X. *Chem. Commun. (Cambridge, U. K.)* **2010**, *46*, 5049.

(11) Kim, K. O.; Choi, T.-L. *ACS Macro Letters* **2012**, *1*, 445.

(12) Xia, Y.; Boydston, A. J.; Grubbs, R. H. *Angewandte Chemie International Edition* **2011**, *50*, 5882.

(13) Sheiko, S. S.; Sumerlin, B. S.; Matyjaszewski, K. *Prog. Polym. Sci.* **2008**, *33*, 759.

(14) Sankaran, N. B.; Rys, A. Z.; Nassif, R.; Nayak, M. K.; Metera, K.; Chen, B.; Bazzi, H. S.; Sleiman, H. F. *Macromolecules* **2010**, *43*, 5530.

(15) Claesson, P. M.; Makuska, R.; Varga, I.; Meszaros, R.; Titmuss, S.; Linse, P.; Pedersen, J. S.; Stubenrauch, C. *Adv. Colloid Interface Sci.* **2010**, *155*, 50.

(16) Beers, K. L.; Gaynor, S. G.; Matyjaszewski, K.; Sheiko, S. S.; Möller, M. *Macromolecules* **1998**, *31*, 9413.

(17) Börner, H. G.; Beers, K.; Matyjaszewski, K.; Sheiko, S. S.; Möller, M.

Macromolecules **2001**, *34*, 4375.

(18) Cheng, G.; Böker, A.; Zhang, M.; Krausch, G.; Müller, A. H. E. *Macromolecules* **2001**, *34*, 6883.

(19) Kriegel, R. M.; Rees, W. S.; Weck, M. *Macromolecules* **2004**, *37*, 6644.

(20) Runge, M. B.; Dutta, S.; Bowden, N. B. *Macromolecules* **2005**, *39*, 498.

(21) Deffieux, A.; Schappacher, M. *Macromolecules* **1999**, *32*, 1797.

(22) Gao, H.; Matyjaszewski, K. *J. Am. Chem. Soc.* **2007**, *129*, 6633.

(23) Schappacher, M.; Deffieux, A. *Macromolecules* **2005**, *38*, 7209.

(24) Gerle, M.; Fischer, K.; Roos, S.; Müller, A. H. E.; Schmidt, M.; Sheiko, S. S.; Prokhorova, S.; Möller, M. *Macromolecules* **1999**, *32*, 2629.

(25) Tsukahara, Y.; Mizuno, K.; Segawa, A.; Yamashita, Y. *Macromolecules* **1989**, *22*, 1546.

(26) Tsukahara, Y.; Tsutsumi, K.; Yamashita, Y.; Shimada, S. *Macromolecules* **1990**, *23*, 5201.

(27) Wintermantel, M.; Gerle, M.; Fischer, K.; Schmidt, M.; Wataoka, I.; Urakawa, H.; Kajiwara, K.; Tsukahara, Y. *Macromolecules* **1996**, *29*, 978.

(28) Ito, K.; Tanaka, K.; Tanaka, H.; Imai, G.; Kawaguchi, S.; Itsuno, S. *Macromolecules* **1991**, *24*, 2348.

(29) Nomura, E.; Ito, K.; Kajiwara, A.; Kamachi, M. *Macromolecules* **1997**, *30*, 2811.

(30) Wintermantel, M.; Schmidt, M.; Tsukahara, Y.; Kajiwara, K.; Kohjiya, S. *Macromol. Rapid Commun.* **1994**, *15*, 279.

(31) Sheiko, S. S.; Gerle, M.; Fischer, K.; Schmidt, M.; Möller, M. *Langmuir* **1997**, *13*, 5368.

(32) Dziezok, P.; Fischer, K.; Schmidt, M.; Sheiko, S. S.; Möller, M. *Angewandte Chemie International Edition in English* **1997**, *36*, 2812.

(33) Wintermantel, M.; Fischer, K.; Gerle, M.; Ries, R.; Schmidt, M.; Kajiwara, K.; Urakawa, H.; Wataoka, I. *Angewandte Chemie International Edition in English* **1995**, *34*, 1472.

(34) Tsukahara, Y.; Ohta, Y.; Senoo, K. *Polymer* **1995**, *36*, 3413.

(35) Grassl, B.; Rempp, S.; Galin, J. C. *Macromol. Chem. Phys.* **1998**, *199*, 239.

(36) Ishizu, K.; Furukawa, T. *Polymer* **2001**, *42*, 7233.

(37) Ishizu, K.; Yukimasa, S.; Saito, R. *Journal of Polymer Science Part A: Polymer Chemistry* **1993**, *31*, 3073.

(38) Zhang, M.; Breiner, T.; Mori, H.; Müller, A. H. E. *Polymer* **2003**, *44*, 1449.

(39) Runge, M. B.; Yoo, J.; Bowden, N. B. *Macromol. Rapid Commun.* **2009**, *30*, 1392.

(40) Cheng, C.; Khoshdel, E.; Wooley, K. L. *Nano Lett.* **2006**, *6*, 1741.

(41) Sumerlin, B. S.; Neugebauer, D.; Matyjaszewski, K. *Macromolecules* **2005**, *38*, 702.

(42) Benson, S. W.; Cruickshank, F. R.; Golden, D. M.; Haugen, G. R.; O'Neal, H. E.; Rodgers, A. S.; Shaw, R.; Walsh, R. *Chem. Rev. (Washington, DC, U. S.)* **1969**, *69*, 279.

(43) Xia, Y.; Kornfield, J. A.; Grubbs, R. H. *Macromolecules* **2009**, *42*, 3761.

(44) Xia, Y.; Olsen, B. D.; Kornfield, J. A.; Grubbs, R. H. *J. Am. Chem. Soc.* **2009**, *131*, 18525.

(45) Li, Z.; Ma, J.; Cheng, C.; Zhang, K.; Wooley, K. L. *Macromolecules* **2010**, *43*,

1182.
(46) Li, Z.; Zhang, K.; Ma, J.; Cheng, C.; Wooley, K. L. *J. Polym. Sci., Part A: Polym. Chem.* **2009**, *47*, 5557.
(47) Heroguez, V.; Breunig, S.; Gnanou, Y.; Fontanille, M. *Macromolecules* **1996**, *29*, 4459.
(48) Héroguez, V.; Amédro, E.; Grande, D.; Fontanille, M.; Gnanou, Y. *Macromolecules* **2000**, *33*, 7241.
(49) Murphy, J. J.; Nomura, K. *Chem. Commun. (Cambridge, U. K.)* **2005**, 4080.
(50) Hilf, S.; Kilbinger, A. F. M. *Macromol. Rapid Commun.* **2007**, *28*, 1225.
(51) Jha, S.; Dutta, S.; Bowden, N. B. *Macromolecules* **2004**, *37*, 4365.
(52) Matson, J. B.; Grubbs, R. H. *J. Am. Chem. Soc.* **2008**, *130*, 6731.
(53) Camm, K. D.; Martinez Castro, N.; Liu, Y.; Czechura, P.; Snelgrove, J. L.; Fogg, D. E. *J. Am. Chem. Soc.* **2007**, *129*, 4168.
(54) Choi, T.-L.; Grubbs, R. H. *Angewandte Chemie International Edition* **2003**, *42*, 1743.
(55) Rajaram, S.; Choi, T.-L.; Rolandi, M.; Fréchet, J. M. J. *J. Am. Chem. Soc.* **2007**, *129*, 9619.
(56) Rzayev, J. *Macromolecules* **2009**, *42*, 2135.
(57) Lee, H. I.; Matyjaszewski, K.; Yu-Su, S.; Sheiko, S. S. *Macromolecules* **2008**, *41*, 6073.
(58) Birshtein, T. M.; Borisov, O. V.; Zhulina, Y. B.; Khokhlov, A. R.; Yurasova, T. A. *Polymer Science U.S.S.R.* **1987**, *29*, 1293.
(59) Fischer, K.; Schmidt, M. *Macromol. Rapid Commun.* **2001**, *22*, 787.
(60) Saariaho, M.; Subbotin, A.; Szleifer, I.; Ikkala, O.; ten Brinke, G. *Macromolecules* **1999**, *32*, 4439.
(61) Leitgeb, A.; Wappel, J.; Slugovc, C. *Polymer* **2010**, *51*, 2927.
(62) Kolonko, E. M.; Pontrello, J. K.; Mangold, S. L.; Kiessling, L. L. *J. Am. Chem. Soc.* **2009**, *131*, 7327.
(63) Lienkamp, K.; Madkour, A. E.; Musante, A.; Nelson, C. F.; NuÃàsslein, K.; Tew, G. N. *J. Am. Chem. Soc.* **2008**, *130*, 9836.
(64) Muir, H. *Biochem. Soc. Trans.* **1983**, *11*, 613.
(65) Li, X.; Prukop, S. L.; Biswal, S. L.; Verduzco, R. *Macromolecules* **2012**.
(66) Colak, S.; Tew, G. N. *Biomacromolecules* **2012**, *13*, 1233.
(67) Colak, S.; Nelson, C. F.; NuÃàsslein, K.; Tew, G. N. *Biomacromolecules* **2009**, *10*, 353.
(68) Massia, S. P.; Hubbell, J. A. *The Journal of Cell Biology* **1991**, *114*, 1089.
(69) Maynard, H. D.; Okada, S. Y.; Grubbs, R. H. *J. Am. Chem. Soc.* **2001**, *123*, 1275.
(70) Maynard, H. D.; Okada, S. Y.; Grubbs, R. H. *Macromolecules* **2000**, *33*, 6239.
(71) Chen, L.-M.; Hong, Z.; Li, G.; Yang, Y. *Adv. Mater. (Weinheim, Ger.)* **2009**, *21*, 1434.
(72) Yu, F.; Spring, A. M.; Li, L.; Qiu, F.; Yamamoto, K.; Maeda, D.; Ozawa, M.; Odoi, K.; Yokoyama, S. *Journal of Polymer Science Part A: Polymer Chemistry* **2013**, *51*, 1278.
(73) Sukegawa, T.; Kai, A.; Oyaizu, K.; Nishide, H. *Macromolecules* **2013**, *46*, 1361.
(74) G√ºnes, S.; Neugebauer, H.; Sariciftci, N. S. *Chem. Rev. (Washington, DC, U. S.)*

2007, *107*, 1324.

(75) Mor, G. K.; Kim, S.; Paulose, M.; Varghese, O. K.; Shankar, K.; Basham, J.; Grimes, C. A. *Nano Lett.* **2009**, *9*, 4250.

(76) Takamizu, K.; Nomura, K. *J. Am. Chem. Soc.* **2012**, *134*, 7892.

(77) Yan, J.; Ye, Q.; Han, X.; Zhou, F. *RSC Advances* **2013**, *3*, 166.

(78) Romulus, J.; Patel, S.; Weck, M. *Macromolecules* **2011**, *45*, 70.

(79) Sveinbj√∂rnsson, B. R.; Weitekamp, R. A.; Miyake, G. M.; Xia, Y.; Atwater, H. A.; Grubbs, R. H. *Proceedings of the National Academy of Sciences* **2012**, *109*, 14332.

(80) Miyake, G. M.; Weitekamp, R. A.; Piunova, V. A.; Grubbs, R. H. *J. Am. Chem. Soc.* **2012**, *134*, 14249.

(81) Miyake, G. M.; Piunova, V. A.; Weitekamp, R. A.; Grubbs, R. H. *Angewandte Chemie International Edition* **2012**, *51*, 11173.

(82) Meli, L.; Arceo, A.; Green, P. F. *Soft Matter* **2009**, *5*, 533.

(83) Lowe, A. B.; Sumerlin, B. S.; Donovan, M. S.; McCormick, C. L. *J. Am. Chem. Soc.* **2002**, *124*, 11562.

(84) Berlin, J. M.; Yu, J.; Lu, W.; Walsh, E. E.; Zhang, L.; Zhang, P.; Chen, W.; Kan, A. T.; Wong, M. S.; Tomson, M. B.; Tour, J. M. *Energy & Environmental Science* **2011**, *4*, 505.

(85) Mazzio, K. A.; Okamoto, K.; Li, Z.; Gutmann, S.; Strein, E.; Ginger, D. S.; Schlaf, R.; Luscombe, C. K. *Chem. Commun. (Cambridge, U. K.)* **2013**, *49*, 1321.

(86) Gregory, A.; Stenzel, M. H. *Prog. Polym. Sci.* **2012**, *37*, 38.

(87) Li, Y.; Zou, J.; Das, B. P.; Tsianou, M.; Cheng, C. *Macromolecules* **2012**, *45*, 4623.

2 Conformational and interactional behaviors of bottlebrush polymer at surface

[The work described in this chapter is published in: Xianyu Li, Stacy L. Prukop, Sibani Lisa Biswal, and Rafael Verduzco, "Surface Properties of Bottlebrush Polymer Thin Films" *Macromolecules*, 2012, 45, 7118-7127]

2.1 Abstract

Bottlebrush polymer thin films may be attractive for the preparation of antifouling and/or stimuli-responsive surface coatings due to the high grafting density and conformational flexibility of polymeric side-chains. Thin polymer films can be easily prepared using solvent-based techniques including spin-coating, dip-coating, and ink-jet printing, but bottlebrush polymer thin films have not been previously reported and their surface properties are unknown. Herein, we report a study of the surface properties of mixed bottlebrush polymer (MBBPs) films. MBBPs with hydrophobic polystyrene (PS) and hydrophilic poly(ethylene glycol) (PEG) side-chains are synthesized using a "grafting-through" ring-opening metathesis polymerization (ROMP) technique. Stimuli-responsive MBBPs films are prepared by spin-casting a solution of MBBPs onto a solid surface, and resulting film morphology and surface properties are characterized using atomic force microscopy (AFM), water contact angle measurements, and x-ray photoelectron spectroscopy (XPS) and grazing-incident small-angle X-ray scattering

(GISAXS). The water contact angles of MBBPs films decrease or increase upon exposure of the MBBPs films to methanol or cyclohexane, which are selective for PEG and PS side-chains, respectively. The degree to which the contact angle changes is dependent on the length of the PEG side-chain; longer PEG side-chains result in greater contact angle changes with solvent exposure. XPS measurements reveal compositional changes of the top film surface due to solvent exposure. Consistent with water-contact angle measurements, XPS indicates enrichment of PEG or PS chains after exposure of the MBBPs film to methanol or cyclohexane solvent vapors, respectively. Finally, it is demonstrated that bottlebrush polymer films can be stabilized by the addition of a radical cross-linker and irradiation with UV light. This work demonstrates that bottlebrush polymers enable the preparation of stimuli-responsive, "brush-like" polymeric coatings using simple solution processing methods.

2.2 Introduction

Bottlebrush polymers are macromolecules with polymeric side-chains on each repeat unit. The dense grafting density of polymeric side-chains results in both backbone and side-chain extension,[1-4] giving rise to large, highly extended macromolecules with individual molecules exceeding 100 nm in backbone length in some cases.[5] As a result of their size and novel structure, bottlebrush polymers are candidates for a number of applications, including rheological modifiers,[6] polymeric photonics,[7] and nanoparticles for drug-delivery.[8-10] While thin films of polymers can be easily prepared using common solvent-based techniques including spin-coating, dip-coating, and ink-jet printing, bottlebrush polymer thin films have not been previously reported and their surface

properties are unknown. Due to the high grafting density and conformational flexibility of the side-chains, such coatings may be attractive for the preparation of antifouling and/or stimuli-responsive surfaces.

Bottlebrush polymer thin films exhibit surface properties characteristic of polymer brush films, which are comprised of polymer chains densely tethered to a surface.[11] Steric interactions in polymer brush films result in chain stretching normal to the surface and give rise to novel and potentially useful surface properties. These types of films are currently of interest for the preparation of non-toxic antifouling surfaces,[12,13] self-cleaning surfaces,[14] stimuli-responsive surfaces,[15-17] organic electronics,[18,19] and other applications.[20,21] However, the use of polymer brush films for some applications may be impractical. Polymer brush films are commonly prepared through surface initiated polymerizations[22,23] which require a functionalized, reactive surface as well as polymerization under inert conditions. Accomplishing this over a large surface, such as a ship's hull for antifouling films, would be costly and technically difficult. Bottlebrush polymers provide a potential alternative and they can be easily applied over any surface using solution processing techniques such as ink-jet printing, dip coating, or spray coating.

The goal of this study is to characterize the surface properties of bottlebrush polymer thin films and, in particular, determine if bottlebrush polymer films can show stimuli-responsive surface properties. In analogy to the switchable wettability that has been observed in polymer brush films,[24-28] bottlebrush polymers with mixed hydrophobic and hydrophilic side-chains may show switchable surface properties on exposure to solvents that selective for one of the chains (Figure 2.1). For a mixed bottlebrush polymer

film with hydrophobic polystyrene (PS) and hydrophilic poly(ethylene glycol) (PEG) side-chains, exposure to cyclohexane (which is selective for PS) may result in enrichment of PS chains at the film surface and an increase of the water contact angle. On the other hand, exposure of the film to methanol (which is selective to PEG) may result in enrichment of PEG chains at the film surface and a decrease in the water contact angle. The length of the side-chains may also play a role. Short side-chains may have little conformational flexibility, while longer side-chains are expected to have more conformational flexibility, potentially resulting in larger contact angle changes with solvent exposure.

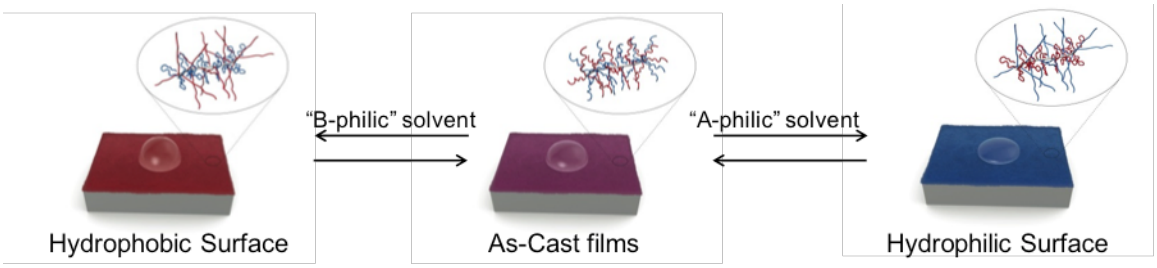

Figure 2.1 Schematic for a bottlebrush polymer films with reversible wettability.

The schematic shows a film of mixed bottlebrush polymers, which have both hydrophilic and hydrophobic side-chains. Exposure to a selective solvent for one side-chain will preferentially swell those chains and lead to enrichment of those chains at the film surface and lead to an increase or decrease in the water contact angle.

Experimental verification of switchable wettability requires the preparation of mixed bottlebrush polymers (MBBPs), which have distinct polymeric side-chains connected to a polymeric backbone. Three general approaches for synthesizing bottlebrush polymers

include "grafting-to," "grafting-from," and "grafting-through."[29] Each strategy has particular advantages and disadvantages, but the "grafting-from" approach has been the most popular method for making bottlebrush polymers,[30-33] including the preparation bottlebrush polymers with block copolymer side-chains as well as nanocapsules with hollow interiors.[10,34-39] However, the "grafting-through" approach, which involves the polymerization of reactive macromonomers, is the only method which guarantees uniform side-chains attached to each repeat unit. Early studies on bottlebrush polymers relied on a "grafting-through" approach, but this generally resulted in polymers with a low degree of polymerization and broad polydispersities.[40-45] Recently, an efficient "grafting-through" scheme for synthesizing bottlebrush polymers based on ring opening metathesis polymerization (ROMP) has been developed.[46-49] Bowden and coworkers demonstrated in 2004 that ROMP was an effective approach for polymerizing macromonomers terminated with a norbornyl group.[47] Subsequently, Grubbs and coworkers showed that using a more reactive modified 2nd or 3rd generation Grubbs catalyst enabled control over the length and polydispersity of molecular brushes. Their approach enabled the preparation of molecular brushes with complex structures, such as random and "blocky" molecular brush copolymers.[9,46,49,50]

Herein, we report a study of the surface properties of mixed bottlebrush polymer (MBBPs) films. Well-defined MBBPs are prepared through a "grafting-through" ROMP technique using a mixture of PEG and PS macromonomers. Gel-permeation chromatography (GPC) and ^{1}H NMR show that well-defined MBBPs with > 90% conversion of the macromonomers can be prepared by ROMP. MBBPs films are prepared by spin-casting a solution of MBBPs onto a solid surface, and the resulting

surface properties are characterized by AFM, contact angle, XPS measurements. The water contact angle and composition of the top film can be modified by exposing the MBBPs film to methanol or cyclohexane vapors, which are selective to PEG or PS side chains, respectively. Furthermore, it is demonstrated that bottlebrush polymers films can be stabilized by the addition of a bifunctional radical cross-linker. This work demonstrates that bottlebrush polymers enable the preparation of stimuli-responsive, "brush-like" polymeric coatings using simple and economically-viable solution processing methods.

2.3 Experimental

2.3.1 Materials

All reagents and solvents were purchased from Aldrich or VWR and were used as received unless otherwise noted. 2,2'-azobis(2-methylpropionitrile) (AIBN) was purified by recrystallization in methanol. Styrene was passed through aluminum oxide column to remove inhibitors before use. Anhydrous dichloromethane (DCM) was dried over molecular sieves (4 Å) before use. Exo-7-oxabicyclo[2.2.1] hept-5-ene-2,3-dicarboxylic anhydride[51], 4-(2-Hydroxyethyl)-10-oxa-4-azatricyclo[5.2.1.02,6]dec-8-ene-3,5-dione[52], modified Grubb's catalyst (H2IMes)(pyr)2(Cl)2RuCHPh[53], and the bifunctional benzophenone molecule bis-3-benzoyl benzoic acid ethylene glycol[54] were synthesized as previously reported. 2K and 5K azide functionalized PEG were purchased from Nanocs.

***N*-(Hydroxypentanyl)-*cis*-5-norbornene-*exo*-2,3-dicarboximide** The synthetic procedure is a slightly modified from a previous report.[49] A round-bottom flask was

charged with *cis*-5-norbornene-*exo*-2,3-dicarboxylic anhydride (0.95 g, 5.8 mmol) and 5-amino-1-pentanol (0.60 g, 5.8 mmol). Toluene (20 ml) and triethylamine (80 μL, 0.58 mmol) were added to the flask, and the reactor was refluxed at 125 °C with a Dean-Stark trap attached. After reacting for at least 4 h, the reaction was cooled down, and the solvent was removed by rotary evaporation. The resulting light yellow oil was re-dissolved in 20 mL DCM and extracted with brine (10 ml,) and then HCl (10 ml). The organic layer was dried by adding $MgSO_4$, and the resulting solution was concentrated under vacuum (1.40 g, 96% yield). ^{1}H NMR (400MHz, CDCl3, ppm): δ 6.27 (2H, CHCH=CHCH), 3.62 (2H, CH2CH2OH), 3.44 (2H, NCH2CH2), 3.27 (2H, CHCHCH) 2.65 (2H, CHCHCO), 1.49-1.56 (5H, CH2CH2CH2CH2; CHCH2CH), and 1.20-1.28 (3H, CH2CH2CH2OH; CHCH2CH).

***N*-(Pentynoylhexanyl)-*cis*-5-norbornene-*exo*-2,3-dicarboximide (1)** The synthetic procedure is a slightly modified from a previous report.[49] *N*-(Hydroxypentanyl)-*cis*-5-norbornene-*exo*-2,3-dicarboximide (0.623 g, 2.5 mmol), 5-hexynoic acid (0.28 g, 2.5 mmol) and *N*, *N*′-dicyclohexylcarbodiimide (DCC) (0.62 g, 3.0 mmol) were dissolved in 10 ml DCM, and cooled in an ice bath. 4-dimethylaminopyridine (DMAP) (0.10 g, 0.82 mmol) was then added. The reaction was stirred at 0 °C for 5 min and then allowed to come to room temperature, then stirring overnight. The organic layer was washed with water (2×10 ml) and brine (10 ml) and then dried with $MgSO_4$. The final product was purified with silica gel chromatography to obtain a light yellow oil (0.72 g, 84% yield). ^{1}H NMR (400 MHz, $CDCl_3$): δ and 6.28 (2H, CHCH=CHCH), 4.06 (2H, CH2CH2O), 3.46 (2H, NCH2CH2), 3.27 (2H,

CHCHCH), 2.67 (2H, CHCHCO), 2.17-2.56 (4H, COCH2CH2CH2), 1.98 (1H, CCH), 1.50-1.55 (5H, CH2CH2CH2CH2; CHCH2CH), 1.18-1.45 (10H, norbornene spacer).

NB-PEG2K and NB-PEG 5K. PEG-azide (1 g) and *N*-(Pentynoylhexanyl)-*cis*-5-norbornene-*exo*-2,3-dicarboximide (1 equiv to prepolymer end group) were dissolved in anhydrous N,N-dimethylformamide and purged by bubbling nitrogen through the solution for 30 minutes. Cu(I)Br was then added before adding a 1/9 v/v mixture of pyridine/toluene which was separately purged with nitrogen. The reaction was heated to 50 °C and allowed to proceed overnight. The produce was passed through a basic alumina column to remove copper catalyst, concentrated under reduced pressure, and precipitated in cold diethyl ether to obtain a white powder. The product was dried under vacuum.

NB-PEG2K (0.99 g, 90% yield) ^{1}H NMR (400 MHz, $CDCl_3$): δ 7.50 (1H, C=CHN), 6.29 (2H, CHCH=CHCH), 4.05 (2H, CH_2CH_2CO), 3.50-3.90 (209H $(CH_2CH_2O)_n$), 3.48 (3H, CH_2OCH_3), 1.2-1.7 (3H, $CH_2CH_2CH_2OH$; $CHCH_2CH$).

NB-PEG 5K (0.95 g, 89% yield) ^{1}H NMR (400 MHz, $CDCl_3$): δ 7.50 (1H, C=CHN), 6.29 (2H, CHCH=CHCH), 4.05 (2H, CH_2CH_2CO), 3.50-3.90 (509H $(CH_2CH_2O)_n$), 3.48 (3H, CH_2OCH_3), 1.2-1.7 (3H, $CH_2CH_2CH_2OH$; $CHCH_2CH$).

Norbornene-functionalized chain-transfer agent (NB-CTA), *N*-(Pentynoyl-2-(dodecylthiocarbonothioylthio)-2-methylpropanyl)-*cis*-5-norbornene -*exo*-2,3-dicarboximide(2)

4-(2-hydroxyethyl)-10-oxa-4-azatricyclo[5.2.1.02,6]dec-8-ene-3,5-dione (1.43 g, 6.85 mmol), 2-(dodecylthiocarbonothioylthio)-2-methylpropionic acid (2.50 g, 6.85 mmol),

and N,N'-dicyclohexylcarbodiimide (1.61 g, 7.82 mmol) were dissolved in anhydrous dichloromethane (60 ml) and allowed to stir at 0 °C for thirty minutes. A solution of 4-dimethylaminopyridine in anhydrous DCM (5 mL 0.65 mmol,) was added dropwise. The reaction was stirred at 0 °C for five minutes and then allowed to come to room temperature while stirring overnight. The product was concentrated under reduced pressure and recrystallized in ethyl acetate/hexanes (1:4) solvent mixture. Crystals were collected by vacuum filtration dried under vacuum (1.57g, 40% yield). ^{1}H NMR (400MHz, $CDCl_3$, ppm) δ 6.52 (2H, CHC<u>H</u>=C<u>H</u>CH), 5.29 (2H, CHC<u>H</u>OCH), 4.22 (2H, $CH_2C\underline{H}_2O$), 3.77 (2H, $NC\underline{H}_2CH_2$), 3.2 (2H, $SC\underline{H}_2(CH_2)_{10}$), 2.89 (2H, CHC<u>H</u>CCH), 1.66 (6H, $C(C\underline{H}_3)_2$), 1.29 (20H, $CH_2(C\underline{H}_2)_{10}CH_3$), 0.90 (3H, $CH_2C\underline{H}_3$).

Synthesis of NB-PS macromonomers. NB-PS6K and NB-PS3K were prepared via reversible-addition fragmentation chain transfer (RAFT) polymerization. For the synthesis of NB-PS6K, styrene (4.84 g, 46.50 mmol), NB-CTA (101.40 mg, 0.182 mmol), and AIBN (3.40 mg, 1.82×10^{-2} mmol) were mixed in a 100 mL RBF, and the solution was purged by bubbling the nitrogen through the solution for 30 minutes. The polymerization was initiated by raising the temperature to 60 °C. After 11 h, the reaction flask was removed from heat and the polymer was recovered by precipitation in methanol. For the synthesis of NB-PS3K, styrene (23.62 g, 227.1 mmol), NB-CTA (0.53 g, 0.92 mmol), and AIBN (0.197 mg, 1.2×10^{-3} mmol) were mixed in a 100 mL RBF, and the solution was purged by bubbling the nitrogen through the solution for 30 minutes. The polymerization was initiated by raising the temperature to 50 °C. After 5days, the reaction flask was removed from heat, quenched by immersing in liquid N_2 and the polymer was recovered by precipitation in methanol

NB-PS6K: (0.75 g, 67.0% yield, based on the conversion of styrene) ^{1}H NMR (400MHz, $CDCl_3$, ppm): δ 6.30-7.25 (317H, styrenyl protons), 6.45 (2H, CHC<u>H</u>=C<u>H</u>CH) 5.20 (2H, CHCOC<u>H</u>CH), 3.62 (2H, CH_2CH_2O), 3.49(2H, $NC\underline{H}_2CH_2$), 3.25 (2H, $SC\underline{H}_2(CH_2)_{10}$), 2.78 (2H, CHC<u>H</u>CCH), 1.52 (6H, $C(C\underline{H}_3)_2$), 1.15-2.15 (127H, PS chain backbone protons), 1.26 (20H, $CH_2(C\underline{H}_2)_{10}CH_3$),0.88 (3H, $CH_2C\underline{H}_3$).

NB-PS3K: (1.68 g, 61.0% yield, based on the conversion of styrene,) ^{1}H NMR (400MHz, CDCl3, ppm): δ 6.30-7.25 (163H, styrenyl protons), 6.45 (2H, CHC<u>H</u>=C<u>H</u>CH) 5.20 (2H, CHCOC<u>H</u>CH), 3.62 (2H, CH_2CH_2O), 3.49(2H, $NC\underline{H}_2CH_2$), 3.25 (2H, $SC\underline{H}_2(CH_2)_{10}$), 2.78 (2H, CHC<u>H</u>CCH), 1.52 (6H, $C(C\underline{H}_3)_2$), 1.15-2.15 (65H, PS chain backbone protons), 1.26 (20H, $CH_2(C\underline{H}_2)_{10}CH_3$),0.88 (3H, $CH_2C\underline{H}_3$).

Synthesis of mixed bottlebrush polymers through ROMP MBBPs were prepared by ROMP using $(H_2IMes)(pyr)_2(Cl)_2RuCHPh$. The macromonomers were added to a dry, 25 mL round bottom flask charged with a stir bar. The flask was then degassed with three pump-purge cycles, and the desired amount of degassed, anhydrous THF (total macromonomer concentration was 0.02-0.05 M) was added. $(H_2IMes)(pyr)_2(Cl)_2RuCHPh$ was dissolved in degassed, anhydrous THF in a separate flask. The catalyst solution was transferred to the reaction flask containing macromonomers via cannula to initiate the polymerization and stirred at room temperature for at least 1 hour. The reaction was quenched by addition of ethyl vinyl ether after completion. The product was collected by precipitation in methanol or diethyl ether and dried under vacuum.

P(NB-PS6K-*m*-NB-PEG5K): (precipitate in methanol, 93% yield, based on the ROMP conversion) M_w (GPC): 307 kg/mol, d*n*/d*c* = 0.0880, PDI = 1.13, DP (NMR) = 51.

^{1}H NMR (400 MHz, $CDCl_3$), δ (ppm): 6.36-7.50 (7630 H; styrenyl protons), 4.95 -5.90 (102 H; -C<u>H</u>=C<u>H</u>-), 3.4-3.89 (12852 H, grafted PEG chain backbone protons), 1.15-2.15 (1H; grafted PS chain backbone protons).

P(NB-PS6K-*m*-NB-PEG2K): (precipitate in methanol, 90% yield, based on the ROMP conversion) M_w (GPC): 302 kg/mol, d*n*/d*c* = 0.0880, PDI = 1.17, DP (NMR) = 69. ^{1}H NMR (400 MHz, $CDCl_3$), δ (ppm): 6.36-7.50 (10324 H; styrenyl protons), 4.95 -5.90 (138 H; -C<u>H</u>=C<u>H</u>-), 3.4-3.89 (7970 H, grafted PEG chain backbone protons), 1.15-2.15 (6194 H; grafted PS chain backbone protons).

P(NB-PS3K-*m*-NB-PEG2K)-1: (precipitate in diethyl ether, 84% yield, based on the ROMP conversion) M_w (GPC): 165 kg/mol, d*n*/d*c* = 0.0870, PDI = 1.22, DP (NMR) = 58. ^{1}H NMR (400 MHz, $CDCl_3$), δ (ppm): 6.36-7.50 (4871 H; styrenyl protons), 4.95 -5.90 (116 H; -C<u>H</u>=C<u>H</u>-), 3.4-3.89 (6457 H, grafted PEG chain backbone protons), 1.15-2.15 (2923 H; grafted PS chain backbone protons).

P(NB-PS3K-*m*-NB-PEG2K)-2: (precipitate in methanol, 87% yield, based on the ROMP conversion)M_w (GPC): 302 kg/mol, d*n*/d*c* = 0.134, PDI = 1.38, DP (NMR) = 30. ^{1}H NMR (400 MHz, $CDCl_3$), δ (ppm): 6.36-7.50 (3080 H; styrenyl protons), 4.95 -5.90 (60 H; -C<u>H</u>=C<u>H</u>-), 3.4-3.89 (2614 H, grafted PEG chain backbone protons), 1.15-2.15 (1848 H; grafted PS chain backbone protons).

P(NB-PS3K-*m*-NB-PEG5K): (precipitate in diethyl ether, 89% yield, based on the ROMP conversion) M_w (GPC): 132 kg/mol, d*n*/d*c* = 0.0813, PDI = 1.15, DP (NMR) = 29. ^{1}H NMR (400 MHz, $CDCl_3$), δ (ppm): 6.36-7.50 (2495 H; styrenyl protons), 4.95 -5.90 (58 H; -C<u>H</u>=C<u>H</u>-), 3.4-3.89 (13920 H, grafted PEG chain backbone protons), 1.15-2.15 (1497 H; grated PS chain backbone protons).

P(NB-PS6K): (precipitate in methanol, 91% yield, based on the ROMP conversion) M_w (GPC): 207 kg/mol, d*n*/d*c* = 0.158, PDI = 1.79, DP (NMR) = 33. ^{1}H NMR (400 MHz, $CDCl_3$), δ (ppm): 6.36-7.50 (10461 H; styrenyl protons), 4.95 -5.90 (66 H; -C<u>H</u>=C<u>H</u>-), 1.15-2.15 (4191H; grafted PS chain backbone protons).

P(NB-PS3K): (precipitate in methanol, 90% yield, based on the ROMP conversion) M_w (GPC): 207 kg/mol, d*n*/d*c* = 0.150, PDI = 107, DP (NMR) = 21. ^{1}H NMR (400 MHz, $CDCl_3$), δ (ppm): 6.36-7.50 (3423 H; styrenyl protons), 4.95 -5.90 (42 H; -C<u>H</u>=C<u>H</u>-), 1.15-2.15 (1365H; grafted PS chain backbone protons).

P(NB-PEG5K): (precipitate in diethyl ether 90% yield) M_w (GPC): 59.6 kg/mol, d*n*/d*c* = 0.030, PDI = 1.07, DP (NMR) = 35. ^{1}H NMR (400 MHz, $CDCl_3$), δ (ppm): 4.95 -5.90 (70H; -C<u>H</u>=C<u>H</u>-), 3.4-3.89 (17815 H, grafted PEG chain backbone protons).

P(NB-PEG2K): (precipitate in diethyl ether, 86% yield) M_w (GPC): 59.6 kg/mol, d*n*/d*c* = 0.030, PDI = 1.07, DP (NMR) = 25. ^{1}H NMR (400 MHz, $CDCl_3$), δ (ppm): 4.95 -5.90 (50 H; -C<u>H</u>=C<u>H</u>-), 3.4-3.89 (5500 H, grafted PEG chain backbone protons)

2.3.2 Instruments

Gel-Permeation Chromatography (GPC) Molecular weights and polydispersities were obtained using an Agilent 1200 module equipped with three PSS SDV columns in series (100, 1000, and 10000 Å pore sizes), an Agilent variable wavelength UV/VIS detector, a Wyatt Technology HELEOS II multi-angle laser light scattering (MALLS) detector (λ = 658 nm), and a Wyatt Technology Optilab reX RI detector. This system enables SEC with simultaneous refractive index (SEC-RI), UV/VIS (SEC-UV/VIS), and

MALLS detection. THF was used as the mobile phase at a flow rate of 1 mL/min at 40 ^{o}C.

Nuclear Magnetic Resonance Spectroscopy (NMR) Hydrogen NMR (^{1}H NMR) spectra were recorded using tetramethylsilane as internal standard in $CDCl_3$ on a 400 MHz Bruker multi-nuclear spectrometer. Samples were placed in 5 mm o.d. tubes with the concentration of 20 mg/ml.

AFM Atomic force microscopy (AFM) images were obtained with a nanoscope V scanning probe controller (Digital Instruments, Veeco Mtrology Group) in tapping mode in air at room temperature using silicon tips (resonance frequency = 270-330 kHz, and tip radius of curvature < 10 nm).

Contact Angle Measurements Static contact angle measurements of DI water on MBBPs thin films were carried out using a CAM 200 optical contact angle meter (KSV instruments, Monroe, CT) at ambient conditions. Water contact angles were measured after letting the water droplet equilibrate on the surface for 180s. Measurements were repeated three times, and differences between the measurements were found to be less than 1.3^{o} for all surfaces (see Figure S8 as an example).

XPS X-ray photoelectron spectroscopy (XPS, PHI Quantera SXM) was performed using monochromatic aluminum Kα X-rays. The incident angle of the beam to the sample is 45°. XPS data were analyzed with the MultiPak software. The samples were prepared by spin-casting solutions onto freshly cleaned silica wafers.

Grazing-Incidence Small-Angle X-ray Scattering (GISAXS). GISAXS measurements were carried out on the undulator-based beamline X9 at the National

Synchrotron Light Source at Brookhaven National Laboratory. The monochromator was adjusted to select a photon energy of 14 keV (wavelength 0.886 nm). A Kirkpatrick-Biaz mirror system was used to focus the beam at the sample position (approximately 100 μm wide by 60 μm tall). Samples were measured under vacuum (~40 Pa), and the instrument was calibrated using a silver behenate powder as a standard. Data processing was carried out using a Python script developed on the X9 beamline. All measurements were carried out at an incident angle of 0.15°, which was measured by reflectivity to be above the critical angle. All films were measured on ITO substrates.

2.3.3 The preparation and solvent treatment of MBBPs films on ITO glass

ITO glass substrates were immersed and sonicated for 60 minutes in each of the following solvents: 2% solution of basic cleaning solution Hellmanex in DI water, pure DI water, and isopropyl alcohol. The substrates were dried by under stream of compressed air and then under vacuum. Next, a MBBPs solution in chloroform (20 mg/ml) was prepared by stirring for 30 minutes before filtering using a 0.45 mm syringe filter. The filtered solution was then spin-cast onto the freshly cleaned ITO surfaces at a spin rate of 1500 rpm and spinning time of 60s. For solvent treatment, freshly prepared MBBPs film samples were dried under vacuum for 30 min and then placed in a sealed chamber with either methanol or cyclohexane under reduced pressure (-10 mm Hg) and at room temperature overnight. After solvent-treatment, samples were removed from the sealed chamber and immediately dried under a flow of nitrogen before placing the film samples under vacuum overnight to remove residual solvents before testing.

2.4 Results and discussions

2.4.1 Synthesis of bottlebrush polymers

Mixed bottlebrush polymers were prepared via "grafting-through" synthetic approach that relies on ROMP of ω-norbornenyl macromonomers using a highly-active, 3rd generation Grubb's catalyst. This approach ensures that each repeat unit has a side-chain attached and can be used to prepare bottlebrush polymers with controlled side-chain and backbone length as well as low polydispersity.[46,49] PEG macromonomers were prepared by coupling azide-terminated PEG (purchased from Nanocs) to alkynyl terminated *exo*-norbornene though a copper-catalyzed azide-alkyne "click" coupling reaction (Figure 2.2, top). PS macromonomers were prepared via reversible addition-fragmentation chain transfer (RAFT) from a *exo*-norbornene-functionalized chain-transfer agent (CTA) (Figure 2.2, bottom). Two different molecular weights for each macromonomer (summarized in Table 2.1) were prepared and used in the synthesis of bottlebrush polymers.

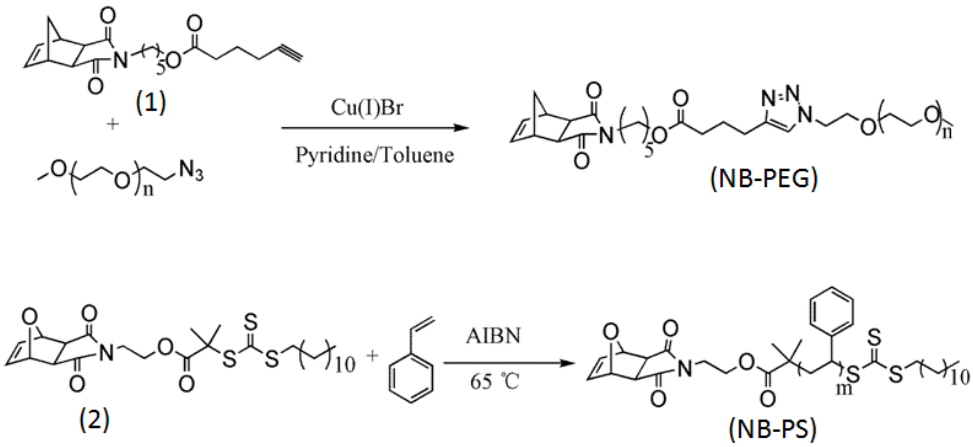

Figure 2.2 Synthetic scheme for the preparation of ω-norbornenyl poly(ethylene glycol) (NB-PEG) (top) and polystyrene (NB-PS) (bottom) macromonomers.

^{1}H NMR provides evidence of quantitative end-group control for both macromonomers. In the case of NB-PEG5K (Figure 2.3, top), protons corresponding to the terminal norbornene as well as the proton on the triazole ring are clearly resolved by ^{1}H NMR. NB-PEG2K shows similar features. For the polystyrene macromonomer NB-PS6K (Figure 2.3, bottom), peaks corresponding to the norbornene end group and the trithiocarbonate functionality are clearly resolved by ^{1}H NMR, and similar features are observed for NB-PS3K. Calculation of polymer molecular weights using ^{1}H NMR integrated intensities are in good agreement with the estimate provided by GPC for all polymers, indicating good control over the polymer end group. The polydispersity (PDI) of all macromonomers is less than 1.2 (Table 2.1).

Table 2.1 Characteristics of norbornene-functionalized macromonomers

Macromonomer[a]	Polymer	$M_{w,\,GPC}$[b] (kg/mol)	DP_{GPC}[c]	DP_{NMR}[d]	PDI[b]
NB-PS3K	Polystyrene	3400	28	34	1.18
NB-PS6K	Polystyrene	6600	55	61	1.14
NB-PEG2K	Poly(ethylene glycol)	2300	48	55	1.09
NB-PEG5K	Poly(ethylene glycol)	5600	125	120	1.02

[a]The sample name reflects the type and molecular weight of the polymer. [b]Measured by GPC relative to monodisperse PS standards. [c] Number-averaged degree of polymerization (DP) calculated based on the GPC estimate of $M_n = M_w$/PDI. [d]The NMR estimate for DP is calculated by comparing the integrated intensity for H in the polymer backbone to that for H in the norbornene endgroup.

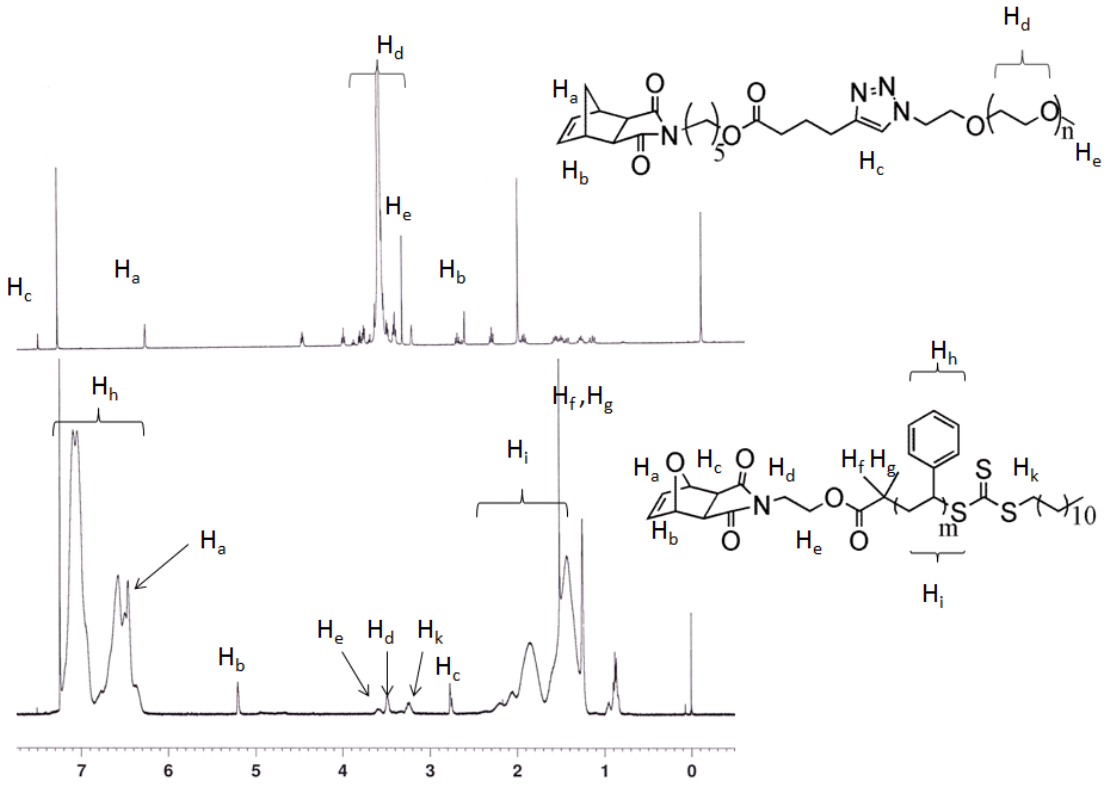

Figure 2.3. ^{1}H NMR spectrum for macromonomers NB-PEG5K (top) and NB-PS6K (bottom).

MBBPs were synthesized via ROMP of ω-norbornenyl macromonomers (Figure 2.4). GPC with refractive index (RI) and multi-angle laser light scattering (MALLS) detection was used to monitor the reaction and provide a quantitative measure of conversion and bottlebrush polymer molecular weight and polydispersity (see Figure 2.5). ^{1}H NMR was used to monitor the conversion of the *exo*-norbornene end group to a poly(norbornene) or poly(oxanorbornene) backbone. The content of PS and PEG side-chains in the MBBPs is determined by comparing the ^{1}H NMR integrated intensities corresponding to each side-chain. The initial molar ratio of PS to PEG macromonomers was 1:1 for all MBBPs except for P(NB-PS3K-*m*-NB-PEG2K)-2, for which the initial

ratio was 2:1. This latter sample was prepared due to the difficultly in extracting a reliable water contact angle for P(NB-PS3K-*m*-NB-PEG2K)-1 films, as described below.

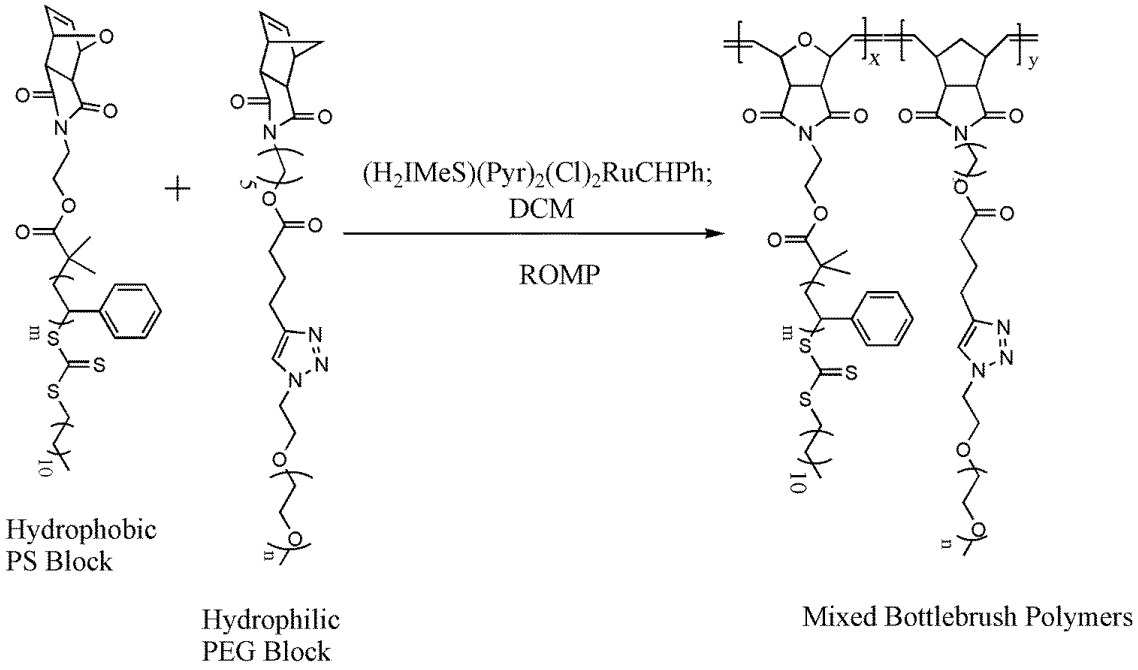

Figure 2.4 Mixed bottlebrush polymers (MBBPs) are prepared via ROMP of NB-PS and NB-PEG macromonomers, resulting in bottlebrush polymers with mixed hydrophobic and hydrophilic side chains.

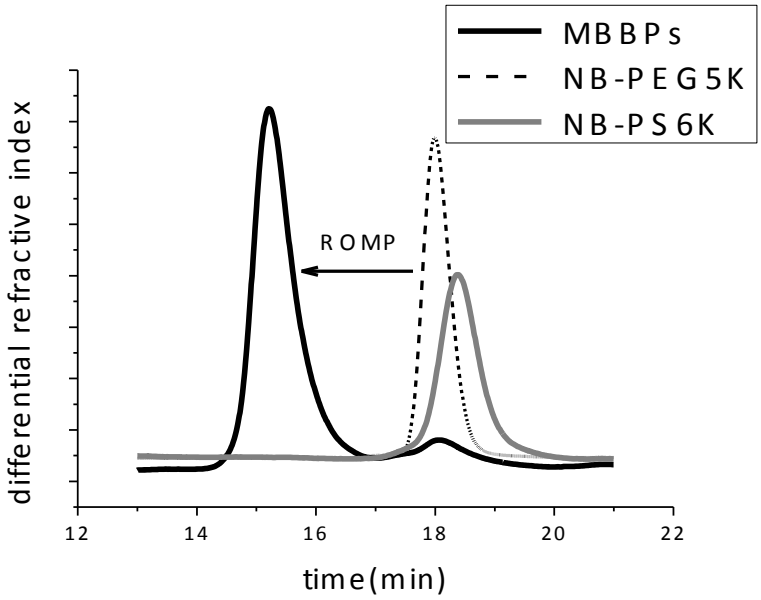

Figure 2.5 GPC traces for MBBPs P(PS6K-*m*-PEG5K) (black line) and corresponding NB-PS6K (gray line) and NB-PEG5K (dashed line) macromonomers.

The GPC shows a clear shift in the molecular weight after ROMP as well as some residual (< 5 wt %) macromonomer.

Table 2.2 Characteristics of bottlebrush polymers prepared for this study

Samples[a]	M_W[b] (kg/mol)	DP $_{GPC}$	PDI	Conversion[c]	PEG Content[d] (mol %)	PEG Content[d] (mass %)
P(NB-PS6K-*m*-NB-PEG5K)	307	51	1.13	95	52.5	48.0
P(NB-PS6K-*m*-NB-PEG2K)	302	67	1.17	93	52.5	30.0
P(NB-PS3K-*m*-NB-PEG2K)-1	165	66	1.22	91	50.6	41.7
P(NB-PS3K-*m*-NB-PEG2K)-2	93.2	35	1.38	94	39.6	30.4
P(NB-PS3K-*m*-NB-PEG5K)	132	33	1.15	97	50.6	63.1
P(NB-PS6K)	207	35	1.79	96	0.00	0.00
P(NB-PS3K)	68.7	20	1.02	96	0.00	0.00
P(NB-PEG2K)	59.6	30	1.07	93	100	100
P(NB-PEG5K)	195	35	1.11	90	100	100

[a] The sample name reflects the molecular weight and type of side-chains in the MBBPs. All samples that involve two different side-chains are mixed bottlebrush polymers with a molar ratio of 1:1, except for PS3K-PEG2K-2:1 which was prepared with a 2:1 molar ratio of PS3K to PEG2K; [b] M_w are determined by GPC with MALLS analysis; [c] Conversion of the

macromonomers after ROMP polymerization are calculated using GPC with RI detection by comparing the peak area of MBBPs to the peak area of residual macromonomers. [d] The final ratio of PEG to PS is calculated by comparing the ^{1}H NMR integrated intensities corresponding to each side-chain.

As demonstrated in Table 2.2, the ROMP-based "grafting-through" approach is effective for preparing a series of well-defined MBBPs with systematically varying side-chain lengths and composition. In a typical polymerization reaction, conversion of the macromonomers was > 90%. The MBBPs have backbone DPs ranging from 30 - 60 (corresponding to total molecular weights of 100 - 300 kg/mol) and relatively low polydispersities (approximately 1.2 or lower) for most samples prepared. Finally, ^{1}H NMR indicates complete conversion of the *exo*-norbornene functionality to a poly(norbornene) or poly(oxanorbornene) backbone and proves incorporation of both PS and PEG side-chains into the bottlebrush polymers.

2.4.2 Preparation bottlebrush polymer thin films

Bottlebrush polymer thin films can be prepared by spin-casting a dilute solution of MBBPs onto a clean indium tin oxide (ITO) surface. ITO was used for all measurements due to problems with film dewetting on silica wafer, as has been previously reported for PS films[54]. Smooth films can be achieved by spin-casting a sufficiently thick (100 nm or greater) polymer film. The film thickness and surface coverage depends on the concentration used for spin-coating; for this study, all films are spin-cast at 1500 rpm/sec for 30s and then at 500 rpm/sec for an additional 30s. Spin-casting a 20 mg/mL solution of MBBPs in chloroform results in a smooth film with complete surface coverage (Figure

2.6). MBBPs films appear uniform by visual inspection and under optical microscopy, and AFM indicates that the surface roughness is approximately 5 nm (Figure 10). On the other hand, when a dilute (1 mg/ml) chloroform solution is used, surface coverage is incomplete and individual polymers can be imaged by AFM (Figure 2.6b, right). The bottlebrush polymers are cylindrical in shape with a length of 40 – 50 nm. Recent results show that the backbone can be extended fully with the l_m approximate of 0.25nm[5], and the backbone length is independent of the side chain length. Assuming the -CH_2-CH_2- bond of the 5-carbone polynorbornene backbone repeat unit is fully stretched, and the length is 0.25 nm[5], from GPC data, the backbone DP is 51, therefore the calculating backbone length is 63.75 nm. If assuming the MBBPs are Gaussian polymers, the backbone length is proportional to the root of the above calculated value: 7.984 nm. Uniform MBBPs films exposed to methanol and/or cyclohexane vapor in a sealed annealing chamber showed no significant changes to film uniformity after solvent treatment. AFM analysis of surfaces before and after solvent treatment (see Figure 2.10) indicates that film roughness increases slightly (from 5 nm to 10 nm) for both methanol and cyclohexane vapor treatments. No micro-phase separated structure was observed in any MBBPs film, in contrast to what has been observed in some mixed polymer brush films.[55,56] This may be due to the film thickness chosen or the relatively short length of the side-chains in the MBBPs studied. And GISAXS data (Figure 2.11) are also consistent with AFM images, no phase separation were founded for our samples.

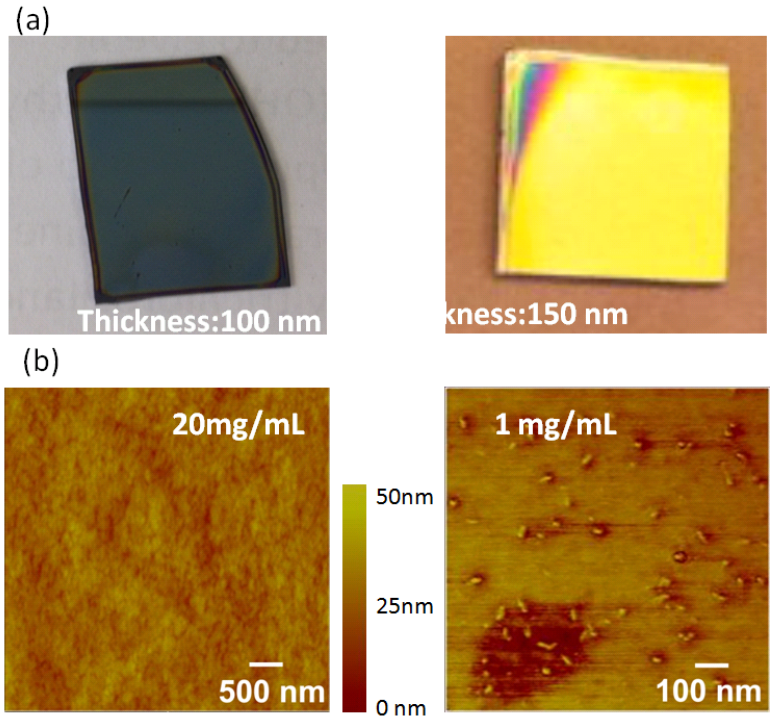

Figure 2.6 Representative images of P(NB-PS6K-*m*-NB-PEG5K) films on silicon (a) and AFM height images for two different spin-casting concentrations (b).

The images in (a) show that uniform films can be prepared on a surface by spin-casting, and the surfaces are approximately 2 cm across. Films shown in were prepared on silicon to allow for visualization from a reflective surface. Film thicknesses are measured by AFM. AFM images (b) show a film with uniform coverage when a 20 mg/ml solution is used, but at lower MBBPs concentrations (1 mg/ml) surface coverage is incomplete and individual polymers can be resolved.

2.4.3 Stimuli-responsive behaviors of bottlebrush polymer thin films

Bottlebrush polymer thin films are prepared by spin-casting a solution of bottlebrush polymer in a good solvent (chloroform) for both side chains. Subsequent treatment by selective solvents may preferentially swell either the PEG or PS side-chains, leading to a measureable change in the surface composition and water contact angle. This responsiveness with solvent treatment may also depend on the length of the side-chains. Solvent-dependent stimuli-responsive properties have been reported for polymer brush films[24-28] but not for bottlebrush polymer films.

Bottlebrush polymer films were prepared on clean ITO-coated glass from a 20 mg/mL solution in chloroform. For comparison to MBBPs films, contact angles were also measured for ITO-coated glass, NB-PS6K and NB-PEG2K macromonomers, and P(NB-PS6K) and P(NB-PEG2K) bottlebrush polymers (Figure 2.7 and Table 2.3). Clean ITO is a very hydrophilic surface on which water completely wets the surface. The water contact angles are higher for polymeric thin film coatings, and the water-contact angles were significantly higher for bottlebrush polymer films compared with corresponding macromonomer films (Table 2.3). NB-PEG2K has a water contact angle of 35°, and P(NB-PEG2K) films have a much higher contact angle (around 80°). As expected, NB-PS6K macromonomer films have a larger contact angle than NB-PEG2K films, with a contact angle of approximately 90°, and P(NB-PS6K) films have a larger contact angle of 102°. MBBPs films have water contact angles that range between those for the macromonomers and bottlebrush polymers, although all have a contact angle greater than 60°. The contact angles measured for bottlebrush polymer and mixed bottlebrush polymer films are consistent with previous measurements on PS and PEG brush films. A variety of polystyrene brush films have been reported with advancing contact angles in

the range of 90° -100°. [28,57-59] A broader range of values has been reported for PEG brushes and self-assembled monolayers (SAMs). PEG brush films have contact angles reported ranging from 30° - 70°, [60] depending on the surface coverage, PEG length, and preparation method.[61-63] SAMs of oligo-ethylene glycol show a contact angle of roughly 68°,[64] while star-shaped PEG surfaces show a contact angle of 64°.[65]

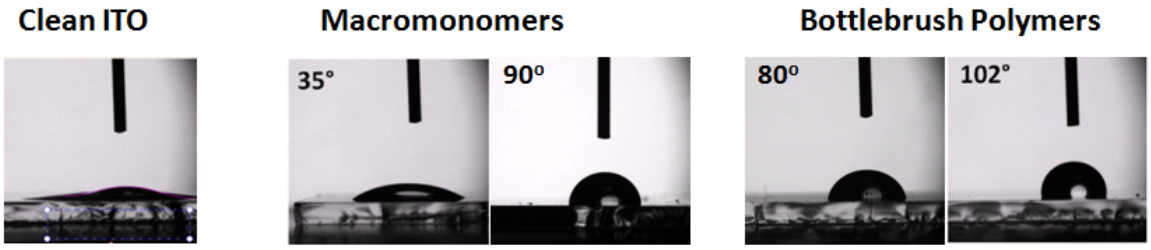

Figure 2.7 Micrographs of water droplets on clean ITO and polymer-coated ITO surfaces.

From left to right: clean ITO, NB-PEG2K, NB-PS6K, P(NB-PEG2K), and P(NB-PS6K). Clean ITO and NB-PEG films are hydrophilic, but all other polymeric films are more hydrophobic.

Table 2.3 Water contact angles for as-cast polymer films

Polymer Sample	Polymer Type	Contact Angle (degrees)	Methanol-treated (degrees)	Cyclohexane-treated (degrees)
Blank ITO	=	= (fully spread)	--	--
NB-PEG2K	Mms[a]	35.0±0.5	--	--
NB-PS6K	Mms	90.4±0.2	--	--
P(NB-PEG2K)	BB[b]	79.5±0.7	--	--
P(NB-PS6K)	BB	102±0.3	--	--
P(NB-PS6K-*m*-NB-PEG5K)	MBB[c]	69.6±0.4	63.8±0.8	72.5±0.6
P(NB-PS6K-*m*-NB-PEG2K)	MBB	73.0±0.6	71.1±0.4	74.8±0.3
P(NB-PS3K-*m*-NB-PEG2K)-1	MBB	69.3±0.7	=	=
P(NB-PS3K-*m*-NB-PEG2K)-2	MBB	75.4±0.3	72.0±0.6	77.0±0.5
P(NB-PS3K-*m*-NB-PEG5K)	MBB	53.6±0.3	46.8±1.3	58.3±0.7

[a] Mms represents macromonomers; [b] BB represents bottlebrush polymers; [c] represents mixed bottlebrush polymers

To test the conformational flexibility of the side-chains, bottlebrush polymer films were exposed to a selective solvent (methanol or cyclohexane) and subsequently dried under vacuum overnight before measurement. Cyclohexane is a theta solvent for PS (at 34.5 °C) but a poor solvent for PEG, and treatment with cyclohexane vapor is thus expected to result in selective swelling and enrichment of NB-PS chains at the air-film interface. Methanol, on the other hand, is a good solvent for PEG but poor solvent for PS, and therefore treatment with methanol vapor is expected to result in swelling and enrichment of NB-PEG side-chains at the air-film surface. This is shown schematically in Figure 2.1, where treatment with a selective solvent results in a change in side-chain conformation and surface wettability.

The measured water contact angles changed for all MBBPs films with solvent treatment, with methanol-treated surfaces exhibiting a decrease in contact angle and cylcohexane-treated surface exhibiting an increase in contact angle relative to as-cast films (Table 2.3 and Figure 2.8). Furthermore, MBBPs with longer PEG side-chains

exhibit larger contact angle changes. For example, for P(NB-PS6K-*m*-NB-PEG5K) films have a contact angle of approximately 69.6° as-cast, and the contact angle increases by approximately 2.9° after cyclohexane vapor treatment but decreases by 5.8° after methanol vapor treatment. A larger change is seen for P(NB-PS3K-*m*-NB-PEG5K) with 6.8° and 4.7° contact angle changes with methanol and cyclohexane treatment, respectively. By comparison, MBBPs films with 3K NB-PS side-chains showed a maximum change of only 3.4° for methanol and cyclohexane treatment. The water contact angle for P(NB-PS6K-*m*-NB-PEG2K) films changed by less than 2° with methanol and cyclohexane treatments. The relatively small change in contact angle for bottlebrush polymers with short PS side-chains may be due to the reduced flexibility of PS chains compared with PEG side-chains. Contact angle data is not available for P(NB-PS3K-*m*-NB-PEG2K)-1 since the films were unstable to solvent treatment. Instead, MBBPs films with the same side-chains but a 2:1 ratio of NB-PS3K and NB-PEG2K side-chains were studied (P(NB-PS3K-*m*-NB-PEG2K)-2). These films show similar contact angles and solvent responsiveness as P(NB-PS6K-*m*-NB-PEG2K), which might be expected due to the similar overall content of NB-PS and NB-PEG side-chains in both MBBPs.

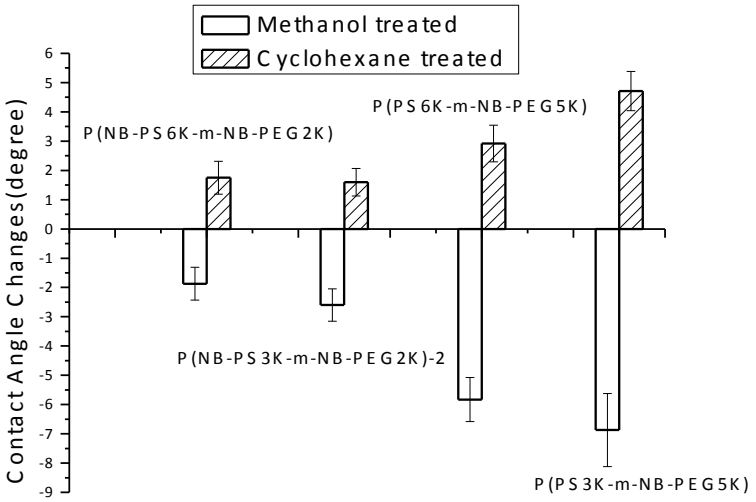

Figure 2.8 Changes in water contact angles for MBBPs films exposed to either methanol or cyclohexane vapors.

The contact angle measurements indicate that MBBPs films show stimuli-responsive behavior. For the materials studied, greater contact angle changes were detected for MBBPs with longer PEG side-chains. This indicates that conformational flexibility of the side-chains is important for the responsiveness of the films and that, for the MBBPs in the present study, the conformational flexibility of the hydrophilic side-chain plays a more significant role in water contact angle changes.

XPS was used to quantify the chemical composition of the top MBBPs film surface. Films were prepared on clean ITO coated glass substrates, and measurements were carried out an incidence angle of 45°. At this incidence angle, XPS measures the composition of roughly the top 5-10 nm of the polymer film and can provide direct evidence for changing composition near the top film surface, as shown in Figure 2.9 for

P(NB-PS6K-*m*-NB-PEG5K) MBBPs films. For the as-cast P(NB-PS6K-*m*-NB-PEG5K) MBBPs film, the molar ratio of carbon to oxygen (C/O) on the surface is 8.5. The ratio increases to 13.3 after treatment with cyclohexane vapor but decreases to 6.5 after methanol vapor treatment. This indicates that solvent treatment does indeed change the composition of the MBBPs film at the film-air interface resulting in a greater NB-PS content after cyclohexane treatment and a greater NB-PEG content after methanol treatment, consistent with contact angle measurements.

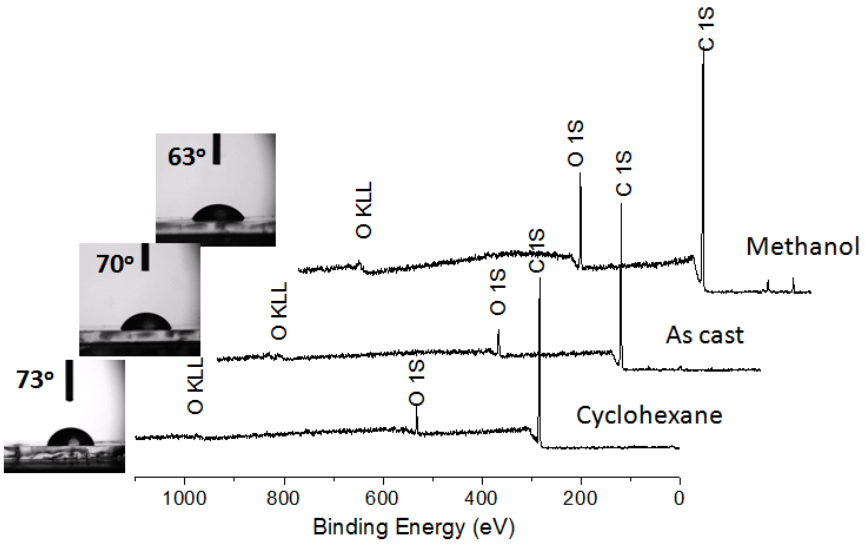

Figure 2.9 XPS spectra and corresponding contact angle images for P(NB-PS6K-m-NB-PEG5K) MBBPs films before and after solvent treatments.

As shown in Table 2.4, the C/O ratio changes with solvent treatment for all MBBPs films and shows trends consistent with those expected from contact angle measurements. All MBBPs films and P(NB-PS6K) and P(NB-PEG2K) bottlebrush polymer films were similarly measured by XPS. For example, a comparison of P(NB-PS6K-*m*-NB-PEG5K) with P(NB-PS6K-*m*-NB-PEG2K) films shows that the former have a lower C/O ratio and

exhibit larger changes in the C/O ratio with solvent treatment. Furthermore, P(NB-PS3K-*m*-NB-PEG5K) films exhibit the lowest C/O ratio for all MBBPs studied, consistent with their relatively low contact angle. P(NB-PS3K-*m*-NB-PEG2K)-2 films show surprisingly large changes in the C/O ratio with solvent vapor treatment, but these MBBPs films still have a larger C/O ratio compared with P(NB-PS3K-*m*-NB-PEG5K) and P(NB-PS6K-*m*-NB-PEG5K) films.

Table 2.4 XPS results of MBBPs or HBBs. The C/O ratio is determined by taking a ratio of the C1s and O1s signals measured by XPS. The value in parentheses shows the percentage change in the C/O ratio relative to the as-cast value.

Sample Polymers	C/O (as-cast)	C/O (methanol-treated)	C/O (cyclohexane-treated)
P(NB-PS6K-*m*-NB-PEG5K)	8.5	6.5 (-24%)	13.3 (+56%)
P(NB-PS6K-*m*-NB-PEG2K)	12.4	11.2 (-12%)	16.2 (+38%)
P(NB-PS3K-*m*-NB-PEG2K)-1	6.4	N/A	N/A
P(NB-PS3K-*m*-NB-PEG2K)-2	9.8	7.3 (-26%)	12.9 (+32%)
P(NB-PS3K-*m*-NB-PEG5K)	6.1	5.3 (-13%)	7.5 (+23%)
P(NB-PS6K)	27.5	N/A	N/A
P(NB-PEG2K)	3.3	N/A	N/A

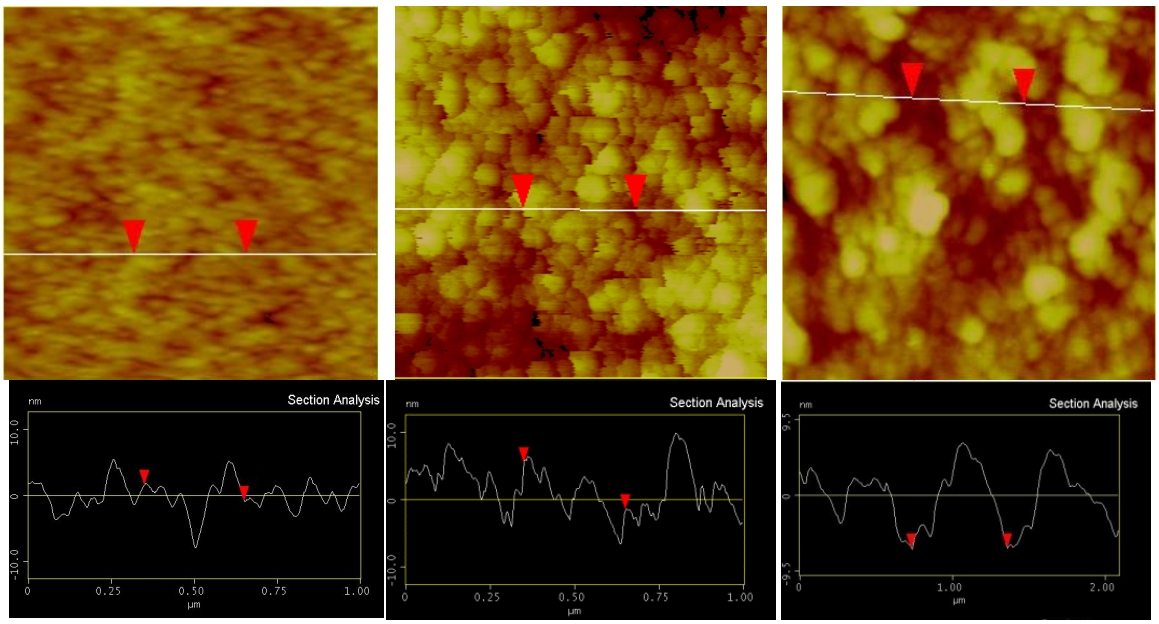

Figure 2.10 AFM roughness of bottlebrush thin films as cast (left); after treated by methanol (middle); and after treated by cyclohexane (right)

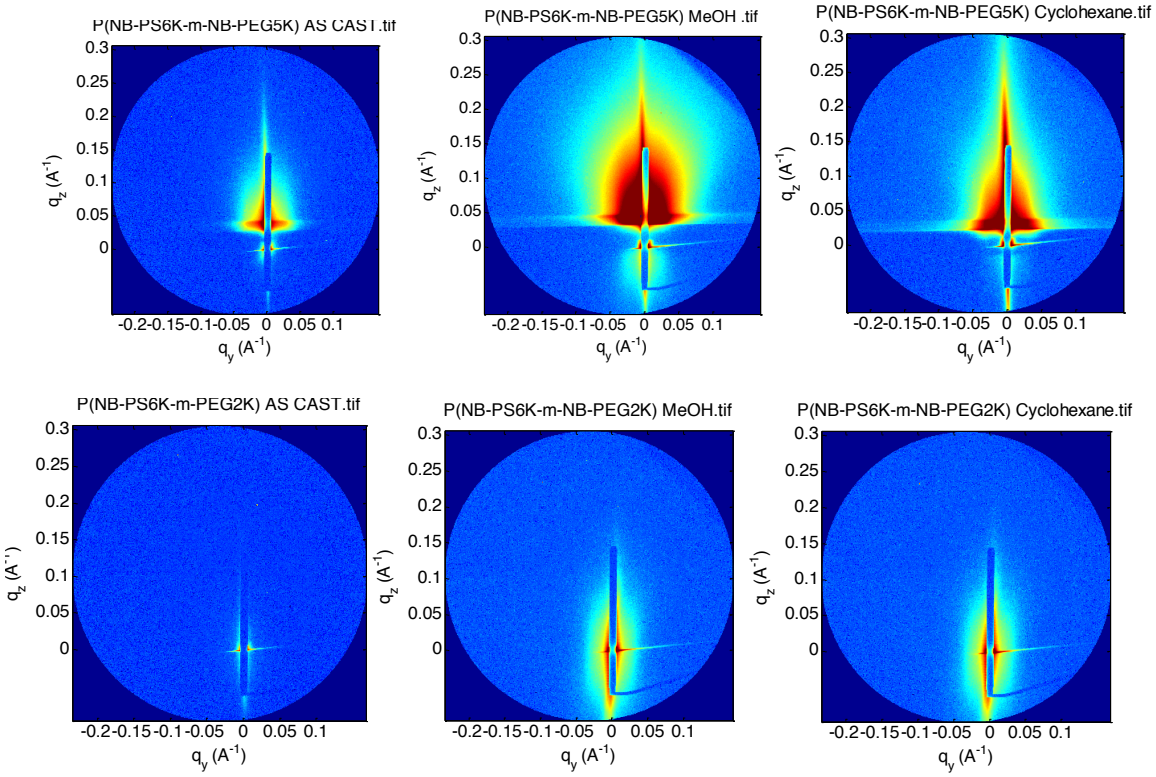

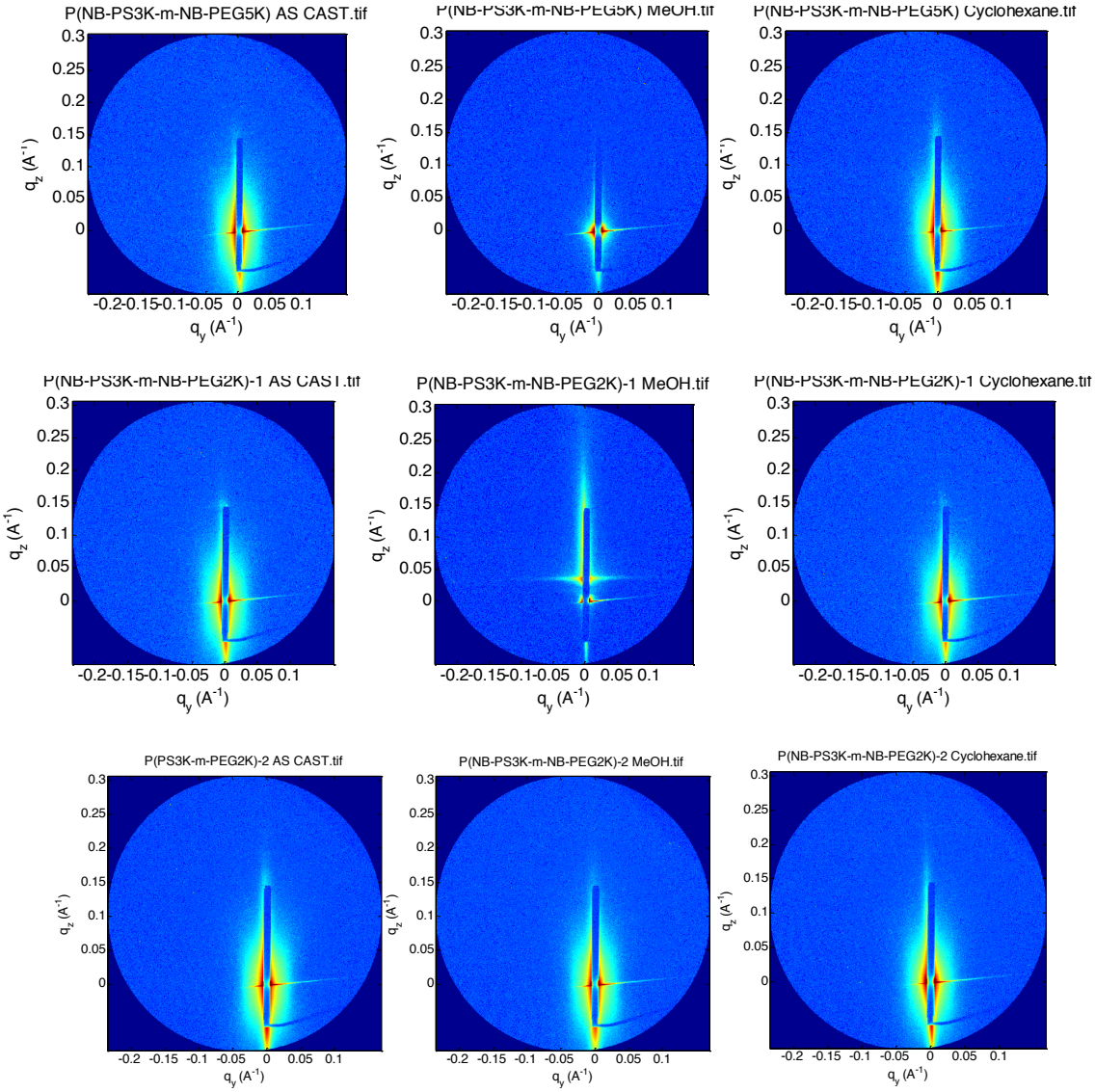

Figure 2.11 2D GISAXS images for 5 mixed bottlebrush polymer films under different conditions. From left to right :as cast films; methanol (MeOH) treated films; Cyclohexane treated films on ITO substrates

2.4.4 Crosslinking and stabilization of bottlebrush polymer thin films

The long-term stability of bottlebrush polymer films is potentially important for applications, for example for the development of non-toxic coatings to inhibit marine

biofouling. The films described above were uncrosslinked and only physically adsorbed to the surface, but chemical crosslinking of MBBPs films is possible using bifunctional benzophenone chromophore bis-3-benzoyl benzoic acid ethylene glycol (Figure 2.12 (c)).[54] To demonstrate film stabilization, P(NB-PS3K-*m*-NB-PEG2K)-1 was dissolved in chloroform (1 wt. %), and the bifunctional, photoactive benzophenone crosslinker was added at a molar ratio of 1:100 relative to P(NB-PS3K-*m*-NB-PEG2K)-1. This MBBPs was chosen since it was the smallest, most soluble, and least stable MBBPs film. The solution was spin-cast onto a clean silicon substrate, and half of the resulting MBBPs film was irradiated by UV light while the other half was protected from exposure using aluminum foil (Figure 2.12 a). After exposure to UV light the film was washed with THF, but only the irradiated portion of the film was remained while the non-irradiated portion dissolved in THF. This indicates that robust MBBPs films can be prepared by addition of a small amount of bifunctional benzophenone chromophore; more detailed studies on the surface properties of crosslinked MBBPs films will be the focus of future work.

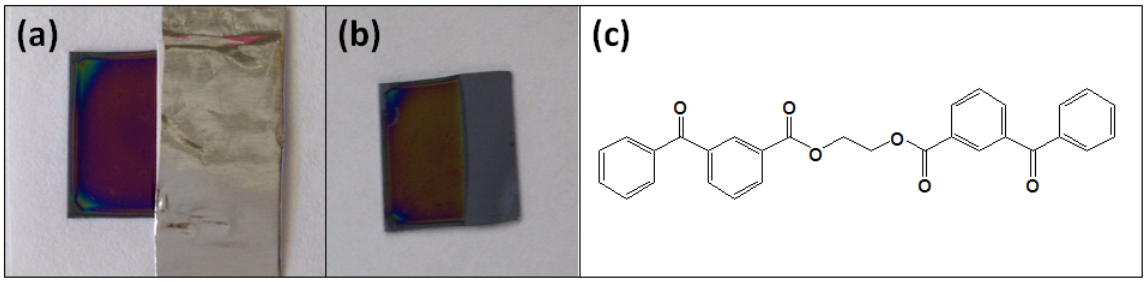

Figure 2.12 Cross-linked films before (a) and after (b) washing with THF, and the chemical structure of the bifunctional benzophenone crosslinker used (c).

Well-defined mixed bottlebrush polymers (MBBPs) with targeted side-chain and backbone molecular weight can be prepared via ROMP of ω-norbornenyl

macromonomers, and polymeric thin films can be prepared by spin-casting a solution of MBBPs onto a surface. Stimuli-responsive surface properties in MBBPs thin films arise due to the conformational flexibility of the polymeric side-chains and are analogous to what has been observed in polymer brush films, in which polymer chains are end-tethered to a surface. Treatment of MBBPs films with methanol vapor results in a more hydrophilic surface, while treatment with cyclohexane vapor results in a more hydrophobic surface, as demonstrated by water contact angle and XPS measurements. The length of the side-chains plays a role in determining contact angle and compositional changes; for the samples studied, MBBPs with longer NB-PEG side-chains exhibited larger contact angle and compositional changes. Additionally, bottlebrush polymer films can be stabilized by addition of a bifunctional benzophenone crosslinker. This work demonstrates that bottlebrush polymers enable the preparation of stimuli-responsive, "brush-like" surface coatings using conventional solution processing methods.

2.5 Bibliography

(1) Fredrickson, G. H. *Macromolecules* **1993**, *26*, 2825.

(2) Hsu, H.-P.; Paul, W.; Binder, K. *Macromol. Symp.* **2007**, *252*, 58.

(3) Rathgeber, S.; Pakula, T.; Wilk, A.; Matyjaszewski, K.; Beers, K. L. *The Journal of Chemical Physics* **2005**, *122*, 124904.

(4) Zhang, B.; Gröhn, F.; Pedersen, J. S.; Fischer, K.; Schmidt, M. *Macromolecules* **2006**, *39*, 8440.

(5) Sheiko, S. S.; Möller, M. *Chem. Rev.* **2001**, *101*, 4099.

(6) Lee, S.; Spencer, N. D. *Science* **2008**, *319*, 575.

(7) Runge, M. B.; Bowden, N. B. *J. Am. Chem. Soc.* **2007**, *129*, 10551.

(8) Johnson, J. A.; Lu, Y. Y.; Burts, A. O.; Xia, Y.; Durrell, A. C.; Tirrell, D. A.; Grubbs, R. H. *Macromolecules* **2010**, *43*, 10326.

(9) Li, Z.; Ma, J.; Cheng, C.; Zhang, K.; Wooley, K. L. *Macromolecules* **2010**, *43*, 1182.

(10) Huang, K.; Rzayev, J. *J. Am. Chem. Soc.* **2009**, *131*, 6880.

(11) Brittain, W. J.; Minko, S. *J. Polym. Sci., Part A: Polym. Chem.* **2007**, *45*, 3505.

(12) Krishnan, S.; Weinman, C. J.; Ober, C. K. *J. Mater. Chem.* **2008**, *18*, 3405.

(13) Rosenhahn, A.; Schilp, S.; Kreuzer, H. J.; Grunze, M. *Phys. Chem. Chem. Phys.* **2010**, *12*, 4275.

(14) Howarter, J. A.; Youngblood, J. P. *Adv. Mater. (Weinheim, Ger.)* **2007**, *19*, 3838.

(15) Chen, T.; Ferris, R.; Zhang, J.; Ducker, R.; Zauscher, S. *Prog. Polym. Sci.* **2010**, *35*, 94.

(16) Stuart, M. A. C.; Huck, W. T. S.; Genzer, J.; Muller, M.; Ober, C.; Stamm, M.; Sukhorukov, G. B.; Szleifer, I.; Tsukruk, V. V.; Urban, M.; Winnik, F.; Zauscher, S.; Luzinov, I.; Minko, S. *Nat. Mater.* **2010**, *9*, 101.

(17) Nath, N.; Chilkoti, A. *Adv. Mater. (Weinheim, Ger.)* **2002**, *14*, 1243.

(18) Alonzo, J.; Chen, J.; Messman, J.; Yu, X.; Hong, K.; Deng, S.; Swader, O.; Dadmun, M.; Ankner, J. F.; Britt, P.; Mays, J. W.; Malagoli, M.; Sumpter, B. G.; Brédas, J.-L.; Kilbey, S. M. *Chem. Mater.* **2011**, *23*, 4367.

(19) Sekovskyy, V.; Khanduyeva, N.; Komber, H.; Oertel, U.; Stamm, M.; Kuckling, D.; Kiriy, A. *J. Am. Chem. Soc.* **2007**, *129*, 6626.

(20) Ayres, J. R. *J. Appl. Phys.* **1993**, *74*, 1787.

(21) Bünsow, J.; Kelby, T. S.; Huck, W. T. S. *Acc. Chem. Res.* **2010**, *43*, 466.

(22) Matyjaszewski, K.; Dong, H.; Jakubowski, W.; Pietrasik, J.; Kusumo, A. *Langmuir* **2007**, *23*, 4528.

(23) Barbey, R. l.; Lavanant, L.; Paripovic, D.; Schüwer, N.; Sugnaux, C.; Tugulu, S.; Klok, H.-A. *Chem. Rev.* **2009**, *109*, 5437.

(24) Mansky, P.; Liu, Y.; Huang, E.; Russell, T. P.; Hawker, C. *Science* **1997**, *275*, 1458.

(25) Zhao, B.; Haasch, R. T.; MacLaren, S. *J. Am. Chem. Soc.* **2004**, *126*, 6124.

(26) Sidorenko, A.; Minko, S.; Schenk-Meuser, K.; Duschner, H.; Stamm, M. *Langmuir* **1999**, *15*, 8349.

(27) Estillore, N. C.; Advincula, R. C. *Langmuir* **2011**, *27*, 5997.

(28) Granville, A. M.; Boyes, S. G.; Akgun, B.; Foster, M. D.; Brittain, W. J. *Macromolecules* **2004**, *37*, 2790.

(29) Lee, H.-i.; Pietrasik, J.; Sheiko, S. S.; Matyjaszewski, K. *Prog. Polym. Sci.* **2010**, *35*, 24.

(30) Börner, H. G.; Beers, K.; Matyjaszewski, K.; Sheiko, S. S.; Möller, M. *Macromolecules* **2001**, *34*, 4375.

(31) Cheng, G.; Böker, A.; Zhang, M.; Krausch, G.; Müller, A. H. E. *Macromolecules* **2001**, *34*, 6883.

(32) Kriegel, R. M.; Rees, W. S.; Weck, M. *Macromolecules* **2004**, *37*, 6644.

(33) Runge, M. B.; Dutta, S.; Bowden, N. B. *Macromolecules* **2006**, *39*, 498.

(34) Beers, K. L.; Gaynor, S. G.; Matyjaszewski, K.; Sheiko, S. S.; Moller, M. *Macromolecules* **1998**, *31*, 9413.

(35) Huang, K.; Canterbury, D. P.; Rzayev, J. *Macromolecules* **2010**, *43*, 6632.

(36) Rzayev, J. *Macromolecules* **2009**, *42*, 2135.

(37) Xie, M.; Dang, J.; Han, H.; Wang, W.; Liu, J.; He, X.; Zhang, Y. *Macromolecules* **2008**, *41*, 9004.

(38) Yamamoto, S.-i.; Pietrasik, J.; Matyjaszewski, K. *Macromolecules* **2007**, *40*, 9348.

(39) Bolton, J.; Bailey, T. S.; Rzayev, J. *Nano Lett.* **2011**, *11*, 998.

(40) Yamada, K.; Miyazaki, M.; Ohno, K.; Fukuda, T.; Minoda, M. *Macromolecules* **1998**, *32*, 290.

(41) Dziezok, P.; Fischer, K.; Schmidt, M.; Sheiko, S. S.; Möller, M. *Angew. Chem. Int. Ed.* **1997**, *36*, 2812.

(42) Wintermantel, M.; Gerle, M.; Fischer, K.; Schmidt, M.; Wataoka, I.; Urakawa, H.; Kajiwara, K.; Tsukahara, Y. *Macromolecules* **1996**, *29*, 978.

(43) Wintermantel, M.; Fischer, K.; Gerle, M.; Ries, R.; Schmidt, M.; Kajiwara, K.; Urakawa, H.; Wataoka, I. *Angew. Chem. Int. Ed.* **1995**, *34*, 1472.

(44) Tsukahara, Y.; Ohta, Y.; Senoo, K. *Polymer* **1995**, *36*, 3413.

(45) Tsukahara, Y.; Kohjiya, S.; Tsutsumi, K.; Okamoto, Y. *Macromolecules* **1994**, *27*, 1662.

(46) Xia, Y.; Olsen, B. D.; Kornfield, J. A.; Grubbs, R. H. *J. Am. Chem. Soc.* **2009**, *131*, 18525.

(47) Jha, S.; Dutta, S.; Bowden, N. B. *Macromolecules* **2004**, *37*, 4365.

(48) Runge, M. B.; Yoo, J.; Bowden, N. B. *Macromol. Rapid Commun.* **2009**, *30*, 1392.

(49) Xia, Y.; Kornfield, J. A.; Grubbs, R. H. *Macromolecules* **2009**, *42*, 3761.

(50) Li, Z.; Zhang, K.; Ma, J.; Cheng, C.; Wooley, K. L. *J. Polym. Sci., Part A: Polym. Chem.* **2009**, *47*, 5557.

(51) France, M. B.; Alty, L. T.; Earl, T. M. *J. Chem. Educ.* **1999**, *76*, 659.

(52) Mantovani, G.; Lecolley, F.; Tao, L.; Haddleton, D. M.; Clerx, J.; Cornelissen, J. J. L. M.; Velonia, K. *J. Am. Chem. Soc.* **2005**, *127*, 2966.

(53) Sanford, M. S.; Love, J. A.; Grubbs, R. H. *Organometallics* **2001**, *20*, 5314.

(54) Carroll, G. T.; Sojka, M. E.; Lei, X.; Turro, N. J.; Koberstein, J. T. *Langmuir* **2006**, *22*, 7748.

(55) Soga, K. G.; Zuckermann, M. J.; Guo, H. *Macromolecules* **1996**, *29*, 1998.

(56) Motornov, M.; Sheparovych, R.; Katz, E.; Minko, S. *ACS Nano* **2008**, *2*, 41.

(57) Ayres, N.; Boyes, S. G.; Brittain, W. J. *Langmuir* **2006**, *23*, 182.

(58) Zhao, B.; Brittian, W. J. *J. Am. Chem. Soc.* **1999**, *121*, 3557.

(59) Rowe, M. D.; Hammer, B. A. G.; Boyes, S. G. *Macromolecules* **2008**, *41*, 4147.

(60) Drumheller, P. D.; Hubbell, J. A. *J. Biomed. Mater. Res.* **1995**, *29*, 207.

(61) Ostaci, R.-V.; Damiron, D.; Grohens, Y.; Léger, L.; Drockenmuller, E. *Langmuir* **2009**, *26*, 1304.

(62) Zdyrko, B.; Klep, V.; Luzinov, I. *Langmuir* **2003**, *19*, 10179.

(63) Xia, N.; Hu, Y.; Grainger, D. W.; Castner, D. G. *Langmuir* **2002**, *18*, 3255.

(64) Lee, S.-W.; Laibinis, P. E. *Biomaterials* **1998**, *19*, 1669.

(65) Groll, J.; Fiedler, J.; Engelhard, E.; Ameringer, T.; Tugulu, S.; Klok, H.-A.; Brenner, R. E.; Moeller, M. *J. Biomed. Mater. Res. Part A* **2005**, *74A*, 607.

3 Solution and phase properties of thermoresponsive PNIPAAM bottlebrush polymers with tailored side-chain length and end-group structure

[Portions of this work have been published: Xianyu Li, Hadi Shamsi Jazeyi, Stacy L. Pesek, Aditya Agrawal, Boualem Hammouda and Rafael Verduzco, "Thermo-responsive PNIPAAM Bottlebrush Polymers with Tailored Side-chain Length and End-group Structure", Soft Matter, 2014,10, 2008-2015; and Stacy Pesek, Xianyu Li, Boualem Hammouda, Kunlun Hong and Rafael Verduzco et al, "Small-Angle Neutron Scattering Analysis of Bottlebrush Polymers made by Grafting-Through Polymerization", Macromolecules, 2013, 46, 6998-7005]

3.1 Abstract

We explore the phase behavior, solution conformation, and interfacial properties of bottlebrush polymers with side-chains comprised of poly(N-isopropylacrylamide) (PNIPAAM), a thermally responsive polymer that exhibits a lower critical solution temperature (LCST) in water. PNIPAAM bottlebrush polymers with controlled side-chain length and side-chain end-group structure are prepared using a "grafting-through" technique. Due to reduced flexibility of bottlebrush polymer side-chains, side-chain end-groups have a disproportionate effect on bottlebrush polymer solubility and phase behavior. Bottlebrush polymers with a hydrophobic end-group have

poor water solubilities and depressed LCSTs, whereas bottlebrush polymers with thiol-terminated side-chains are fully water-soluble and exhibit an LCST greater than that of PNIPAAM homopolymers. The temperature-dependent solution conformation of PNIPAAM bottlebrush polymers in D_2O is analyzed by small-angle neutron scattering (SANS), and data analysis using the Guinier-Porod model shows that the bottlebrush polymer radius decreases as the temperature increases towards the LCST for PNIPAAM bottlebrush polymers with relatively long, 9 kg/mol side-chains. Above the LCST, PNIPAAM bottlebrush polymers can form a lyotropic liquid crystal phase in water.

3.2 Introduction

Bottlebrush polymers are branched macromolecules with novel and potentially useful bulk and interfacial properties. For example, as a result of their large size and highly extended backbone conformation, brush block copolymers self-assemble into polymer photonic crystals with large (100 nm or greater) domains.[1,2] Bottlebrush polymers are also of interest for interfacially-active materials due to dense crowding of the polymeric side-chains. This property can be used in the design of new nanomaterials for drug delivery,[3-5] surfactants,[6] organic electronics,[7] or as responsive surface coatings.[8]

While the size and conformation of the bottlebrush polymer backbone has been analyzed in detail, the conformation and flexibility of the side-chains is poorly understood. Characterizing the conformation of bottlebrush polymer side-chains and backbone simultaneously is challenging due to the dense-crowding of side-chains and proximity of the bottlebrush polymer backbone. However, the side-chain flexibility and

length may be relevant for applications that rely on the interfacial properties of bottlebrush polymers.

PNIPAAM is a well-known thermoresponsive polymer which exhibits a lower critical solution temperature (LCST) of 32 °C.[9,10] In aqueous solution, a reversible coil-to-globule phase transition and chain aggregation is induced by the dehydration of polymer chains when heating the solution above LCST. For bottlebrush polymers with PNIPAAM side chains, we hypothesized that collapse of the side-chains above the LCST might result in backbone extension resulting in, potentially, a larger single-molecule size above the LCST and a greater aspect ratio. The high grafting density of PNIPAAM side-chains may also lead to a change in the LCST temperature and a two-stage collapse, as has been observed for end-tethered PNIPAAM polymer brush films[11] but is absent in surface-tethered PNIPAAM networks.[12]

Here, we report the solution conformation, solubility, phase behavior, and interfacial properties of PNIPAAM bottlebrush polymers. We prepared a series of PNIPAAM bottlebrush polymers with different side-chain molecular weights and side-chain end-groups. We find that side-chain end-groups have a disproportionate effect on bottlebrush polymer solubility and phase behavior, likely due to stretching and reduced flexibility of bottlebrush polymer side-chains,[13,14] Both PNIPAAM bottlebrush solubility and LCST in water is affected by the end-group structure, and a stronger effect is seen for shorter side-chains. SANS measurements reflect a collapse of the side-chains with increasing temperature, with a greater collapse for longer PNIPAAM side-chains. PNIPAAM bottlebrush polymers with relatively long 9 kg/mol side-chains form lyotropic liquid crystal phases at temperatures higher than the LCST.

3.3 Experiment

3.3.1 Materials

All reagents and solvents were purchased from commercial sources and were used as received unless otherwise noted. *N*-isopropylacrylamide (Aldrich, 97%) was purified by recrystallization in hexane for three times. 2,2′-azobis(2-methylpropionitrile) (AIBN) was purified by recrystallization in methanol. Dichloromethane was dried over molecular sieves (4Å). Modified Grubb's catalyst (H2IMes)(pyr)2(Cl2)RuCHPh,[15] exo-7-Oxabicyclo- [2.2.1]hept-5-ene-2,3-dicarboxylic anhydride[16], norbornene-functionalized chain transfer agent (NB-CTA), and *N*-(pentynoyl-2-(dodecylthiocarbonothioylthio)-2-methylpropanyl)-cis-5-norbornene-exo-2, 3-dicarboximide were synthesized as previously reported[8].

3.3.2 Instruments

Gel-Permeation Chromatography (GPC) Molecular weights and polydispersities were obtained using an Agilent 1200 module equipped with three PSS SDV columns in series (100, 1000, and 10000 Å pore sizes), an Agilent variable wavelength UV/VIS detector, a Wyatt Technology HELEOS II multi-angle laser light scattering (MALLS) detector (λ = 658 nm), and a Wyatt Technology Optilab reX RI detector. This system enables SEC with simultaneous refractive index (SEC-RI), UV/VIS (SEC-UV/VIS), and MALLS detection. THF was used as the mobile phase at a flow rate of 1 mL/min at 40 °C.

Nuclear Magnetic Resonance Spectroscopy (NMR) Hydrogen NMR (^{1}H NMR) spectra were recorded using tetramethylsilane as internal standard in CDCl3 on a 400 MHz Bruker multi-nuclear spectrometer. Samples were placed in 5 mm o.d. tubes with the concentration of 20 mg/mL.

Differential Scanning Calorimetry (DSC) Glass transition temperatures (Tg) and lower-critical solution temperatures (LCSTs) were determined by a TA instrument DSC Q20 under N2 purge. For measurement of bulk polymer Tg, samples were subjected to three heating and cooling cycles from 0°C-250 °C. Values from the second and third heating cycle are reported. For measurement of LCST in water, solutions were subjected to three heating and cooling cycles from 10°C-60°C at a scan rate of 5 °C/min. The LCST was taken from second and third heating cycles, which were in good agreement for all samples.

Temperature-dependent UV-VIS analysis. UV-VIS measurements were carried out on a Jasco J815 spectropolarimeter equipped with a PFD-452S/15 peltier temperature controller. For analysis of temperature-dependent transmittance, transmittance at 400 nm was analyzed for 10 mg/mL solutions in the temperature range of 25 °C -50°C with a 0.1 °C/min ramp rate. For UV-VIS absorbance analysis, 1 mg/mL aqueous solutions were analyzed in the wavelength range of 190 nm-700 nm.

Small Angle Neutron Scattering (SANS) SANS measurements were performed at the National Institute of Standards and Technology Center for Neutron Research on the NG3 30 m instrument with a neutron wavelength of λ= 6 Å. Three sample-detector distances were used (1.3 m, 4 m, and 13 m), which

leads to an overall q-range 0.003 Å-1 - 0.4 Å-1. Polymer samples were prepared at 1 wt % in D2O and allowed to equilibrate at RT for at least 4 hours. Model fitting was performed using IGOR PRO software[17] and the Guinier-Porod model.[18]

Polarizing Optical Microscopy (POM). A Zeiss Axioplan 2 was used in a transmission mode, equipped with Linkam TMS 93 hot stage and Linkam LNP cooling pump temperature control system. Pictures were taken by a digital Axiocam HRM camera combined with AxioVision software.

3.4 Results and Discussion

3.4.1 The synthesis of PNIPAAM bottlebrush polymers

Bottlebrush polymers Bottlebrush polymers were prepared in a two-step "grafting through" synthetic approach (Figure 3.1), similar to that reported previously for poly(styrene) bottlebrush polymers.[8,19] First, norbornene functionalized PNIPAAM (NB-PNIPAAM-CTA) macromonomers were prepared by reversible addition−fragmentation chain transfer (RAFT) from an *exo*-norbornene-functionalized chain-transfer agent (NB-CTA). Bottlebrush polymers were synthesized *via* ROMP in the present of Grubbs' third generation catalyst ($(H_2IMeS)(3\text{-Br-Py})_2(Cl_2)RuCHPh$) at room temperature, resulting in PNIPAAM bottlebrush polymer with CTA-terminated side-chains P(PNIPAAM-CTA). This approach was repeated for three different PNIPAAM side-chain lengths, as shown in Table 3.1. Size-exclusion chromatography indicates successful polymerization in all cases, but the presence of unreacted

homopolymers was unavoidable (Figure 3.2). To address potential effects arising from these impurities, we compare measurements on bottlebrush polymer samples with those of pure PNIPAAM homopolymers.

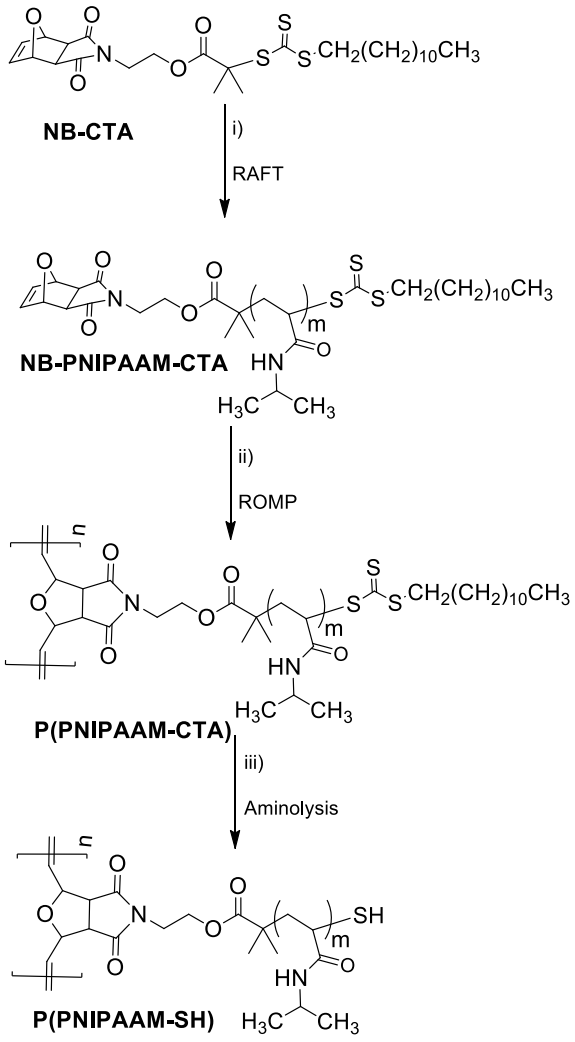

Figure 3.1 Synthetic route for the preparation of bottlebrush polymers with poly(NIPAAM) side-chains.

i) AIBN, 1,4-dioxane, N-isopropylacrylamide, 65°C, ii) CH_2Cl_2, ($(H_2IMeS)(3\text{-Br-Py})_2(Cl_2)RuCHPh$) iii) 1,4-Dioxane, hexylamine, tributylphosphine.

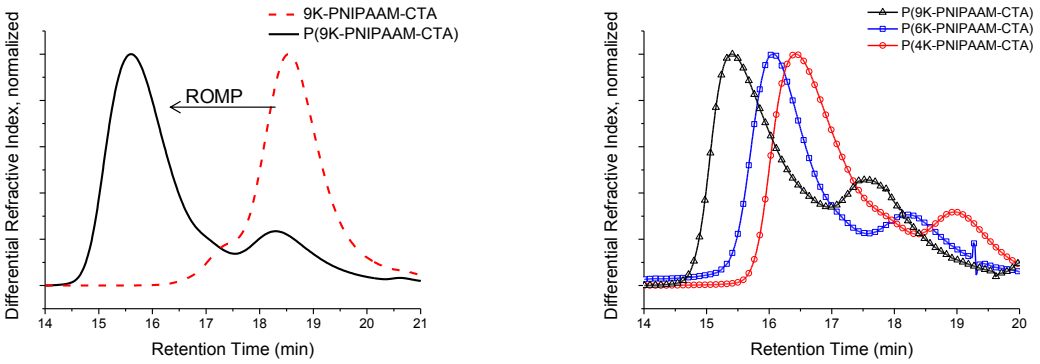

Figure 3.2 Size-exclusion Chromatography analysis of (left) 9K-PNIPAAM-CTA homopolymer and resulting P(9K-PNIPAAM-CTA) after ROMP and (right) all PNIPAAM bottlebrush polymer samples before removal of CTA end-group.

NB-PNIPAAM-CTA: As a representative example, the synthesis of 5.6 kg/mol NB-PNIPAAM-CTA is described. NIPAAM (2.064 g, 18.24 mmol), NB-CTA (94.97 mg, 0.166 mmol), AIBN (2.71 mg, 1.66 $\times 10^{-2}$ mmol) and anhydrous 1,4-dioxane (20 mL) were mixed in a 100 mL RBF, and the solution was purged by bubbling with nitrogen for 30 minutes. The flask was sealed and polymerization was initiated by raising the temperature to 65 °C. Aliquots were withdrawn periodically for analysis by GPC, and when the desired molecular weight was obtained the flask was removed from heat, quenched in an ice bath, and the polymer was recovered by several precipitations in diethyl ether to remove unreacted monomer. All NB-PNIPAAM polymers were prepared using the same approach. ^{1}H NMR (400 MHz, $CDCl_3$, ppm) δ 6.50 (2H, CHC<u>H</u>=C<u>H</u>CH), 5.8−7.1 (mH, CO_2N<u>H</u>CH), 5.23 (2H, CHCHOC<u>H</u>CH), 3.95-4.05 (mH, NHC<u>H</u>$(CH_3)_2$), 3.75 (2H, $CH_2C\underline{H}_2O$), 3.45 (2H, $NC\underline{H}_2CH_2$), 3.32 (2H, $SC\underline{H}_2(CH_2)_{10}$), 2.9 (2H,

CHCHCCH), 1.5-2.5 (3mH; $CH_2CHCONH$), 1.26 (20H, CH_2 $(CH_2)_{10}CH_3$), 1.05-1.20 (6mH, $CH(CH_3)_2$) , 0.88 (3H, CH_2CH_3).

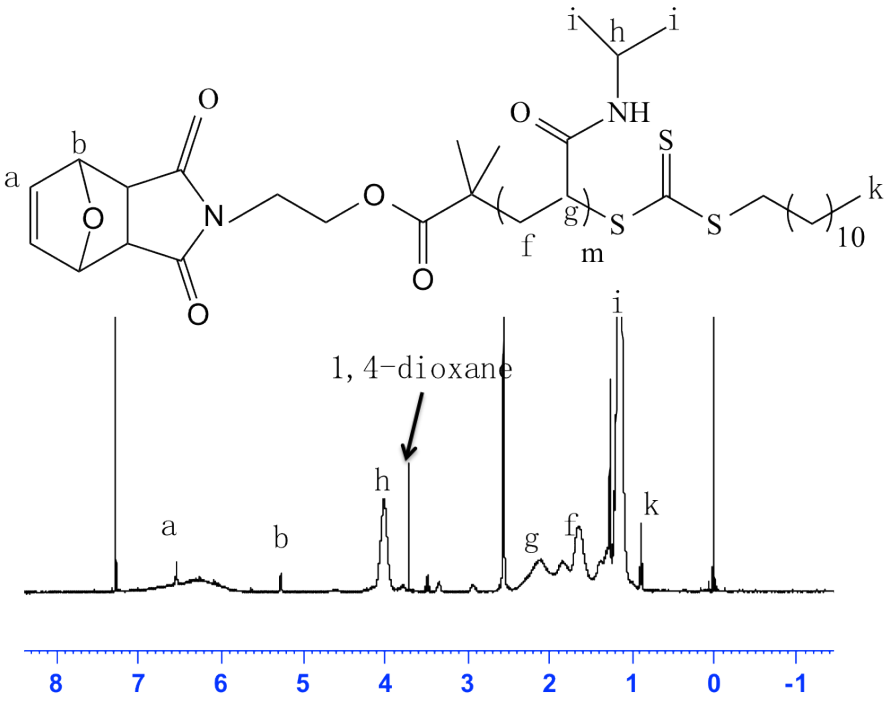

Figure 3.3 ^{1}H NMR spectra for 6 kg/mol NB-PNIPAAM-CTA.

P(PNIPAAM-CTA) All P(PNIPAAM-CTA) were prepared as follows. Norbornenyl macromonomers (NB-PNIPAAM-CTA) were added to a 10mL dry RBF with a stir bar. The flask was then degassed with three pump− purge cycles, and the desired amount of degassed, anhydrous DCM was added (total macromonomer concentration was 0.02−0.05 M). In a separate flask, Grubbs' third generation catalyst $(H_2IMes)(pyr)_2(Cl)_2RuCHPh$ was dissolved in anhydrous, degassed dichloromethane. The catalyst solution was transferred to the macromonomer solution using an airtight syringe to initiate the polymerization, and the reaction was stirred at room temperature

for at least 1 hour (GPC was used to track the reaction conversion). After completion, the reaction was quenched by addition of ethyl vinyl ether. The product was precipitated in cold diethyl ether, filtered and dried under vacuum.

^{1}H NMR (400 MHz, $CDCl_3$, ppm) δ5.8−7.1 (nH, $CO_2N\underline{H}CH$), 3.95-4.05 (mnH, $NHC\underline{H}(CH_3)_2$), 3.3 (mH, $CO_2N\underline{H}CH$), 1.5-2.5 (3mnH; $C\underline{H}_2C\underline{H}CONH$), 1.26 (20H, $CH_2(C\underline{H}_2)_{10}CH_3$), 1.05-1.20 (6mnH, $CH(C\underline{H}_3)_2$) , 0.88 (3H, $CH_2C\underline{H}_3$).

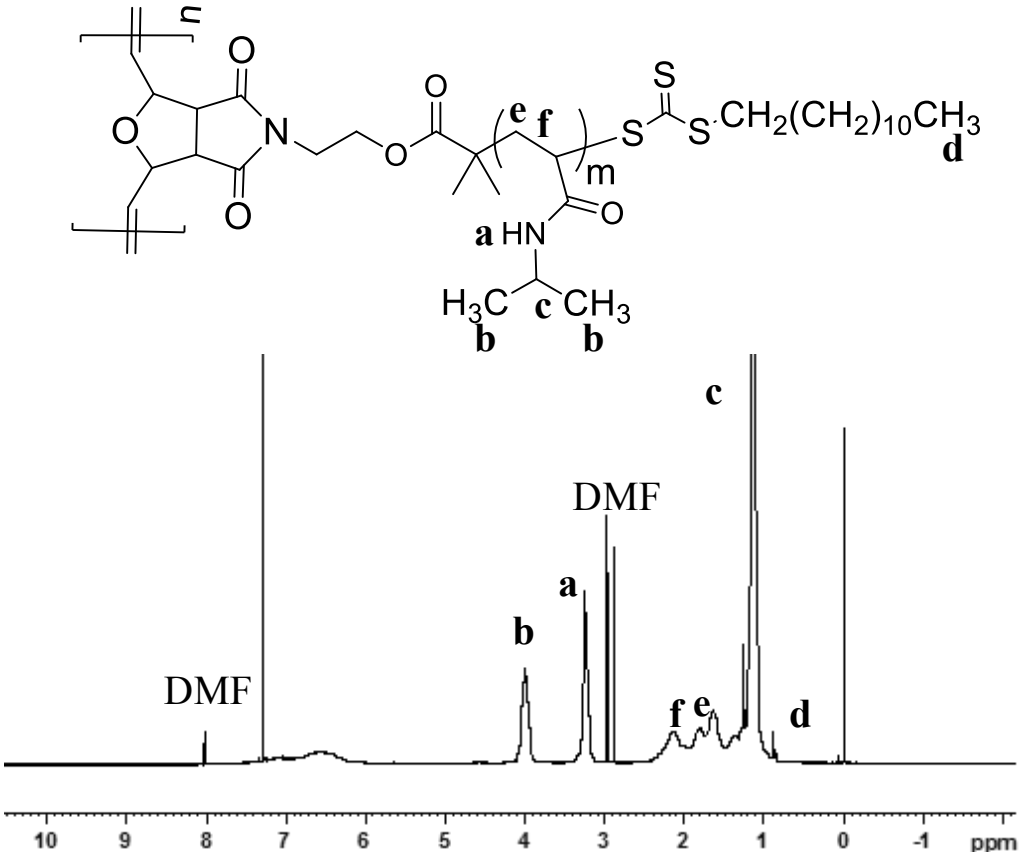

Figure 3.4 ^{1}H NMR spectra for P(6K-PNIPAAM-CTA).

P(PNIPAAM-SH) Thiol-terminated bottlebrush polymers were prepared by removing chain transfer agent (CTA) end-group from P(PNIPAAM-CTA)

bottlebrush polymers using an aminolysis reaction. The reaction was carried out in a nitrogen glovebox. P(NB-PNIPAAM-CTA) was dissolved anhydrous 1,4-dioxane, and hexylamine (10 times that of the amount of CTA end groups present on a molar basis) and tributyphosphine (equal to the amount of CTA end groups present on a molar basis) were added successively. The reaction was stirred at room temperature, after which the solution turned from yellow to a clear, colorless solution, indicating removal of the CTA endgroup. The final product was precipitated in cold diethyl ether and dried under vacuum.

^{1}H NMR (400 MHz, CDCl^{3}, ppm) δ), 5.8−7.1 (mnH, $CO_2N\underline{H}CH$), 3.95-4.05 (mnH, $NHC\underline{H}(CH_3)_2$), 3.3 (mH, $CO_2N\underline{H}CH$), 1.5-2.5 (nH; $C\underline{H}_2C\underline{H}CONH$),. 1.26 (20H, CH_2 $(C\underline{H}_2)_{10}CH_3$), 1.05-1.20 (6mnH, $CH(C\underline{H}_3)_2$)

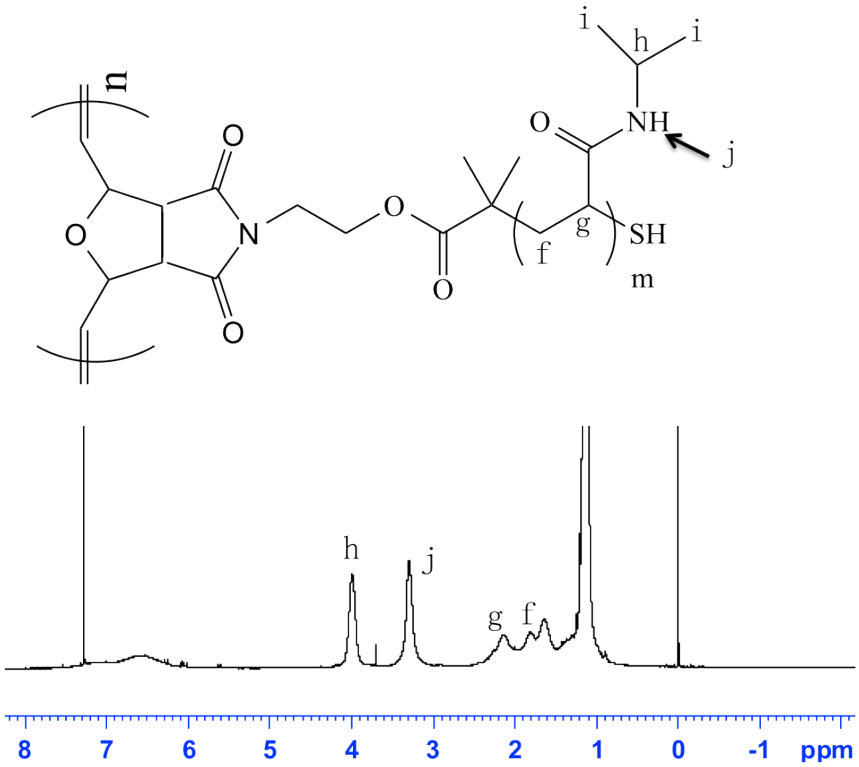

Figure 3.5^{1}H NMR spectra for P(6K-PNIPAAM-SH).

3.4.2 Solubility and lower-critical solution temperature of PNIPAAM bottlebrush polymers

After ROMP, the PNIPAAM bottlebrush polymer side-chains are terminated by a trithiocarbone chain-transfer agent (CTA) with a hydrophobic dodecyl tail. While CTA-terminated PNIPAAM homopolymers are fully water soluble, PNIPAAM bottlebrush polymers with 3.9 and 5.6 kg/mol side-chains are insoluble in water, and PNIPAAM bottlebrush polymers with 9.0 kg/mol side-chains are only partially water-soluble. In order to improve the water-solubility of the bottlebrush polymers, the CTA end-group was removed using a mild aminolysis reaction,[20] resulting in PNIPAAM bottlebrush polymers with thiol-terminated side-chains. Both UV-VIS absorbance measurements and ^{1}H NMR spectroscopy show quantitative removal of the CTA end-group (Figures 2-5). Removal of the CTA end-group reduces the molecular weight of the side-chains and the bottlebrush polymers, but the backbone degree of polymerization (DP) remains constant. We observe only a small increase in the polydispersity (PDI). After removal of the trithiocarbonate CTA, all bottlebrush polymers are water soluble at room temperature. The characteristics of CTA-terminated and thiol-terminated bottlebrush polymers are presented in Table 3.1.

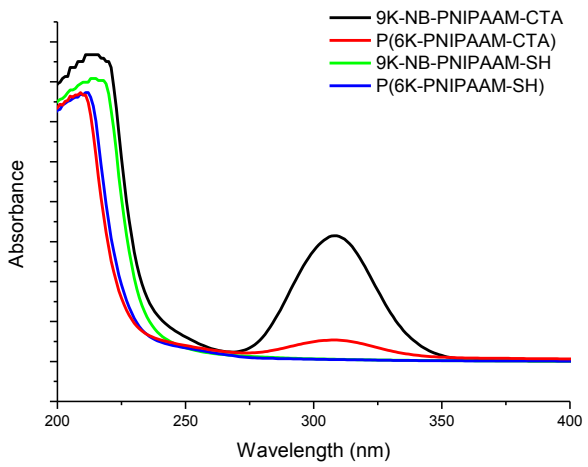

Figure 3.6 UV-Vis absorption spectra (left) of bottlebrush PNIPAAM before (red, black traces) and after (blue, green traces) aminolysis

Table 3.1 Characteristics of PNIPAAM bottlebrush polymers studied. Thiol-terminated bottlebrush polymers were derived from CTA-terminated bottlebrush polymers.

Bottlebrush Polymers	Side-chain M_w[a] (kg/mol)	Overall M_w[b] (kg/mol)	Backbone DP	PDI[a]
P(4K-NIPAAM-CTA)	3.9	154	39	1.06
P(4K-NIPAAM-SH)	3.7	146	39	1.14
P(6K-NIPAAM-CTA)	5.6	204	36	1.06
P(6K-NIPAAM-SH)	5.4	197	36	1.19
P(9K-NIPAAM-CTA)	9.0	292	33	1.14
P(9K-NIPAAM-SH)	8.8	286	33	1.27

[a]measured by size-exclusion chromatography relative to monodisperse polystyrene standards. [b]measured by size-exclusion chromatography with multi-angle laser light scattering detection.

As shown schematically in Figure 3.7, side-chain stretching and length can impact solubility in two different ways. Bottlebrush polymers are expected to have highly stretched, relatively inflexible side-chains due to strong steric interactions. As a result, side-chain end-groups may have a disproportionate impact on solubility. Further, side-chains become more flexible with increasing side-chain length. As a result, the solubility of bottlebrush polymers with longer side-chains should be less sensitive to end-group structure. The solubility behavior of PNIPAAM bottlebrush polymers is consistent with this physical picture. Although the CTA is a relatively small content of the side-chains (roughly 9, 6, and 4 % mass fraction for 4, 6, and 9 kg/mol side-chains, respectively), bottlebrush polymers with CTA-terminated PNIPAAM side-chains exhibit poor solubility in water. Only P(9K-PNIPAAM-CTA) is partially soluble in water compared with the insolubility of P(4K-PNIPAAM-CTA) and P(6K-PNIPAAM-CTA). After removal of the hydrophobic CTA end-group, all bottlebrush polymers are fully water soluble. By comparison, PNIPAAM-CTA homopolymers are fully water soluble.

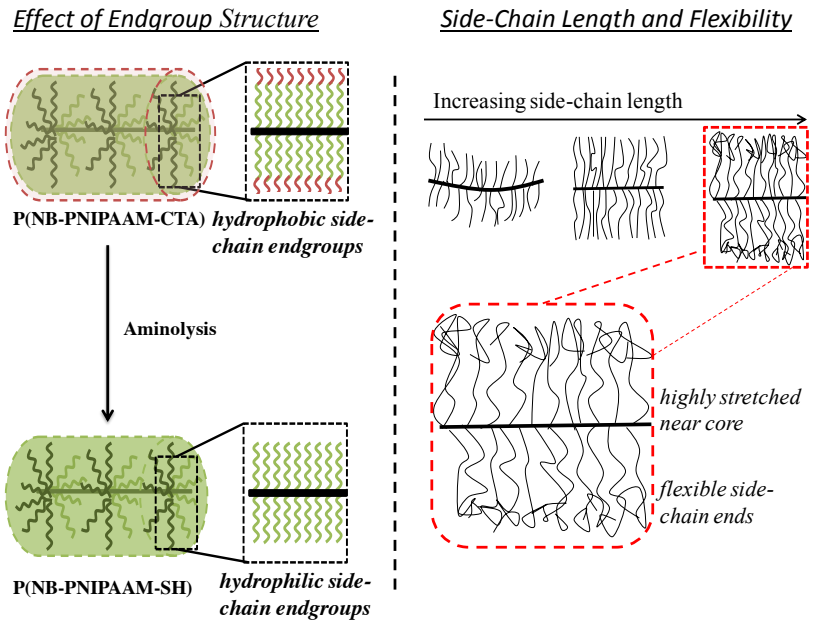

Figure 3.7 Schematic for the solution conformation of bottlebrush polymers and the role of side-chain end-group and length.

Thiol-terminated PNIPAAM bottlebrush polymers exhibit an LCST in water that can be easily observed visually, as shown for 1 % mass fraction (9K-NIPAAM-SH) in Figure 3.8. Prior work has shown the LCST of PNIPAAM can be affected by crowding and by the incorporation of different comonomers.[21,22] In general, increasing the hydrophilicity of PNIPAAM increases the LCST while introducing hydrophobic comonomers de-stabilizes the homogeneous phase and reduces the LCST.[23] Differential scanning calorimetry (DSC) was used to measure the LCST for PNIPAAM-CTA homopolymers on all bottlebrush polymers, including those with pendant CTAs. PNIPAAM-CTA bottlebrush polymers are partially water soluble, and a thermoreversible LCST can be detected by DSC for all samples. DSC measurements show that 9 kg/mol NB-PNIPAAM-CTA homopolymer has an LCST near 32°C, similar to that of linear

PNIPAAM.[9] Shorter PNIPAAM-CTA homopolymers have a reduced CTA, with the greatest reduction measured for 4 kg/mol PNIPAAM-CTA. Thus, the presence of the CTA destabilizes the water-soluble phase, as expected due to the greater hydrophobic character of shorter PNIPAAM-CTA polymers. Further, the impact of the CTA end-group is more significant for shorter side-chains, with P(4K-NIPAAM-CTA) exhibiting an LCST near 25 degrees. For all bottlebrush polymers, the LCST increases upon removal of the CTA. The LCST increases by more than 6 °C on aminolysis of P(4K-NIPAAM-CTA) and 1°C for P(9K-NIPAAM-CTA). The glass transition temperatures were also measured for all bottlebrush polymers, and these were relatively insensitive to side-chain end-group structure. LCST and T_g values are shown for all bottlebrush polymers and their corresponding macromonomers in Table 3.2.

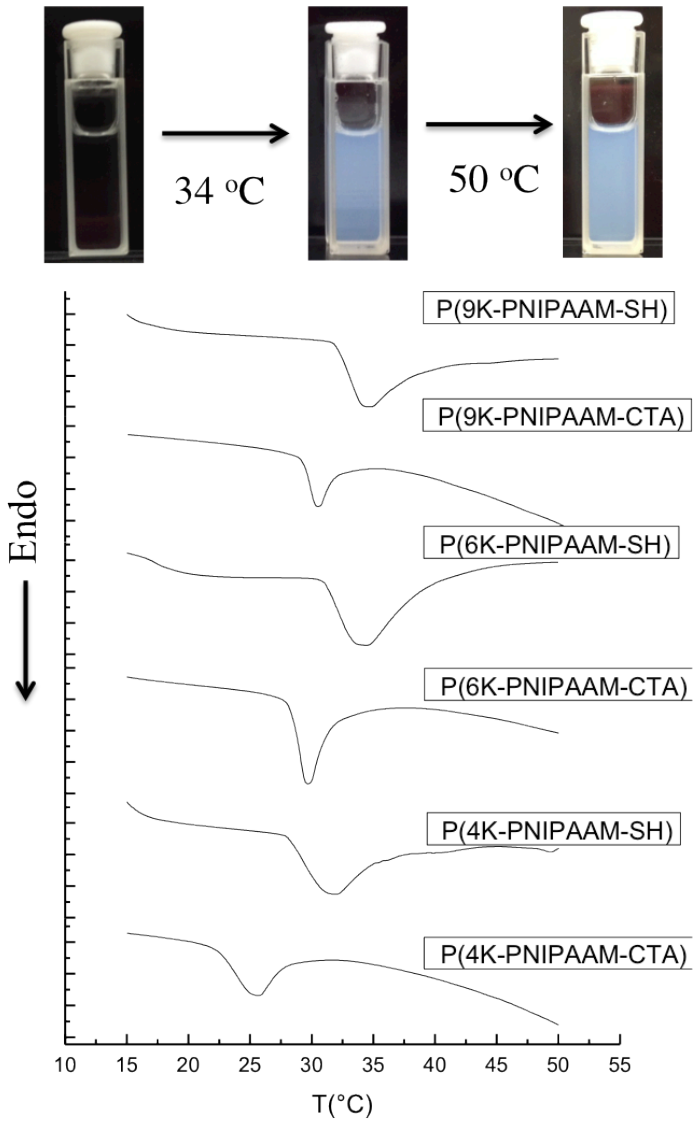

Figure 3.8 (top) Images of 1 % mass fraction P(9K-NIPAAM-SH) in water at different temperatures and (bottom) DSC thermograms of PNIPAAM bottlebrush polymer in water.

The second heating cycle of a heat/cool/heat sequence is shown, using a heating rate of 5 °C/min. The data show a reduced LCST for bottlebrush polymers with CTA terminated side-chains and for shorter side-chains.

Table 3.2 LCST and T_g of PNIPAAM bottlebrush polymers determined by DSC analysis.

Sample	LCST(°C)	T_g(°C)
4K-PNIPAAM-CTA	27.3	142
P(4K-NIPAAM-CTA)	25.5	145
P(4K-NIPAAM-SH)	31.8	145
6K-PNIPAAM-CTA	31.0	144
P(6K-NIPAM-CTA)	29.8	145
P(6K-NIPAM-SH)	34.3	144
9K-PNIPAAM-CTA	32.3	144
P(9K-NIPAAM-CTA)	33.3	145
P(9K-PNIPAAM-SH)	34.3	146

The LCST can be also determined by turbidity measurements (see Figure 3.9). This method gave LCST values in good agreement with those measured by DSC. Interestingly, the transmittance of bottlebrush polymer solutions decreased slowly with temperature over a wide temperature range above the LCST while PNIPAAM homopolymers exhibit a much sharper drop in transmission above the LCST.

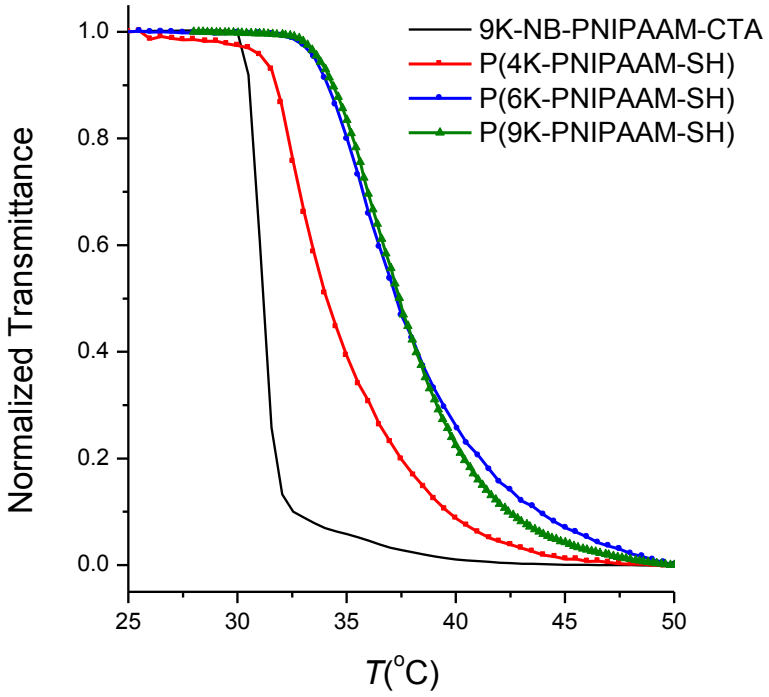

Figure 3.9 Temperature-dependent transmittance.

Obtained for the aqueous solutions of macronomers 9K-NB-PNIPAAM-CTA (black trace); bottlebrush polymers P(4K-PNIPAAM-SH) (red trace); P(6K-PNIPAAM-SH) (blue trace); P(9K-PNIPAAM-SH) (pink trace) at a concentration of 0.5 wt%.

3.4.3 Solution Conformation of Bottlebrush Polymers

Our former studies of series PS bottlebrush polymers with varying side-chain length and backbone length (Table 3.3) by Small angle neutron scattering (SANS) in d_8-toluene illustrated that bottlebrush polymer cross-sectional area depends primarily on side-chain DP, and the R_g exhibits a power-law dependence with side-chain DP. We also observe a sphere-to-cylinder transition with increasing backbone DP, with the transition occurring

at approximately a backbone DP of 120 for the polystyrene bottlebrush polymers studied (Figure 3-10)

Table 3.3 Properties of PS bottlebrush polymers P(NB-PS*N*)*M*, where *N* denotes the side-chain DP and *M* the backbone DP.

	Side-chains			Bottlebrush		
	Mw (kg/mol)	DP	PDI	*Mw* (kg/mol)	DP	PDI
P(NB-PS14)45	2.3	14	1.1.5	105.0	45	1.16
P(NB-PS14)264	2.3	14	1.15	881.0	264	1.67
P(NB-PS20)11	3.1	20	1.18	36.6	11	1.23
P(NB-PS20)15	3.1	20	1.18	63.0	20	1.65
P(NB-PS24)120	3.6	24	1.16	453.0	120	1.22
P(NB-PS42)148	5.6	42	1.14	1100.0	148	1.52
P(NB-PS54)216	6.9	54	1.12	3140.0	216	2.34

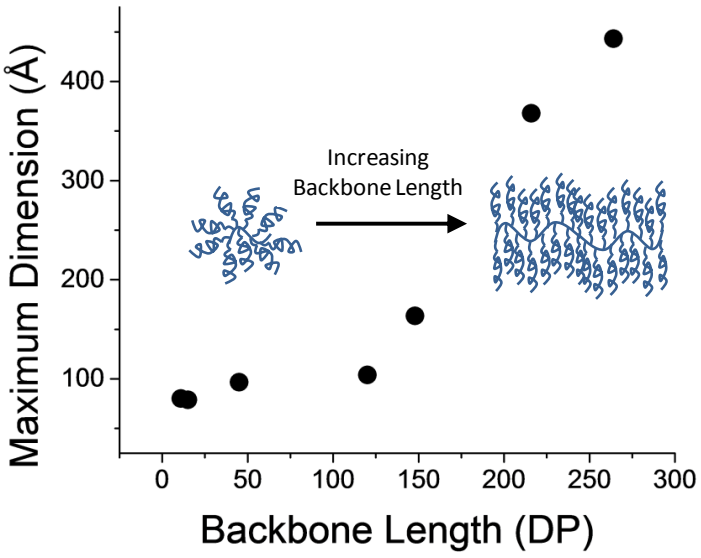

Figure 3.10 Proposed structure for bottlebrush polymers for small (left) and large (right) backbone DPs.

Bottlebrush polymers assume a spherical conformation at low backbone DPs and a more extended conformation at larger backbone DPs.

For temperature dependent PNIPAAM bottlebrush polymers, small angle neutron scattering (SANS) measurements were carried out to quantitatively analyze the size and conformation in solution, with particular interest in detecting collapse of the side-chains on approaching the LCST. We expected that bottlebrush polymers would exhibit a collapse of the PNIPAAM side-chains on approaching the LCST which might, due to steric interactions between side-chains, result in greater backbone extension. Due to increased flexibility with increasing molecular weight of the side-chains (shown schematically in Figure 3.7), we would also expect a greater change in the side-chain length with temperature for bottlebrush polymers with longer PNIPAAM side-chains. SANS measurements were carried out on the NG3 instrument at the National Institute of Standards and Technology (NIST). Samples were loaded into a 1 mm thick cell and sealed by two quartz discs. Samples were equilibrated for 10 min at each temperature. Three bottlebrush samples with 4K, 6K, and 9K side-chains were measured at 7 different temperatures, ranging from 10 °C to 50 °C.

At temperatures below the LCST, SANS traces for P(4K-NIPAAM-SH) and P(6K-NIPAAM-SH) exhibit a clear plateau at low q (< 0.01 $Å^{-1}$) with a small amount of aggregation as indicated by a small upturn at very low q (< 0.007 $Å^{-1}$). This is consistent with a spherical conformation of the bottlebrush polymers[19]. By comparison, the SANS trace for P(9K-NIPAAM-SH) does not exhibit a plateau at low q and instead increases with decreasing q. This suggests an extended bottlebrush polymer conformation in

solution, as has been observed for bottlebrush polymers with long backbone lengths[19] and other rod-like macromolecules. For all samples, the scattering intensity increases with temperature at low-q. This increase is modest below the LCST, but near the LCST the intensity is observed to rapidly increase with temperature (Figure 3.11).

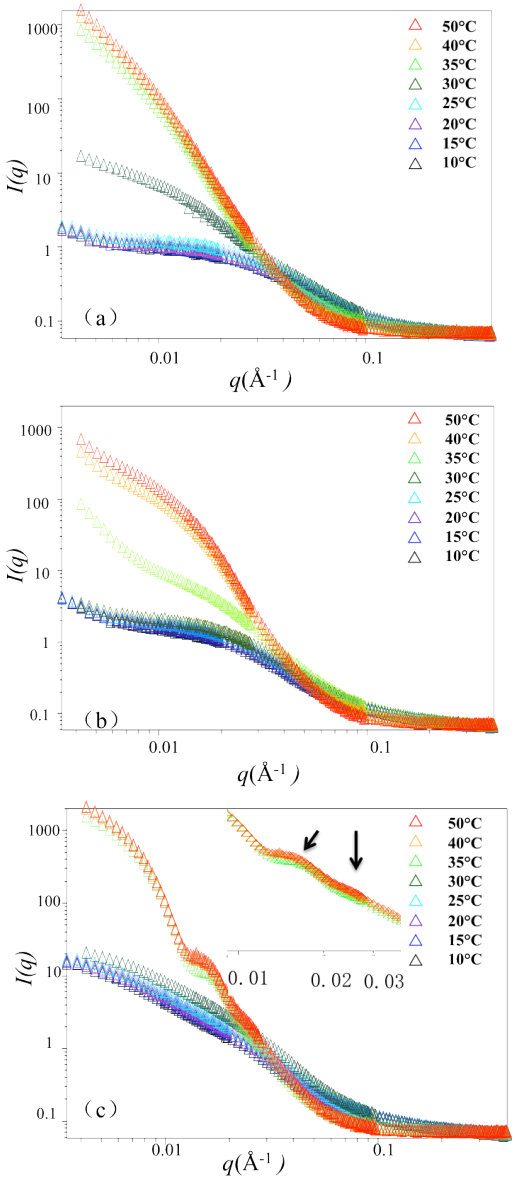

Figure 3.11 SANS data for different bottlebrush polymers

P(4K-PINPAAM-SH) (a); P(6K-PNIPAAM-SH) (b); P(9K-PNIPAAM-SH) (c) and enlarged part for P(9K-PNIPAAM-SH) at 35°C, 40°C and 50°C. Error bars are smaller than the plotting symbols.

A quantitative estimate of bottlebrush polymer size and anisotropy can be obtained by fitting the data to a Guinier-Porod model[19] or a cylindrical model.[19,24,25] Here, we restrict our analysis to the Guinier-Porod model since recent work has demonstrated that this model is more appropriate for bottlebrush polymers with relatively short (DP < 100) backbones. The Guinier-Porod model also makes no assumptions about the bottlebrush polymer shape, which may be spherical or cylindrical in solution. As shown in Figure 3.12, SANS traces for samples at temperatures below the LCST can be fit using the Guinier-Porod model. Model fitting provides an estimate of both the radius of the bottlebrush polymers R and anisotropy through the dimensionless parameter s (Table 3.4).

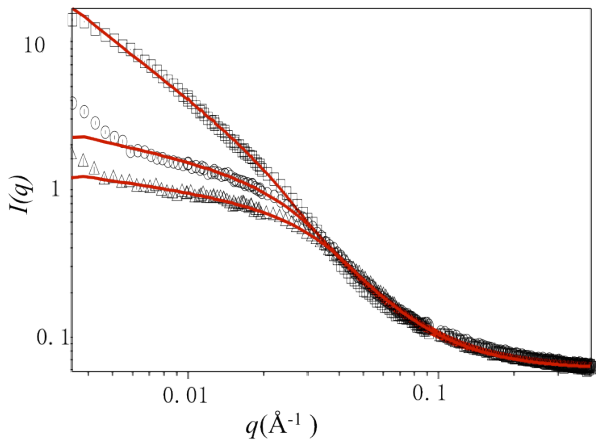

Figure 3.12 Representative SANS data and Guinier-Porod model fits.

SANS data for P(9K-PNIPAAM-SH) (square), P(6K-PNIPAAM-SH) (circle), and P(4K-PNIPAAM-SH) (triangle) at 10°C are shown along with corresponding Guinier-Porod model fits in red.

Comparing three bottlebrush polymer samples at the lowest temperature studied, 10 °C, the radius increases with side-chain molecular weight, as expected, from 3.9 nm to 6.0 nm. The dimension parameter *s* is near 0.2 for both P(4K-PNIPAAM-SH) and P(6K-PNIPAAM-SH), indicating a slightly extended ellipsoidal globule, but 1 for P(9K-PNIPAAM-SH), reflecting a more extended shape in solution. With increasing temperature, the radius of P(9K-PNIPAAM-SH) continuously decreases with temperature while that of P(4K-PNIPAAM-SH) and P(6K-PNIPAAM-SH) are roughly constant with temperature (Figure 3.13).

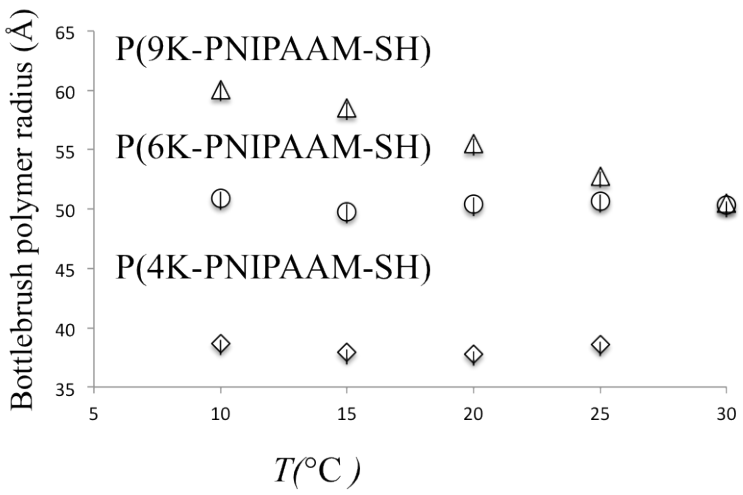

Figure 3.13 Polymer radius of gyration obtained from Guinier-Porod fitting for all three samples with temperature.

Above the LCST, bottlebrush polymers become insoluble and scattering at low-*q* is dominated by large aggregates for all bottlebrush polymer samples. Consistent with DSC and turbidity measurements, aggregates are detected at 30°C for P(4K-PNIPAAM-SH) but only above 30°C for P(6K-PNIPAAM-SH) and P(9K-PNIPAAM-SH). Data for P(4K-PNIPAAM-SH) and P(6K-PNIPAAM-SH) can be fit to a Guinier-Porod model at temperatures above the LCST. This analysis indicates the radius increases above the LCST. By contrast, the shape of the SANS trace for P(9K-PNIPAAM-SH) is qualitatively different than P(4K-PNIPAAM-SH) and P(6K-PNIPAAM-SH), and the SANS data for P(9K-PNIPAAM-SH) solutions cannot be fit by a Guinier-Porod model. Notably, the SANS trace P(9K-PNIPAAM-SH) exhibits two peaks at *q* values of 0.0147 $Å^{-1}$ and 0.0246 $Å^{-1}$. The ratio of these peaks is close to √3, which is characteristic of cylindrical packing. Small changes in the peak positions are observed with temperature.

The peaks shift to lower-*q* from with increasing temperature from 35°C to 40 °C, but little change is seen on further heating to 50°C.

The SANS data reflect significant conformational changes on heating up to and beyond the LCST. In the case of P(4K-PNIPAAM-SH) and P(6K-PNIPAAM-SH), the side-chain length is invariant with temperature below the LCST. Only a small decrease in the dimension parameter *s* is observed with increasing temperature. Above the LCST, SANS traces are dominated by scattering from large aggregates, and featureless traces reflect disordered aggregates. In the case of P(9K-PNIPAAM-SH), a significant reduction in bottlebrush polymer radius is observed, roughly 15%, when heating from 10 to 35 °C. Interestingly, prior work has observed that end-tethered PNIPAAM brushes do not collapse on crossing the LCST due to steric interactions between chains.[26,27] The results presented here indicate that significant side-chain collapse is only present for PNIPAAM bottlebrush polymers with long (~ 9kg.mol) side-chains.

Above the LCST, P(9K-PNIPAAM-SH) forms structured aggregates, indicated by the presence of peaks in the SANS traces. The positions of these peaks indicate cylindrically packed bottlebrush polymers, as shown schematically in Figure 3.14. The changes in the peak position on heating from 35 to 40 °C potentially reflect further collapse of the side-chains in this temperature range.

Table 3.4 Guinier-Porod fitting data for P(PNIPAAM-SH) with temperature.

T	P(4K-PNIPAAM-SH)		P(6K-PNIPAAM-SH)		P(9K-PNIPAAM-SH)	
(°C)	R (Å)	s	R (Å)	s	R (Å)	s
10	38.7±0.5	0.22±0.01	50.9±0.6	0.25±0.01	60.1±0.3	1.00±0.00
15	37.9±0.5	0.22±0.01	49.8±0.6	0.26±0.01	58.5±0.3	1.00±0.00
20	37.8±0.4	0.22±0.01	50.4±0.6	0.24±0.01	55.5±0.2	1.00±0.00
25	38.6±0.4	0.19±0.01	50.7±0.5	0.21±0.01	52.8±0.2	1.00±0.00
30	81.3±1.1	0.73±0.01	50.3±0.4	0.20±0.01	50.5±0.1	1.00±0.00
35	181.2±0.3	1.00±0.00	49.9±0.1	1.00±0.00	N/A	N/A
40	186.0±0.3	1.00±0.00	97.9±0.1	1.00±0.00	N/A	N/A
50	192.5±0.3	1.00±0.00	104.9±0.1	1.00±0.00	N/A	N/A

Early work with bottlebrush polymers reported the formation of lyotropic liquid crystal phases[28,29]. However, more recent studies have failed to observe lyotropic liquid crystal phases in bottlebrush polymers prepared using a "grafting-from" technique.[24,30] Lyotropic liquid crystal phases are expected for ratios of the persistence length to bottlebrush polymer radius greater than 10.[30,31] To determine if liquid crystal phases were present in any of the bottlebrush polymer solutions, 1 % mass fraction solutions in glass capillaries were analyzed by polarizing optical microscopy under crossed polarizers. All

solutions are clear near room temperature and become visibly turbid above the LCST. However, as shown in Figure 3.14, solution birefringence is observed only in the case of P(9K-PNIPAAM-SH) at temperatures above the LCST. The birefringence reversibly appears and disappears on heating and cooling the sample. This is consistent with lyotropic liquid crystal ordering at temperatures above the LCST. Together with the SANS data, these results indicate the formation of a lyotropic liquid crystal phase with cylindrical packing of P(9K-PNIPAAM-SH) bottlebrush polymers above the LCST. The temperature-dependent conformation of all bottlebrush polymers is depicted schematically in Figure 3.15.

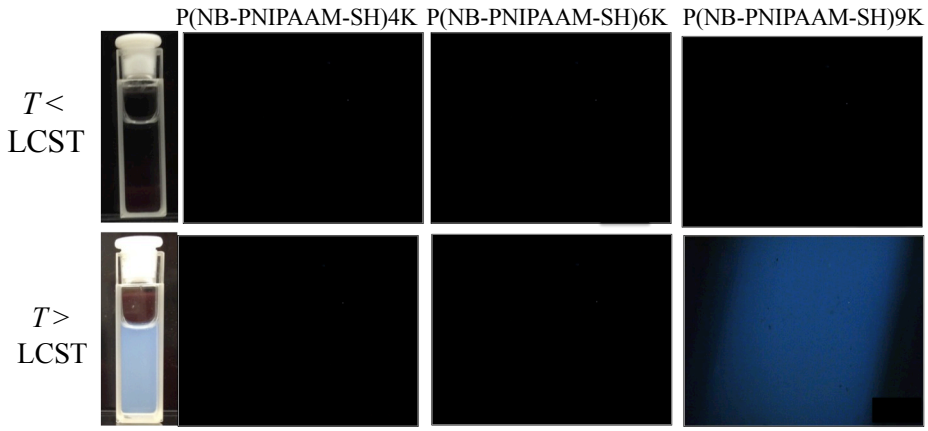

Figure 3.14 POM images of P(4K-PNIPAAM-SH) (left), P(6K-PNIPAAM-SH) (middle), and P(9K-PNIPAAM-SH) (right) viewed under crossed polarizers at temperatures below (top) and above (bottom) LCST.

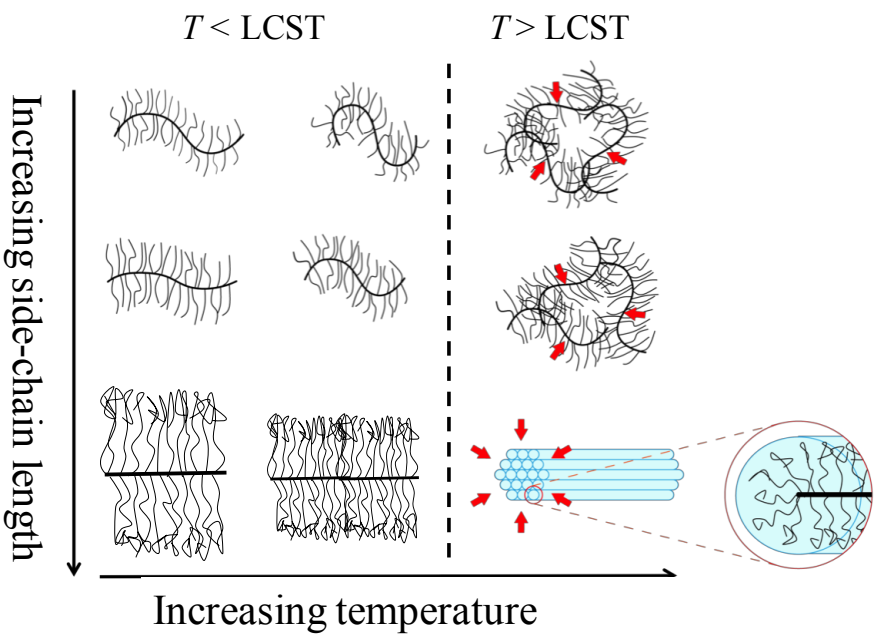

Figure 3.15 Schematic for changing bottlebrush polymer conformation with temperature.

For short side-chains, the side-chain length is invariant with temperature. Above the LCST, bottlebrush polymers form disordered aggregates. For long side-chains, the side-chain length decreases with temperature, and above the LCST bottlebrush polymers exhibit lyotropic liquid crystal ordering due to the formation of structured aggregates.

Well-defined water-soluble PNIPAAM bottlebrushes were synthesized via grafting through method, combining with "ROMP" and "RAFT" polymerization techniques. Both side-chain end-groups and side-chain lengths impact solubility, phase behavior, lower-critical solution temperature in water, and interfacial properties. PNIPAAM bottlebrush polymers with 9kg/mol side-chains exhibit a temperature dependent

conformation below the LCST, and above the LCST they exhibit lyotropic liquid crystal phases.

3.5 Bibliography

(1) Miyake, G. M.; Piunova, V. A.; Weitekamp, R. A.; Grubbs, R. H. *Angewandte Chemie International Edition* **2012**, *51*, 11173.

(2) Runge, M. B.; Bowden, N. B. *J. Am. Chem. Soc.* **2007**, *129*, 10551.

(3) Johnson, J. A.; Lu, Y. Y.; Burts, A. O.; Lim, Y.-H.; Finn, M. G.; Koberstein, J. T.; Turro, N. J.; Tirrell, D. A.; Grubbs, R. H. *J. Am. Chem. Soc.* **2010**, *133*, 559.

(4) Burts, A. O.; Li, Y.; Zhukhovitskiy, A. V.; Patel, P. R.; Grubbs, R. H.; Ottaviani, M. F.; Turro, N. J.; Johnson, J. A. *Macromolecules* **2012**, *45*, 8310.

(5) Li, Z.; Ma, J.; Cheng, C.; Zhang, K.; Wooley, K. L. *Macromolecules* **2010**, *43*, 1182.

(6) Li, Y.; Zou, J.; Das, B. P.; Tsianou, M.; Cheng, C. *Macromolecules* **2012**, *45*, 4623.

(7) Ahn, S.-k.; Pickel, D. L.; Kochemba, W. M.; Chen, J.; Uhrig, D.; Hinestrosa, J. P.; Carrillo, J.-M.; Shao, M.; Do, C.; Messman, J. M.; Brown, W. M.; Sumpter, B. G.; Kilbey, S. M. *ACS Macro Letters* **2013**, 761.

(8) Li, X.; Prukop, S. L.; Biswal, S. L.; Verduzco, R. *Macromolecules* **2012**.

(9) Heskins, M.; Guillet, J. E. *Journal of Macromolecular Science: Part A - Chemistry* **1968**, *2*, 1441.

(10) Schild, H. G. *Prog. Polym. Sci.* **1992**, *17*, 163.

(11) Yim, H.; Kent, M. S.; Satija, S.; Mendez, S.; Balamurugan, S. S.; Balamurugan, S.; Lopez, G. P. *Physical Review E* **2005**, *72*, 051801.

(12) Vidyasagar, A.; Majewski, J.; Toomey, R. *Macromolecules* **2008**, *41*, 919.

(13) Hsu, H.-P.; Paul, W.; Rathgeber, S.; Binder, K. *Macromolecules* **2010**, *43*, 1592.

(14) Birshtein, T. M.; Borisov, O. V.; Zhulina, Y. B.; Khokhlov, A. R.; Yurasova, T. A. *Polymer Science U.S.S.R.* **1987**, *29*, 1293.

(15) Sanford, M. S.; Love, J. A.; Grubbs, R. H. *Organometallics* **2001**, *20*, 5314.

(16) France, M. B.; Alty, L. T.; Earl, T. M. *J. Chem. Educ.* **1999**, *76*, 659.

(17) Kline, S. *J. Appl. Crystallogr.* **2006**, *39*, 895.

(18) Hammouda, B. *J. Appl. Crystallogr.* **2010**, *43*, 716.

(19) Pesek, S. L.; Li, X.; Hammouda, B.; Hong, K.; Verduzco, R. *Macromolecules* **2013**.

(20) Harvison, M. A.; Lowe, A. B. *Macromol. Rapid Commun.* **2011**, *32*, 779.

(21) Elisabetta, R.; et al. *Biomedical Materials* **2010**, *5*, 035012.

(22) Rahimian-Bajgiran, K.; Chan, N.; Zhang, Q.; Noh, S. M.; Lee, H.-i.; Oh, J. K. *Chem. Commun. (Cambridge, U. K.)* **2013**, *49*, 807.

(23) Xia, Y.; Burke, N. A. D.; St√∂ver, H. D. H. *Macromolecules* **2006**, *39*, 2275.

(24) Zhang, B.; Gröhn, F.; Pedersen, J. S.; Fischer, K.; Schmidt, M. *Macromolecules* **2006**, *39*, 8440.

(25) Rathgeber, S.; Pakula, T.; Wilk, A.; Matyjaszewski, K.; Beers, K. L. *The Journal of Chemical Physics* **2005**, *122*, 124904.

(26) Zhu, X.; Yan, C.; Winnik, F. M.; Leckband, D. *Langmuir* **2006**, *23*, 162.

(27) Plunkett, K. N.; Zhu, X.; Moore, J. S.; Leckband, D. E. *Langmuir* **2006**, *22*, 4259.

(28) Wintermantel, M.; Fischer, K.; Gerle, M.; Ries, R.; Schmidt, M.; Kajiwara, K.; Urakawa, H.; Wataoka, I. *Angewandte Chemie International Edition in English* **1995**, *34*, 1472.

(29) Tsukahara, Y.; Ohta, Y.; Senoo, K. *Polymer* **1995**, *36*, 3413.

(30) Rathgeber, S.; Pakula, T.; Wilk, A.; Matyjaszewski, K.; Lee, H.-i.; Beers, K. L. *Polymer* **2006**, *47*, 7318.

(31) van der Schoot, P. *The Journal of Chemical Physics* **1996**, *104*, 1130.

4 Thin film phase behavior in athermal blends of bottlebrush and linear polymers

4.1 Abstract

The novel architecture of bottlebrush polymers might be attractive for tailoring the surface properties of blends due to the high grafting density and conformational flexibility of polymeric side-chains. Previous work with blends of linear and branched polymers has reported preferential surface segregation of branched polymers due to entropic effects. This provides a potentially straightforward and cost-effective way to tailor the surface properties of polymer film coatings using small amounts of bottlebrush polymer additives. Herein, we report a study of the surface segregation behaviors of blends of well-defined bottlebrush and linear polymer thin films. Bottlebrush polymers with hydrogenated 6 kg/mol polystyrene (PS) side-chains were mixed with deuterated linear polystyrene chains with the molecular weight ranging from 2 kg/mol to 260 kg/mol. Blend thin films were prepared by spin casting from a solution mixture solution of hydrogenated bottlebrush polymers and deuterated linear polymers onto freshly cleaned silica wafers. Secondary ion mass spectromery (SIMS), neutron reflectivity, and microcopy demonstrate the segregation of deuterated bottlebrushes to the film-air and film-substrate interface. This work demonstrates that bottlebrush polymers segregate at both “hard” substrate-polymer interface and “soft” air-polymer interface, due to the dominant conformational entropy, bottlebrush polymers exhibit a slight preference for the “hard” substrate-polymer interface; the relative length of linear PS matrix to bottlebrush polymer side-chain length governs both the thermodynamics by controlling segregation

profiles and kinetics by modulating the diffusion rates in matrix linear polymers; and in the limit where the matrix linear polymer length is sufficiently above the critical molecular weight for deuterated PS entanglements, the extent of segregation is constrained by bottlebrush diffusion in the viscous melt.

4.2 Introduction

Bottlebrush polymers are macromolecular brushes with highly branched side-chains and have recently attention for applications including drug-delivery,[1,2] polymeric photonics,[3,4] surface modification,[5] and rheological modifiers.[6] Due to the highly branched architecture of bottlebrush polymers, bottlebrush polymers can be used to control surface and interfacial structures of soft materials. Surface segregation behaviors in miscible polymer blends have been investigated previously both theoretically and experimentally,[7-12] including work with branched polymer additives.[13-17] For athermal blend, in which there is no enthalpic interactions and segregation is driven by entropic effects, segregation is predicted to increase with branching degree and disparity between branching polymer size and linear polymer length.[18] Segregation and phase behavior can also be affected by subtle differences between two blending components, such as the chemical microstructures,[11,19] branching degree,[15] type and degree of isotopic labeling,[20] and tacticity.[21]

Here, we explore segregation in blends of bottlebrush polymers and linear polymers. Bottlebrush polymers can be prepared with control side-chain length and composition and thus represent a potentially promising additive to modify polymer thin films. In this work, we focus on athermal blends in which the side-chains of the bottlebrush polymer

match that of the linear polymer matrix. The linear polymers are fully deuterated, enabling quantitative analysis of segregation through SIMS and Neutron Reflectivity. A schematic for the experiments carried out here is shown in Figure 4.1. As shown, we expect the entropic driving force for segregation to increase with increasing linear polymer molecular weight due to reduced mixing between linear chains and bottlebrush side-chains at higher molecular weights.

Below, we present the results of the studies and show that bottlebrush polymers preferentially segregate to film interfaces after annealing. Little or no segregation is observed for short linear polymer chains, but segregation to both the film-air and film-substrate interface is observed for larger linear matrices. These results are consistent with studies of branched polymer additives and single-molecule studies of bottlebrush polymer solubility blended with linear polymers, and suggests bottlebrush polymers can be used as speciality additives to tailor polymer film interfaces.

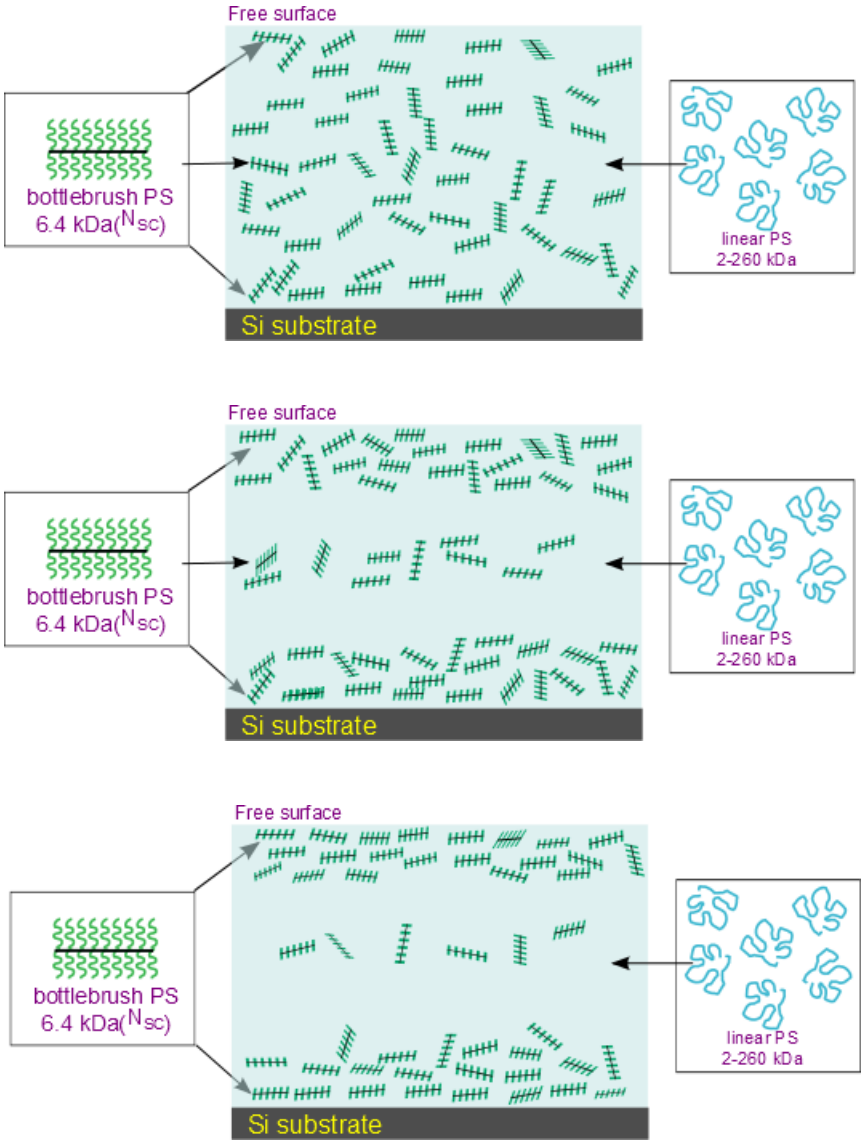

Figure 4.1 Thermodynamic behaviors of bottlebrush polymer/linear polymer blend thin films.

As cast film (top) shows as film with uniform distribution of bottlebrush polymers in linear matrix. 7-day annealed film (bottom) shows the segregation of bottlebrush polymers at both air-polymer and polymer-substrate interfaces. 2 -day annealed film (middle) shows the mid transition process of uniform mixture and re-distribution of bottlebrush polymers.

4.3 Experimental

4.3.1 Materials

All reagents and solvents were purchased from commercial sources and were used as received unless otherwise noted. Styrene was passed through aluminum oxide column to remove inhibitors before use. 2,2´-azobis(2-methylpropionitrile) (AIBN) was purified by recrystallization in methanol. Dichloromethane was dried over molecular sieves (4Å). Modified Grubb's catalyst (H2IMes)(pyr)2(Cl2)RuCHPh,[22] exo-7-Oxabicyclo-[2.2.1]hept-5-ene-2,3-dicarboxylic anhydride,[23] norbornene functionalized chain transfer agent (NB-CTA), were synthesized as previously reported.[5] Deuterated linear polystyrene polymers with different molecular weights were synthesized by anionic polymerization.

Norbornene-functionalized chain-transfer agent (NB-CTA), N-(Pentynoyl-2-(dodecylthiocarbonothioylthio)-2-methylpropanyl)-cis-5-norborne ne-exo-2,3-dicarboximide

4-(2-hydroxyethyl)-10-oxa-4-azatricyclo[5.2.1.02,6]dec-8-ene-3,5-dione (1.43 g, 6.85 mmol), 2-(dodecylthiocarbonothioylthio)-2-methylpropionic acid (2.50 g, 6.85 mmol), and N,N'-dicyclohexylcarbodiimide (1.61 g, 7.82 mmol) were dissolved in anhydrous dichloromethane (60 ml) and allowed to stir at 0 °C for thirty minutes. A solution of 4-dimethylaminopyridine in anhydrous DCM (5 mL 0.65 mmol,) was added dropwise. The reaction was stirred at 0 °C for five minutes and then allowed to come to room temperature while stirring overnight. The product was concentrated under reduced

pressure and recrystallized in ethyl acetate/hexanes (1:4) solvent mixture. Crystals were collected by vacuum filtration dried under vacuum (1.57g, 40% yield). ^{1}H NMR (400MHz, $CDCl_3$, ppm) δ 6.52 (2H, CHC<u>H</u>=C<u>H</u>CH), 5.29 (2H, CHC<u>H</u>OCH), 4.22 (2H, $CH_2C\underline{H}_2O$), 3.77 (2H, $NC\underline{H}_2CH_2$), 3.2 (2H, $SC\underline{H}_2(CH_2)_{10}$), 2.89 (2H, CHC<u>H</u>CCH), 1.66 (6H, $C(C\underline{H}_3)_2$), 1.29 (20H, $CH_2(C\underline{H}_2)_{10}CH_3$), 0.90 (3H, $CH_2C\underline{H}_3$).

Synthesis of NB-PS-CTA macromonomers. NB-PS-CTA was prepared via reversible-addition fragmentation chain transfer (RAFT) polymerization. For the synthesis of NB-PS6K-CTA, styrene (4.84 g, 46.50 mmol), NB-CTA (101.40 mg, 0.182 mmol), and AIBN (3.40 mg, 1.82×10^{-2} mmol) were mixed in a 100 mL RBF, and the solution was purged by bubbling the nitrogen through the solution for 30 minutes. The polymerization was initiated by raising the temperature to 60 °C. After 11 h, the reaction flask was removed from heat and the polymer was recovered by precipitation in methanol.

NB-PS6K-CTA: (0.75 g, 67.0% yield, based on the conversion of styrene) ^{1}H NMR (400MHz, $CDCl_3$, ppm): δ 6.30-7.25 (317H, styrenyl protons), 6.45 (2H, CHC<u>H</u>=C<u>H</u>CH) 5.20 (2H, CHCOC<u>H</u>CH), 3.62 (2H, $CH_2C\underline{H}_2O$), 3.49(2H, $NC\underline{H}_2CH_2$), 3.25 (2H, $SC\underline{H}_2(CH_2)_{10}$), 2.78 (2H, CHC<u>H</u>CCH), 1.52 (6H, $C(C\underline{H}_3)_2$), 1.15-2.15 (127H, PS chain backbone protons), 1.26 (20H, $CH_2(C\underline{H}_2)_{10}CH_3$),0.88 (3H, $CH_2C\underline{H}_3$).

P(NB-PS6K-CTA): Bottlebrush polymers were prepared by ROMP using $(H_2IMes)(pyr)_2(Cl)_2RuCHPh$. The macromonomers were added to a dry, 10 mL round bottom flask charged with a stir bar. The flask was then degassed with three pump-purge cycles, and the desired amount of degassed, anhydrous

dichloromethane (total macromonomer concentration was 0.02-0.05 M) was added. $(H_2IMes)(pyr)_2(Cl)_2RuCHPh$ was dissolved in degassed, anhydrous dichloromethane in a separate flask. The catalyst solution was transferred to the reaction flask containing macromonomers via cannula to initiate the polymerization and stirred at room temperature for at least 1 hour. The reaction was quenched by addition of ethyl vinyl ether after completion. The product was collected by precipitation in methanol dried under vacuum. (95% yield, based on the ROMP conversion). M_w (GPC): 585.4 kg/mol, PDI = 1.19, NMR spectra is shown in Figure 4.5 (top).

P(NB-PS-SH) Thiol-terminated bottlebrush polymers were prepared by removing chain transfer agent (CTA) end-group from P(NB-PS-CTA) bottlebrush polymers using an aminolysis reaction. The reaction was carried out in a nitrogen glovebox. P(NB-PS-CTA) was dissolved anhydrous THF, and hexylamine (10 times that of the amount of CTA end groups present on a molar basis) and tributyphosphine (equal to the amount of CTA end groups present on a molar basis) were added successively. The reaction was stirred at room temperature, after which the solution turned from yellow to a clear, colorless solution, indicating removal of the CTA end-group. The final product was precipitated in cold methanol and dried under vacuum. NMR data was presented in Figure 4.5 (bottom).

4.3.2 Polymer Characterization

Gel-Permeation Chromatography (GPC). Molecular weights and polydispersities of the polymers were obtained using an Agilent 1200 module equipped with three PSS SDV columns in series (100, 1000, and 10000 Å pore

sizes), an Agilent variable wavelength UV/vis detector, a Wyatt Technology HELEOS II multiangle laser light scattering (MALLS) detector (λ = 658 nm), and a Wyatt Technology Optilab reX RI detector. This system enables SEC with simultaneous refractive index (SEC-RI), UV/vis (SEC-UV/vis), and MALLS detection. THF was used as the mobile phase at a flow rate of 1 mL/min at 40 °C.

Nuclear Magnetic Resonance Spectroscopy (NMR). Hydrogen NMR (^{1}H NMR) of spectra were recorded using tetramethylsilane as internal standard in $CDCl_3$ on a 400 MHz Bruker multinuclear spectrometer. Samples were placed in 5 mm o.d. tubes with the concentration of 20 mg/mL.

4.3.3 The preparation and thermal treatment of thin films

To investigate the effect of relative length of linear matrix to the size of bottlebrush polymers, different length of linear polymers were blended with bottlebrush polymer. Different ratios of bottlebrush polymers to linear polymer were investigated, when the ratio of 10 wt % bottlebrush polymers can give both significant signal and less surface roughness. Therefore the following polymers (summarized in Table 4.1) blends were prepared with an approximate concentration of 2.3% polymer (bottlebrush + linear) in toluene. Blend thin films were prepared from the above solutions by spinning coating onto freshly UV-ozone cleaned silica wafers with around 200 ± 5 nm of silicon dioxide (SiO_2). Thermal annealing was conducted in vacuum oven at the temperature of 165 °C for different annealing time: 2 days and 7 days. For each molecular weight of the linear polymer we made three sets of samples one as-cast, the other two being 2

day and 7 day annealed. Since the linear polymer is deuterated and bottlebrush polymer is hydrogenated we generate a cover layer which will help us in calibrating the depth of the film of mass spectrometry data. The cover layer of roughly around 80 nm is generated from any arbitrary molecular weight deuterated linear polystyrene. We spin coat the deuterated polystyrene on a glass slide and float the film on the top of polymer blend film.

Table 4.1 Linear polymer length and mass ratio

Sample	Linear PS length (kg/mol)	Bottlebrush polymer: linear polymer (w/w)
1	2	1：9
2	10	1：9
3	51	1：9
4	125	1：9
5	260	1：9

4.3.4 Characterization of blended thin films

Optical Microscopy. Optical microscopy images of blended films were acquired using an Axioplan 2 imaging microscope (reflective mode) before and after annealing. Films were obtained by spin-casting of 20mg/mL solutions (bottlebrush polymer:linear polymer=1:9, weight ratio) onto freshly uv-ozone cleaned silica wafers.

Thickness Characterization. Thickness of the silicon dioxide wafer and the thickness of the blended films were measured using JA Wollam M-2000 spectroscopic ellipsometer.

Secondary Ion Mass Spectrometry (SIMS): Depth profiles were measured using a PHI D-SIMS 6600 system at Department of Chemistry, University of Houston with focused Cs primary ion beam which can eject the secondary ions with positive or negative charge. A quadrupole mass analyzer separates the masses by resonant electric fields, where only masses of choice are able to pass and be detected by the detector. The chamber was kept in the ultra-high vacuum of low 10^{-10} Torr by a standard ion pump. The Cs+ ion bombardment included a beam size of 30 μm with 30 nA primary current at an angle of 30^0 normal to the surface rastered over an area of 500 ×500 μm^2 with 5 keV impact energy and mass resolution m/Δm of 200. In Figure 4.1 we show the schematics of the SIMS procedure we employed in the study.

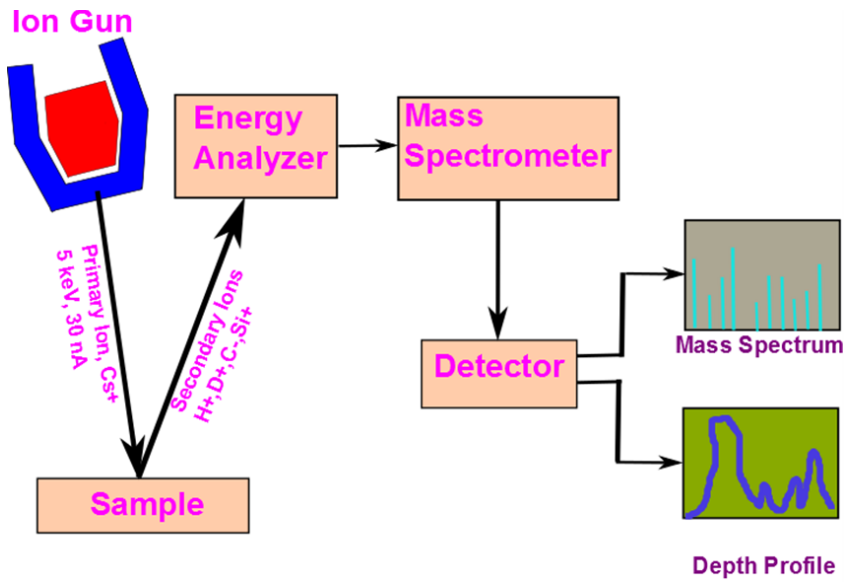

Figure 4.2 Schematic layout of the dynamic SIMS procedure

Neutron Reflectometry: Neutron reflection measurements were performed at Spallation Neutron Source of Oak Ridge National Lab liquid reflectometer (beamline 4B) with the source to sample distance of 13.6 m, sample to detector distance of 1.5m,

wavelength range 2.5Å -17.5Å, bandwidth 3.5 Å, Q range $0Å^{-1}$ to $0.3Å^{-1}$ and minimum reflectivity $1x10^{-7}$.

4.4 Results and discussions

4.4.1 Synthesis of bottlebrush polymers

Bottlebrush polymers were synthesized *via* "grafting through" method by combing with reversible addition-fragmentation chain transfer polymerization (RAFT) and ring-opening metathesis polymerization (ROMP). As shown in Figure 4.3, norbornene functionalized chain transfer agent (NB-CTA) was used to grow polystyrene side-chains (NB-PS-CTA), and later, in present of 3rd generation Grubbs' catalyst, well defined bottlebrush polymers P(NB-PS-CTA) were obtained. GPC spectrum of bottlebrush polymer shows significant shift compared to that of macromonomer NB-PS-CTA, (Figure 4.3). Well-defined bottlebrush were obtained with narrow PDI and high ROMP conversion (~95%). Former studies showed the existence of CTA end-group formed core-shell structure of bottlebrush polymers, and the shell of CTA end-groups affect the whole properties of bottlebrush polymer significantly,[24] to reduce the end-groups effect, aminolysis was applied to remove the CTA end-group of bottlebrush polymers as shown in the following Figure 4.3.

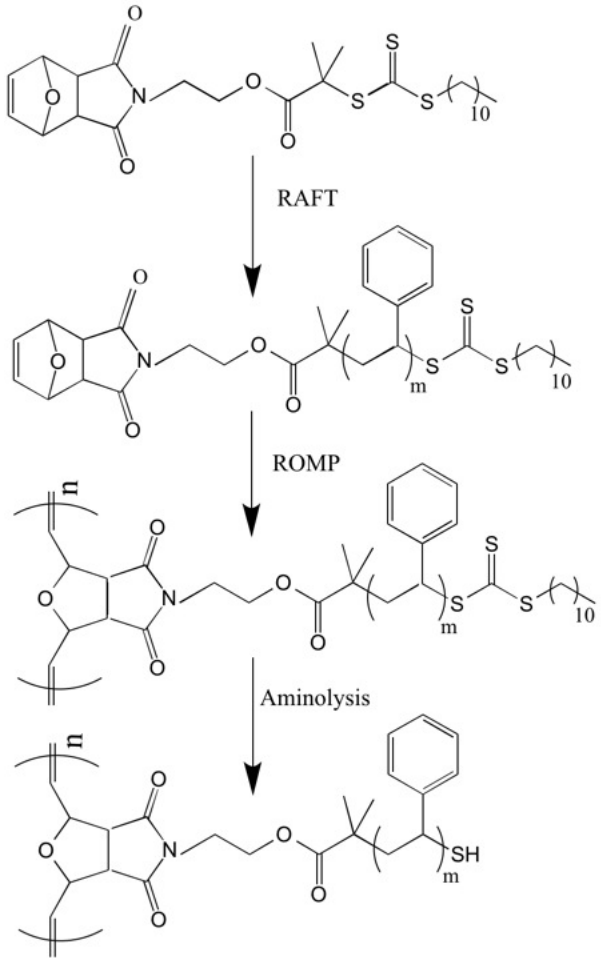

Figure 4.3 Chemical structure of bottlebrush polymer synthesis route for the preparation of bottlebrush polymers with PS side-chains.

i) AIBN, styrene, 60°C, ii) CH_2Cl_2, $((H_2IMeS)(3\text{-Br-Py})_2(Cl_2)RuCHPh)$ iii) THF, hexylamine, tributylphosphine.

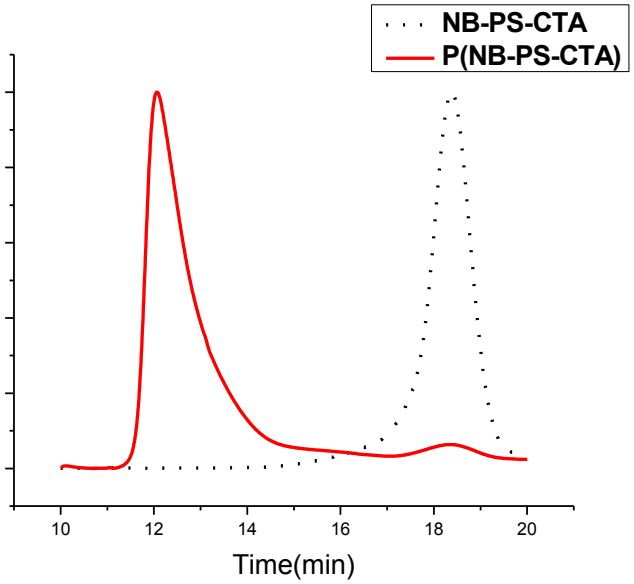

Figure 4.4 GPC spectra of macromonomer (black dish line) and bottlebrush polymers (red line)

P(NB-PS-SH) Thiol-terminated bottlebrush polymers were prepared by removing chain transfer agent (CTA) end-group from P(NB-PS-CTA) bottlebrush polymers using an aminolysis reaction carried out in a nitrogen glovebox. Due to existence of CTA end-group, P(NB-PS-CTA) solution exhibits light yellow color, when color changes from light yellow to colorless, the removal of CTA end-group was completed. Figure 4.5 shows the chemical structure and reaction route of bottlebrush polymers with thiol end-groups. The removal of the hydrophobic dodecyl chain was also confirmed by ^{1}H NMR characterization. The hydrogen (Ha on the Figure 4.5, top) at the position of 3.25ppm, corresponding to the one the dodecyl chain near thiol group disappeared after the cut off the CTA end-groups.

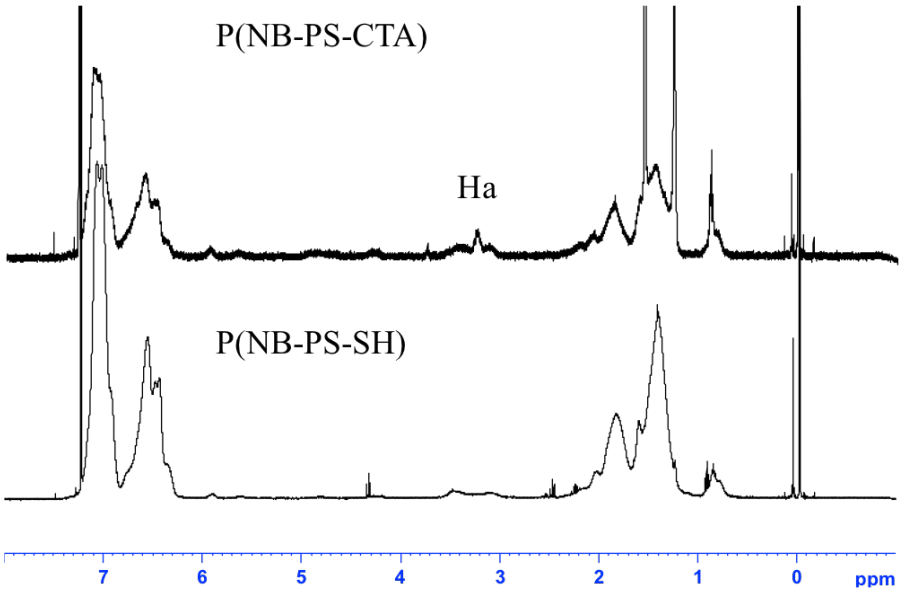

Figure 4.5 H NMR spectra of P(NB-PS-CTA) (top); and P(NB-PS-SH) (bottom)

4.4.2 Preparation of thin films

To investigate the film thickness effect and the annealing time effect on the segregation behaviors. Two different film thickness 150 nm and 200 nm were prepared, and the annealing time ranges from 2 days to 7 days at 165 °C. Blend thin films were prepared by spinning cast 20mg/ml mixture polymer solutions onto silica wafers at different speed rates to obtain desired film thickness.

Microcopy is a direct method to obtain morphology information of thin films. As shown in Figure 4.6, 150nm films with different linear polymer blends were prepared.

For as cast films, shorter linear polymer matrix blends (2K and 10K) show smoother and uniform surfaces, while longer linear polymer matrix blends show more phase separation and less uniform surfaces (51k, 125k and 260k). After annealing for 2 days, morphology of different films changed, polymer blend with 125K linear polymer matrix show significantly more aggregation compared to the corresponding as cast film. After annealing for 7 days, all surfaces of different samples trend to be more uniform.

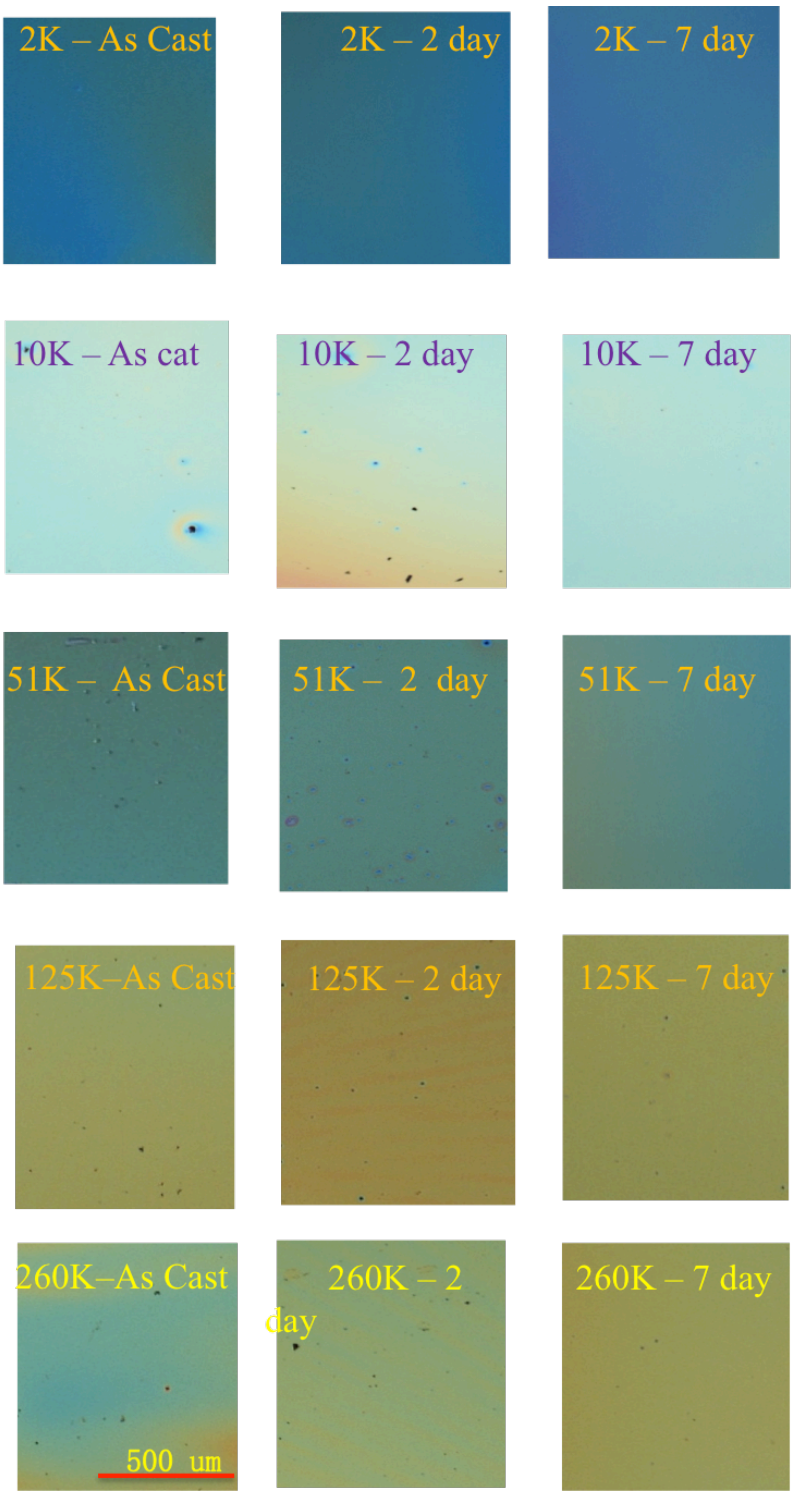

Figure 4.6 150nm blend films with different linear polymers for different annealing time

200nm films with different blends were also prepared. As shown in Figure 4.7, similar to 150nm thin films, for as cast films, shorter linear polymer matrix blends show smoother and uniform surfaces, while longer linear polymer matrix blends show more segregation, however, thin films with 260K linear polymers were uniform without aggregation, compared to the one of 150nm film. After annealing for 2 days, polymer blend with 125K linear polymer matrix show significant less uniform compared to the corresponding as cast film, this is consistent with 150 nm film. After annealing for 7 days, blend films with linear matrix polymers of 2k, 10k and 51k shows less uniform compared to corresponding films. Blend films of 125k and 260k linear polymers did not show significant changes. In general, after annealing for longer time (7 days), surface showed better uniformity for almost all films.

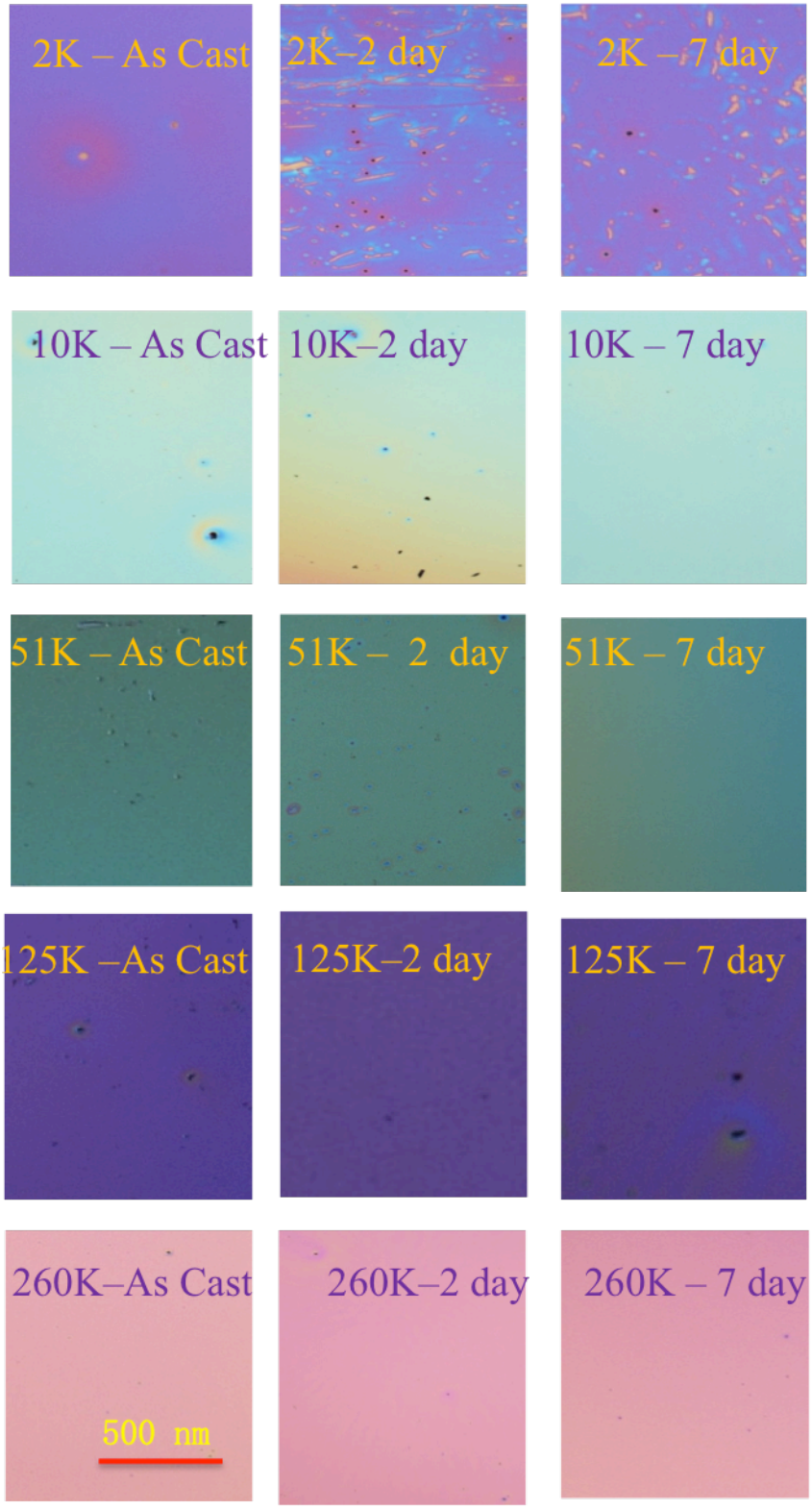

Figure 4.7 200nm blend films with different linear polymers for different annealing time

4.4.3 Phase segregation behaviors of bottlebrush polymers in linear polymer matrix by SIMS

Segregation behaviors of blend films have diverse applications, especially in the controlling of surface properties. SIMS has excellent sensitivity for most elements. To investigate the bottlebrush polymer concentration profile with the position in films, dynamic SIMS was applied.

The only difference between bottlebrush polymer and linear polymer in our studies is the architecture. Compared to linear polymers, bottlebrush analogy side-chains have reduced entanglement due to high grafting density, the surface free energy is relatively higher compared to linear polymers. The linear polymer chain length is an important factor affects the entanglement or entropy, therefore the blend films with different molecular weight of linear polymers were characterized by SIMS as shown in Figure 4.8. For 2K linear polymers, bottlebrush polymers prefer substrate surface at all three conditions: as cast, annealed for 2 days and annealed for 7 days. However more and more bottlebrush polymers goes to substrate interface after annealing. For 10K linear polymer matrix, bottlebrush polymer prefers air-polymer interface for as cast films, annealing process enables new distribution of bottlebrush polymers in linear polymer matrix, both air-polymer surface and polymer-substrate surface show aggregation of bottlebrush polymers, and with annealing time, more and more bottlebrush polymers go to the polymer-substrate interface. For shorter linear matrix, we found that the segregation is not significant even after longer annealing time. Interesting phenomena was found for

51K linear polymer matrix, bottlebrush polymer prefers polymer-substrate interface slightly for as cast films. Significant diffusion of bottlebrush polymers to polymer-substrate interface was observed after 2-day annealing, however after longer annealing time, Significant diffusion of bottlebrush polymers to air-polymer interface was observed. This might be due to the concentrated bottlebrush layer at the substrate surfaces exceed the critical concentration, and this inhibits further aggregation of bottlebrush polymers, therefore bottlebrush polymers prefer to diffuse in the opposite direction. When the linear polymer length is long enough, aggregation is significant, and bottlebrush polymers prefer "hard" substrate surface instead of "soft" air interface, and the concentration of bottlebrush polymers middle layer is relative low (~0.04 w/w) compared to shorter the value (0.08~0.1) in shorter linear matrix.

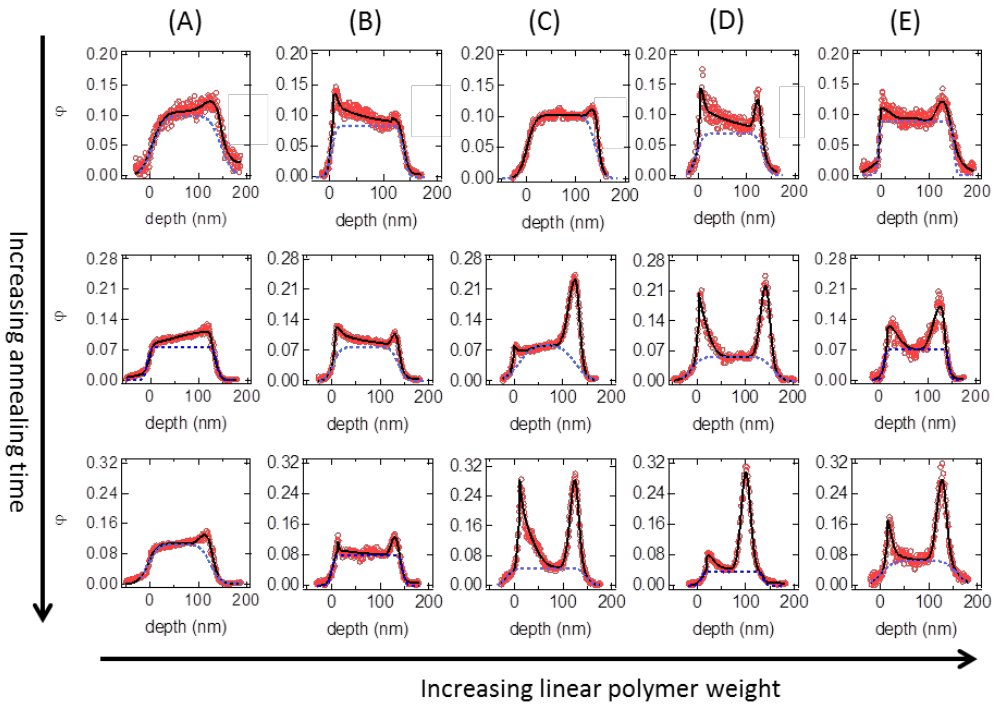

Figure 4.8 SIMS profile (red dote) and fitting curves (black line) for 150 nm 5 blend films

: as cast (left); annealing for 2 days (middle); and annealing for 7 days (right). (A): blend films of bottlebrush with 2K linear matrix; (B) blend films of bottlebrush with 10K linear matrix; (C) blend films of bottlebrush with 51K linear matrix; (D) blend films of bottlebrush with 125K linear matrix; (E) blend films of bottlebrush with 260K linear matrix

To have a direct expression of bottlebrush polymer distribution with matrix polymer length, the surface excess profiles Z^* were evaluated as the function of linear polymer repeat unit. As shown in Figure 4.9 for 150nm films and Figure 4.10 for 200nm films. Z^* was defined as using volume fraction of hydrogenated bottlebrush polymers φ:

$$Z^* = \int [\varphi(Z) - \varphi(\infty)] dZ$$

Where φ(Z) and φ(∞) denote the surface and bulk volume fraction of bottlebrush polymer component. Substrate surface access increases with linear polymer length and annealing time. With the increasing of annealing time, the value of Z* increases. For as cast films, surface excess increases with linear polymer length, while for annealed films, maximum Z* value of top at substrate exists when linear polymer has about 500 N_M for 2 day annealing film and 1250 N_M for 7 day annealing.

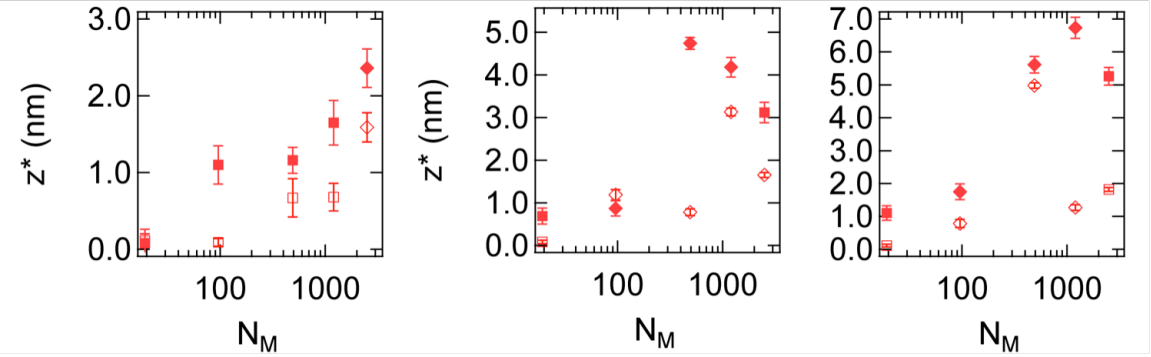

Figure 4.9 150nm films segregation profiles

of bottlebrush polymer 1 at substrate (solid square) and surface (open square) and bottlebrush polymer 2 at substrate (solid diamond) and surface (open diamond). Left image: as cast films; middle image: annealing for 2 days; right image: annealing for 7days.

Based on the microscopy images, we know film thickness can affect the surface components slightly, SIMS measurements of 200nm thick films were also taken into consideration, and to express the relationship of the segregation with molecular weight, segregation profiles were conducted and shown in Figure 4.10. Z* does not change much with the film thickness

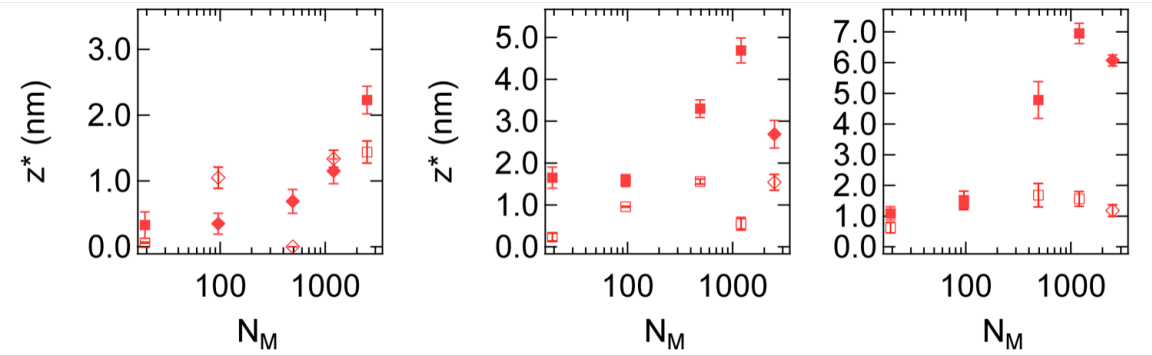

Figure 4.10 200nm films segregation profiles

of bottlebrush polymer 1 at substrate (solid square) and surface (open square) and bottlebrush polymer 2 at substrate (solid diamond) and surface (open diamond). Left image: as cast films; middle image: annealing for 2 days; right image: annealing for 7days.

4.4.4 Phase segregation behaviors of bottlebrush polymers in linear polymer matrix by neutron reflectivity

Neutron reflectivity (NR) is also a commonly used method to analyze the surface or interface interactions. In our studies, only the 150nm blend films, as cast and annealed for 2days, were studied by neutron reflectivity The collected data were fitted by the 3-layer model.[25] The fitting program divides the thin into three layers: top layer, middle layer and bottom layer, however, even within each layer, the concentration of bottlebrush polymers still depends on the depth, therefore the fitting results can not be as accurate as SIMS data. In addition, neutron reflectivity measurements are not as sensitive as SIMS, so some samples shows very weak signal, and it is difficult to fit the data. However, the fitting data can still reflect the general distribution of bottlebrush polymers, and can be compared to SIMS data, Figure 4.11 gives the representative neutron reflectivity data and fitting results, it can be told that fitting at lower Q is better than that of higher Q region. Based on the fitting results, thickness, roughness and bottlebrush centration information can be obtained and were summarized in Table 4.2. It shows similar thickness values and segregation trend as obtained from SIMS data. NR measurements confirm the presence of strong surface segregation observed by SIMS for the bottlebrush/linear blend.

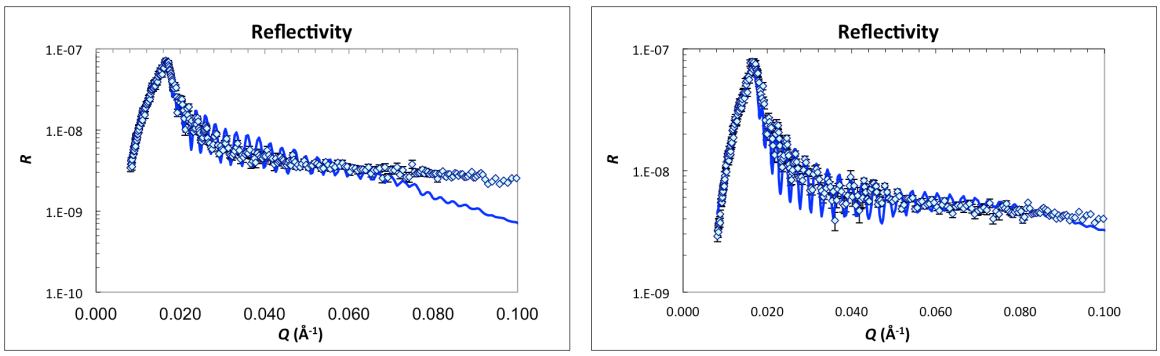

Figure 4.11 Representative sample (blend film with 260k linear matrix) neutron reflectivity data (open circle) and fitting curve (blue line) of as cast film (top) and annealed film (bottom)

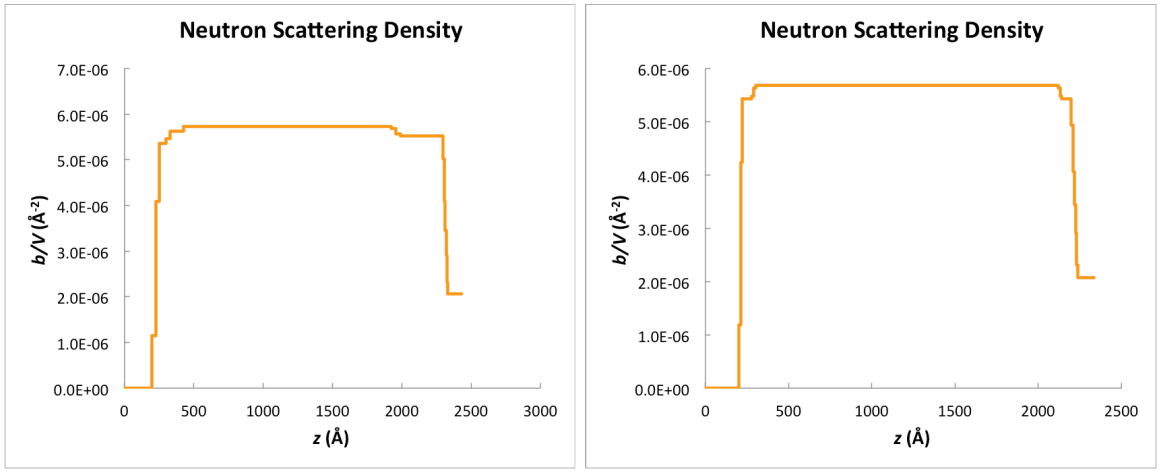

Figure 4.12 Representative sample (blend film with 2k linear matrix) neutron scattering density fitting curve of as cast film (top) and annealed film (bottom)

Table 4.2 Neutron reflectivity fitting data

Sample	Thickness/nm			Roughness/nm			Ratio/nm		
	Top	Mid	Bottom	Top	Mid	Bottom	Top	Mid	Bottom
2K as cast	5	142.5	6.5	1.5	3	5	.085	.095	.12
2K annealed	20	115	20	1.5	3	5	.078	.106	.11
10K as cast	20	112	20	2	.8	.5	.14	.10	.085
10K annealed	7.5	130.5	8	0	.5	2	.13	.101	.105
51K as cast	10	150	6	2	2	1	.13	.101	.11
51K annealed	8	133.5	10	2	.8	.5	.093	.095	.24
125K as cast	15	95	30	2	8	2	.13	.093	.12
125K annealed	6.5	131.5	6.5	2	.8	.5	.14	0.1	.13
260K as cast	10	165	35	4	15	5	.185	.088	.13
260K annealed	8	184	8	1.7	1.7	1.7	.15	.095	.15

4.5 Bibliography

(1) Johnson, J. A.; Lu, Y. Y.; Burts, A. O.; Xia, Y.; Durrell, A. C.; Tirrell, D. A.; Grubbs, R. H. *Macromolecules* **2010**, *43*, 10326.

(2) Johnson, J. A.; Lu, Y. Y.; Burts, A. O.; Lim, Y.-H.; Finn, M. G.; Koberstein, J. T.; Turro, N. J.; Tirrell, D. A.; Grubbs, R. H. *J. Am. Chem. Soc.* **2010**, *133*, 559.

(3) Sveinbj√∂rnsson, B. R.; Weitekamp, R. A.; Miyake, G. M.; Xia, Y.; Atwater, H. A.; Grubbs, R. H. *Proceedings of the National Academy of Sciences* **2012**, *109*, 14332.

(4) Miyake, G. M.; Weitekamp, R. A.; Piunova, V. A.; Grubbs, R. H. *J. Am. Chem. Soc.* **2012**, *134*, 14249.

(5) Li, X.; Prukop, S. L.; Biswal, S. L.; Verduzco, R. *Macromolecules* **2012**.

(6) Lee, S.; Spencer, N. D. *Science* **2008**, *319*, 575.

(7) Jones, R. A. L.; Kramer, E. J. *Polymer* **1993**, *34*, 115.

(8) Affrossman, S.; Hartshorne, M.; Kiff, T.; Pethrick, R. A.; Richards, R. W. *Macromolecules* **1994**, *27*, 1588.

(9) Schaub, T. F.; Kellogg, G. J.; Mayes, A. M.; Kulasekere, R.; Ankner, J. F.; Kaiser, H. *Macromolecules* **1996**, *29*, 3982.

(10) Genzer, J.; Composto, R. J. *EPL (Europhysics Letters)* **1997**, *38*, 171.

(11) Vanden Eynde, X.; Bertrand, P. *Surf. Interface Anal.* **1999**, *27*, 157.

(12) Hirata, T.; Matsuno, H.; Tanaka, M.; Tanaka, K. *Phys. Chem. Chem. Phys.* **2011**, *13*, 4928.

(13)Foster, M. D.; Greenberg, C. C.; Teale, D. M.; Turner, C. M.; Corona-Galvan, S.; Cloutet, E.; Butler, P. D.; Hammouda, B.; Quirk, R. P. *Macromol. Symp.* **2000**, *149*, 263.

(14) Greenberg, C. C.; Foster, M. D.; Turner, C. M.; Corona-Galvan, S.; Cloutet, E.; Quirk, R. P.; Butler, P. D.; Hawker, C. *Journal of Polymer Science Part B: Polymer Physics* **2001**, *39*, 2549.

(15) Lee, J. S.; Foster, M. D.; Wu, D. T. *Macromolecules* **2006**, *39*, 5113.

(16) Yethiraj, A. *Phys. Rev. Lett.* **1995**, *74*, 2018.

(17) Walton, D. G.; Mayes, A. M. *Physical Review E* **1996**, *54*, 2811.

(18) Fredrickson, G. H.; Liu, A. J.; Bates, F. S. *Macromolecules* **1994**, *27*, 2503.

(19) Rhee, J.; Crist, B. *Macromolecules* **1991**, *24*, 5663.

(20) Graessley, W. W.; Krishnamoorti, R.; Balsara, N. P.; Fetters, L. J.; Lohse, D. J.; Schulz, D. N.; Sissano, J. A. *Macromolecules* **1993**, *26*, 1137.

(21) Beaucage, G.; Stein, R. S.; Hashimoto, T.; Hasegawa, H. *Macromolecules* **1991**, *24*, 3443.

(22) Sanford, M. S.; Love, J. A.; Grubbs, R. H. *Organometallics* **2001**, *20*, 5314.

(23) France, M. B.; Alty, L. T.; Earl, T. M. *J. Chem. Educ.* **1999**, *76*, 659.

(24) Li, X.; ShamsiJazeyi, H.; Pesek, S. L.; Agrawal, A.; Hammouda, B.; Verduzco, R. *Soft Matter* **2014**, *10*, 2008.

(25)Lokitz, B. S.; Wei, J.; Hinestrosa, J. P.; Ivanov, I.; Browning, J. F.; Ankner, J. F.; Kilbey, S. M.; Messman, J. M. *Macromolecules* **2012**, *45*, 6438.

5 Potential Application and Outlook of Bottlebrush Polymers

[Portions of this work have been published: Xianyu Li, Hadi Shamsi Jazeyi, Stacy L. Pesek, Aditya Agrawal, Boualem Hammouda and Rafael Verduzco, "Thermo-responsive PNIPAAM Bottlebrush Polymers with Tailored Side-chain Length and End-group Structure", Soft Matter, 2014,10, 2008-2015]

5.1 Abstract

The flexibility of the bottlebrush side-chains and the relatively rigid backbone make bottlebrush polymers a great potential candidate for diverse applications. In this chapter, we explore the potential application of bottlebrush polymers as surfactants for reducing the oil-water interfacial tension and as crosslinked, antifouling films. Interfacial tension measurements show that bottlebrush polymers reduce the IFT between chloroform and water to levels comparable to PNIPAAM homopolymers without the formation of microemulsions, and the interfacial tension is dependent on temperature due to the lower-critical solution temperature of PNIPAAN. A mixture of commercial surfactant 4,5-orthoxylene sulfonate (OXS) and small amounts of PNIPAAM bottlebrush polymers was studied and found to give lower interfacial tensions at higher salinities. Stable thin films of PNIPAAM bottlebrush polymers were prepared by introducing UV-cross-linker: poly(acroyl benzophene) (PABP) as co-macromonomer of bottlebrush polymers and an anchoring layer to the substrate. The resulting PNIPAAM bottlebrush polymer films are

stable in water for extended periods of time and exhibit cell resistance comparable to PEG brush coatings.

5.2 Introduction

The flexibility of the bottlebrush side-chains and the relatively rigid backbone make bottlebrush polymers a great potential candidate for diverse applications. In this chapter, we present preliminary work on the development of bottlebrush polymers for two applications: surfactants for enhanced oil recovery and non-toxic antifouling coatings.

The flexibility of the bottlebrush side-chains may enable reduction of surface tension at liquid-liquid interfaces[3], and recent work has demonstrated the potential of bottlebrush polymers to stabilize emulsions[4]. Below, we show that PNIPAAM bottlebrush polymers and blends of PNIPAAM with surfactant show promise as surfactant additives. PNIPAAM bottlebrush polymers were added into the chloroform/water system, and bottlebrush polymers are shown to be interfacially active and can reduce the interfacial tension (IFT) between chloroform and water to values comparable to PNIPAAM homopolymer. PNIPAAM bottlebrush polymers/4,5-orthoxylene sulfonate mixture can reduce interface tension significantly, and have better salinity tolerance compared to pure 4,5-orthoxylene sulfonate.

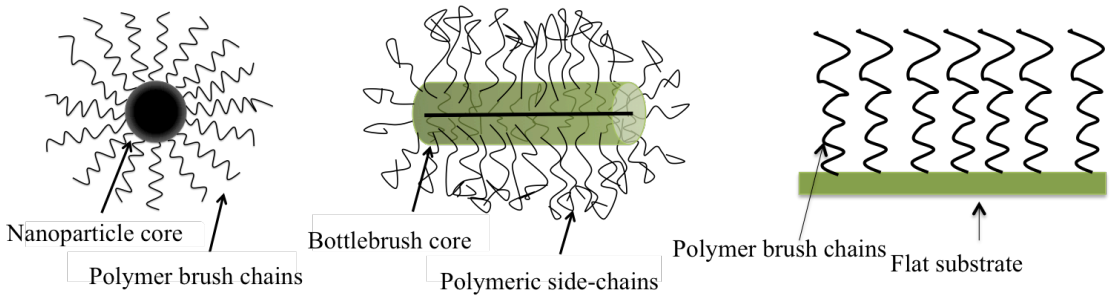

Figure 5.1 Schematic for polymer-coated nanoparticle (left) bottlebrush polymers (middle) and surface attached polymer brushes (right).

A second potential application of bottlebrush polymers is as non-toxic antifouling coatings. Polymer brush coatings have been extensively explored for antifouling films, but the preparation of polymer brush coatings on large surfaces is impractical. Bottlebrush films can be easily prepared by spray casting, spin casting or dip-casting, since bottlebrush is solution processible. Here, we explore the antifouling properties of PNIPAAM bottlebrush polymer films. Stable films can be obtained by cross-linking of PNIPAMM bottlebrush polymers. The proper ratio of cross-linker can keep both high flexibility of polymer chains and also film stability in presence of water. Temperature dependent cell absorption studies on cross-linked PNIPAAM bottlebrush polymer thin films show that PNIPAAM bottlebrush thin films have higher cell-resistant ability at lower temperature, while lower cell-resistant ability at higher temperature.

These results demonstrate two potential applications of bottlebrush polymers and promising directions for future research.

5.3 Experiment

5.3.1 Experimental materials

All reagents and solvents were purchased from commercial sources and were used as received unless otherwise noted. *N*-isopropylacrylamide (Aldrich, 97%) was purified by recrystallization in hexane for three times. 2,2′-azobis(2-methylpropionitrile) (AIBN) was purified by recrystallization in methanol. Dichloromethane was dried over molecular sieves (4Å). Modified Grubb's catalyst (H2IMes)(pyr)2(Cl2)RuCHPh,[8] exo-7-Oxabicyclo- [2.2.1]hept-5-ene-2,3-dicarboxylic anhydride[9], norbornene-functionalized chain transfer agent (NB-CTA), and NB-PNIPAAM were synthesized as previously report.[2]

Synthesis of poly(acroyl benzophene) macromonomer (NB-PABP): NB-PABP was synthesized as follows: first acroylbenzophenone (ABP) was prepared by the coupling of 4-hydroxybenzophenone (HBP,) with acryloyl chloride: HBP (2.5g) and triethylamine (TEA, 2mL) were dissolved in 20mL acetone with a stir bar, place the reaction flask onto ice batch to cool down to 0°C. Dissolve acryloyl chloride (1.27g) into 5ml acetone, and add it to the above solution drop by drop with an addition funnel. Stir at 0°C for 3hrs, and then stir at R.T. for overnight. Product was filtered and then extract with 10ml 1M HCl twice, 10mL 1M Na_2CO_3 aqueous solution once, and 10 mL DI water once. Dried the solution by $MgSO_4$, and removed the residual solvent, white crystals ABP were obtained (1.87g). NB-PABP were synthesized by RAFT: NB-CTA (50.9mg), ABP (1.34g), AIBN (1.46mg) were dissolved in 5mL 1,4-dioxane, followed by purging with N_2 for 30min. Reaction was initiated on the oil batch at 65°C, and quenched after 17hrs. Concentrated

solution was precipitate in cold methanol for 3 times until ^{1}H NMR shows there is no ABP left. GPC results: *Mw*=2918g/mol, PDI=1.262

Synthesis of poly(glycidyl methacrylate) (PGMA): 3.65 g glycidyl methacrylate, 0.1178g 2,2'-bipiridine were dissolved in 3.6mL THF, and solution was purged by N_2 for 15min, add the catalyst Cu(I)Br 36mg under N_2 protection, stirred for 10min, and then added initiator Ethyl α-bromoisobutyrate 36$\boldsymbol{\mu L}$. Reacted on oil batch at 80°C for 1hr, and then quenched on ice batch. GPC results: *Mw*=27.52 kg/mol, PDI=1.292

5.3.2 Experimental characterization

Gel-Permeation Chromatography (GPC) Molecular weights and polydispersities were obtained using an Agilent 1200 module equipped with three PSS SDV columns in series (100, 1000, and 10000 Å pore sizes), an Agilent variable wavelength UV/VIS detector, a Wyatt Technology HELEOS II multi-angle laser light scattering (MALLS) detector (λ = 658 nm), and a Wyatt Technology Optilab reX RI detector. This system enables SEC with simultaneous refractive index (SEC-RI), UV/VIS (SEC-UV/VIS), and MALLS detection. THF was used as the mobile phase at a flow rate of 1 mL/min at 40 ^{o}C.

Nuclear Magnetic Resonance Spectroscopy (NMR) Hydrogen NMR (^{1}H NMR) spectra were recorded using tetramethylsilane as internal standard in $CDCl_3$ on a 400 MHz Bruker multi-nuclear spectrometer. Samples were placed in 5 mm o.d. tubes with the concentration of 20 mg/ml.

Fluorescent microscopy: Cell resistant ability was measured on fluorescent microscopy (Olympus 1X71) with Lumen 200 (PRIOR) fluorescent illumination systems. And images were analyzed by the software of cellsens dimension.

Pendant drop tensiometer Interfacial tension measurements of pure PNIPAAM bottlebrush polymers at interface of chloroform and water were carried out using a CAM 200 optical contact angle meter (KSV instruments, Monroe, CT) at ambient and higher temperature conditions.

Spinning drop tensiometer Interfacial tension measurements of pure 4,5-orthoxylene sulfonate and mixture of 4,5-orthoxylene sulfonate/PNIPAAM bottlebrush polymers at interface of chloroform and water were carried out using Grace M6500 with the range of 10^{-6} to 5 mN/m.

5.3.2 Sample preparation for interfacial tension measurement

For the pendent drop tensiometer: make the solution of the brush polymers in DI water. To prepare samples, 5 (g) of a 0.1 % solution of brush polymer in water was stirred with a magnetic stirrer in contact with 20 (g) of chloroform phase over night at room temperature or in 32 °C in a water bath. The chloroform was first purified using molecular sieves of the type 4A. The chloroform phase was used as the external phase and the water was used as the water drop in pendent drop measurement. The needle has to be chosen with the right size so that the bond number is between 0.1 and 1 so that the effect of gravitational forces is negligible compared to interfacial tension.

For the spinning drop tensiometer, all samples were measured as follows: the prepared surfactant rich solution (2ml) was gently introduced into a capillary tube using a

syringe, the capillary tube was sealed by a lid with a hole in the center. Chloroform was injected into the capillary tube to form a suspend drop by a micro syringe, the rotation speed was set at proper rate. After about 10min, the droplet size was measured to calculate the interfacial tension by the following equation:

$$\gamma = 522.03 * (T_0)^{-2} D_0^3 \Delta S (\frac{N_w}{N})^3$$

Where γ is IFT is mN/m; T_0 is the spinning time period (ms/rev); D_0 is the diameter of oil droplet (mm); ΔS: specific gravity difference between two solutions; N_w and N are refractive index of water and denser fluid respectively.

5.3.3 Stable PNIPAAM bottlebrush polymer thin films preparation

Si substrates (1inch by 1inch) were sonicated in the 2 v/v % cuvette washing aqueous solution for 20min, after rinse by DI water thoroughly, substrates were sonicated in DI water for another 20 min, and finally 20min sonication in IPA followed by drying the substrates by air flow.

Freshly cleaned Si substrates were placed in piranha solution (3:1 concentrated H_2SO_4: 30% H_2O_2) at 80 °C for 1 hr, then all substrates were rinsed thoroughly by a large amount of DI water to introduce hydrophilic surfaces with hydroxyl end-groups.

Spin cast 0.05 wt% Poly(glycidyl methacrylate) (PGMA) solution in THF at the speed rate of 1500 rpm for 30 sec. PGMA layer were treated at 110°C for 20min under vacuum to form a chemical bounding between Si substrate and PGMA layer.

Bottlebrush polymers with cross-linker and thiol end-group were dissolve in dichloromethane at the concentration of 2 wt%, and spin casted onto freshly prepared PGMA layer at the speed rate of 1500 rpm for 30sec. After annealing at 250 °C for overnight in the glovebox to form chemical bounding between PGMA and bottlebrush polymers, the samples were exposed to UV light (360 nm) for another 1hrs to obtain stable films.

5.3.4 Sample preparation for fluorescent microscopy measurement

The stable films were place into DI water for swelling for overnight, and dried by air flow. Freshly swollen thin films were incubated with cells: pseudomonas aeruginosa 700829 shaking for 1hr at room temperature or higher temperature at 36 °C. After rinse by PBS, the samples were observed by fluorescent microcopy, and the cell numbers were counted for 3 different regions for each sample. PS thin films were used as control group.

5.4 Results and Discussion

5.4.1 Synthesis of PNIPAAM bottlebrush polymers with/out cross-linker

PNIPAAM bottlebrush polymers with thiol end-group were synthesized via "grafting through" method as previously reported[2]: macromonomer of NB-PNIPAAM-CTA was synthesized by reversible addition-fragmentation chain transfer polymerization (RAFT), and obtained bottlebrush polymers by ring-opening metathesis polymerization (ROMP) by 3rd generation Grubbs' catalyst, and finally, the water soluble bottlebrush polymer with thiol end-groups were obtained by aminolysis in presence of hexylamine and tributylphosphine.

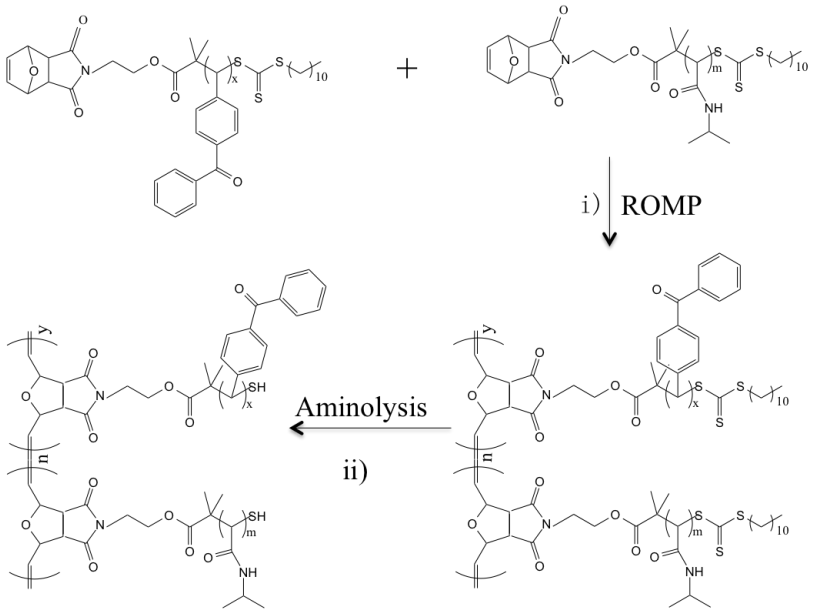

Figure 5.2 Synthetic route for the preparation of PNIPAAM bottlebrush polymers with cross-linker side-chains.

i) CH_2Cl_2, $((H_2IMeS)(3\text{-Br-Py})_2(Cl_2)RuCHPh)$ ii) 1,4-Dioxane, hexylamine, tributylphosphine.

Figure 5.2 shows the chemical structure of NB-PNIAAM macromonomer and NB-PABP macromonomer. For bottlebrush polymer with cross-linker, two macromonomers were prepared: NB-PNIPAAM and cross-linker: NB-PABP poly(acroyl benzophene). The two macromonomers were dissolved in dried dichloromethane (cross-liker 3 wt%), desired amount 3rd Grubbs' catalyst were added into the above solution, stir at R.T. for several hours until reaction completed, GPC was used to track the reaction conversion. As shown in Figure 5.3, the bottlebrush polymers were synthesized successfully with residual unreacted NB-PNIPAAM. Final product was receipted in cold diethyl ether, can dried under vacuum for overnight.

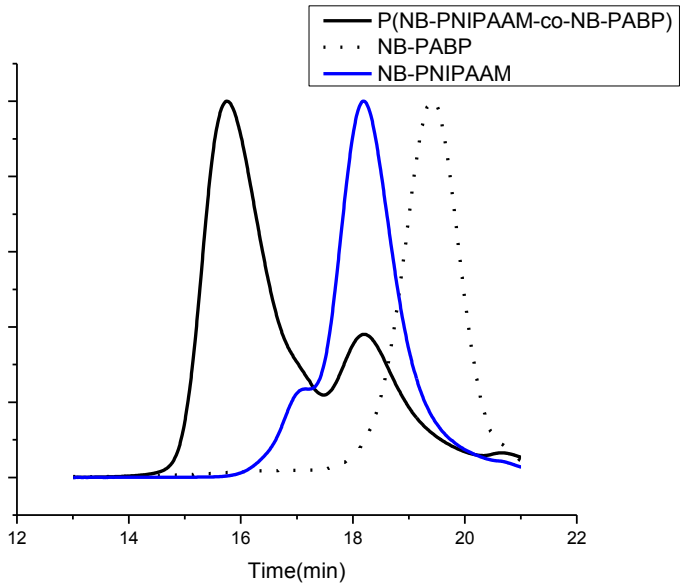

Figure 5.3 GPC spectra of bottlebrush polymer with cross-linker side-chains (black line); macrmonomer NB-PNIPAAM (blue line); and macromonomer NB-PABP (black dots)

5.4.2 Interfacial properties of bottlebrush polymers

Prior work has shown that polymer-coated nanoparticles and branched polymers are interfacially active materials.[1,10] Bottlebrush polymers have the advantage that the side-chain and backbone length can be precisely controlled, and the results above show that the side-chain flexibility can be tuned by changing the side-chain length. Here, we explored the reduction in interfacial tension (IFT) between water and chloroform with the addition of PNIPAAM bottlebrush polymers.

To analyze the interfacial properties of PNIPAAM bottlebrush polymers, 1 wt % solutions of bottlebrush polymers in chloroform were prepared. These solution were mixed with water (50 % v/v) and the mixture was equilibrated for at least 24 h. Visually,

a noticeable change in the curvature at the interface between water and chloroform is observed with the addition of bottlebrush polymers (Figure 5.4). Compared with a chloroform/water control, solutions containing bottlebrush polymer exhibited a noticeably flatter interface at temperatures below the LCST. When heated above the LCST, the interface curvature increased, indicating an increase in the interfacial tension. This suggests that PNIPAAM bottlebrush polymers reduce the IFT between chloroform and water below the LCST.

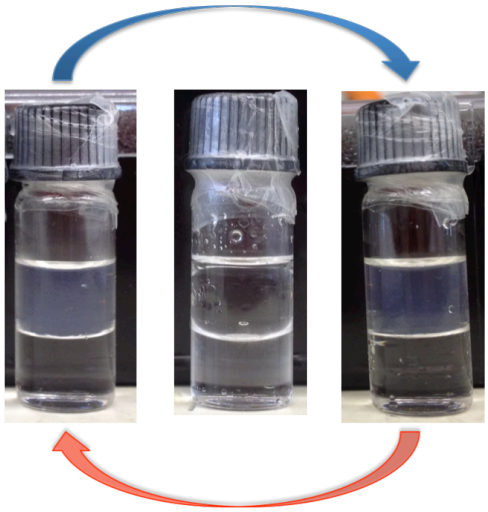

Figure 5.4 Micrographs of water/chloroform two-phase mixtures with no polymer added (middle), with 0.1 % mass fraction at room temperature (left) and at higher temperature T>LCST (right)

Quantitative values for the IFT were obtained using the pendant drop method (Table 5.1). At room temperature, both linear PNIPAAM (3.4± 0.32 mN/m) and bottlebrush PNIPAAM (4.99± 0.78 mN/m) reduce the IFT by one order of magnitude. Above the LCST, the IFT increases for all solutions due to the reduced hydrophilicity of PNIPAAM. The IFT values for bottlebrush polymer and PNIPAAM homopolymer solutions are

comparable, with PNIPAAM homopolymer solutions exhibiting lower IFT values at temperatures below the LCST. Since IFT is strongly dependent on the salinity of aqueous phase and bottlebrush polymers may be of interest for applications such as enhanced oil recovery, we explored the IFT between chloroform and brine.[11,12] As shown in Table 3.5, IFT values are consistently lower in the presence of brine, but the trends are qualitatively the same as in water.

A difference between homopolymer and bottlebrush polymer solutions is observed on vigorous shaking of the chloroform/water solutions. In homopolymer solutions, a thick emulsion forms that does not settle for up to several weeks, but bottlebrush polymer solutions show mostly clear phases (see Figure 5.5). This may indicate the inability for bottlebrush polymers to stabilize highly curved interfaces, as has been observed for bottlebrush polymers and nanoparticles at liquid-liquid interfaces.[13] These results suggest that bottlebrush polymers may be useful as interfacially active materials, but further work is needed to understand the role of side-chain length and interface curvature.

Table 5.1 Interfacial tension (IFT) between water and chloroform at different temperatures and salinities. Where applicable, 0.1 wt% polymer added to aqueous phase

System	IFT mN/m	
	R.T.	35 °C
No added polymer	28.84±1.53	N/A
P(4K-PNIPAAM-SH), 0% NaCl	6.89 ± 1.79	12.22 ± 0.31
P(6K-PNIPAAM-SH), 0% NaCl	4.99 ± 0.78	20.28 ± 1.14
P(9K-PNIPAAM-SH), 0% NaCl	11.75±0.94	20.62±1.59
6K-PNIPAAM-SH, 0% NaCl	3.40 ± 0.32	18.86 ± 0.93
P(4K-PNIPAAM-SH), 10% NaCl	4.29 ± 1.16	8.54 ± 1.27
P(6K-PNIPAAM-SH), 10% NaCl	1.50 ± 0.65	26.44 ± 1.65
P(9K-PNIPAAM-SH), 10% NaCl	7.58 ± 0.28	11.58 ± 0.68
6K-PNIPAAM-SH, 10% NaCl	2.21 ± 0.35	27.16 ± 1.36

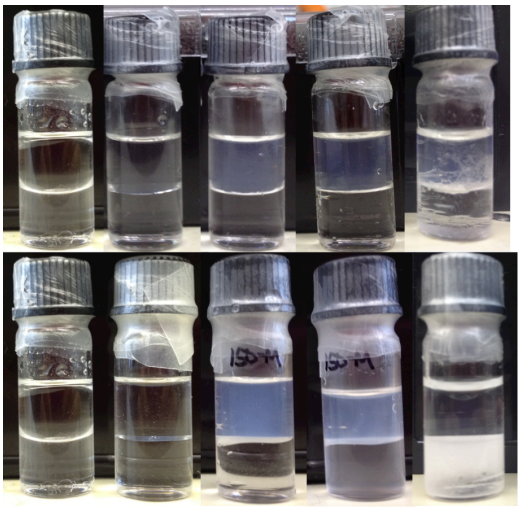

Figure 5.5 A comparison of the interfacial behavior and stability of P(9K-PNIPAAM-SH) bottlebrush polymers and 9K-PNIPAAM-SH homopolymer in chloroform/water mixtures.

Both bottlebrush polymer and macromonomer reduce the IFT, reflected by a reduced interfacial curvature with added polymer. After vigorous shaking (right), a stable emulsion is present in the chloroform phase of 9K-PNIPAAM-SH homopolymer solution, but both phases remain clear for P(9K-PNIPAAM-SH) solution

PNIPAAM bottlebrush polymer reduces the interfacial tension between chloroform and water but do not stabilize the formation of microemulsions. These results demonstrate the role of side-chain conformation and flexibility on macroscopic and interfacial properties. Therefore, we conducted the similar studies of the mixture of bottlebrush polymers with surfactants. As a control group, interfacial tension was also conducted for pure surfactants. Since the much lower IFT value, spinning droplet can provide more accurate results than pendant droplet method. As shown in Table 5.2, the same concentration (0.1wt%) bottlebrush polymers with 6K side-chains were prepared at different salt concentrations with 2% surfactant. The data show that the optimal sanity is shifted with the addition of just 0.1 wt % bottlebrush. With the addition of bottlebrush, lower IFTs are observed at higher salinities. This may be due to complexation between bottlebrush polymer and surfactant and a reduction in the critical micelle concentration. More work is needed to illustrate the mechanism, including more careful IFT measurements over a broad range of salinities, measurements of the IFT at each point, and a study of possible complexation between bottlebrush polymers and surfactant.

Table 5.2 Interfacial tension measured by spinning droplet method

	IFT in different salt concentration (mN/m)		
Sample	1.4%	1.5%	2.0%
Pure surfactant	$2.02\ 10^{-2}$	N/A	$6.07\ 10^{-2}$
Surfactant+0.1wt% bottlebrush	$4.13\ 10^{-2}$	$2.20\ 10^{-2}$	$2.11\ 10^{-2}$

5.4.3 Anti-fouling properties of bottlebrush polymers

Former studies show that PNIPAAM can be used as anti-fouling materials. Our former research results show that the side-chains of bottlebrush polymers have enough flexibility, which makes bottlebrush polymers a possible candidate replacement for polymer brushes.[1] Since PNIPAAM bottlebrush polymer is soluble in water at temperatures below its LCST, therefore films prepared by spin-casting bottlebrush polymer solution onto substrates directly will dissolve when exposed to aqueous solutions. The stable film consistent of two layers: PGMA bottom bonding layer and top cross-linked bottlebrush polymers. Epoxy end-group can react with hydroxyl groups on piranha treated Si wafer and also thiol end-group of bottlebrush polymers. Cross-linking is necessary to form a stable 100 nm thick PNIPAAM bottlebrush polymers, the ratio of cross-linker to bottlebrush polymers is about 3wt%, which can keep the flexibility of PNIPAAM side-chains.

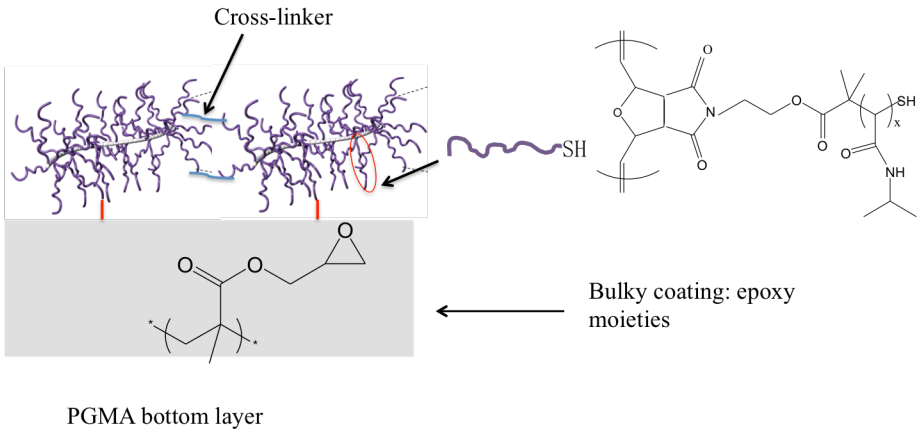

Figure 5.6 Schematic structure of two-layer stable PNIPAAM bottlebrush thin films

Fluorescent microscopy is an efficient method to characterize the cell numbers absorbed on polymer films.

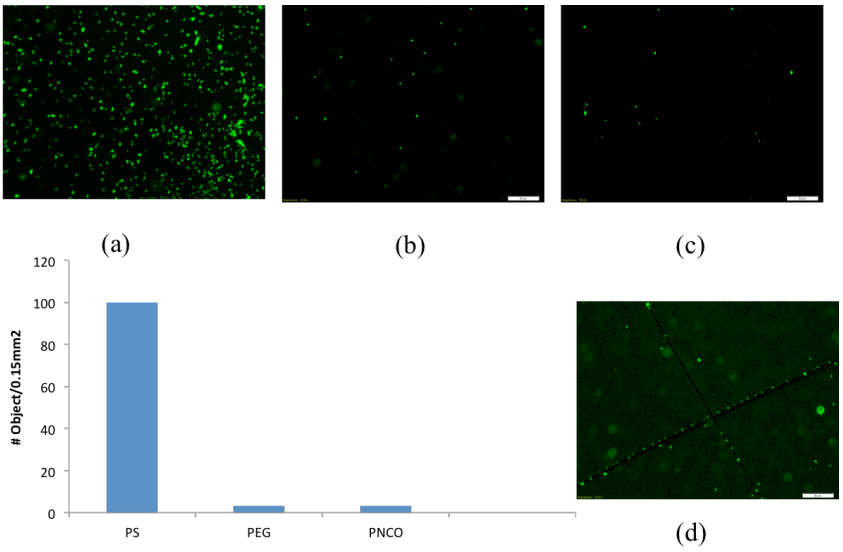

Figure 5.7 Fluorescent images of cell absorption on different films:

PS (a); PEG (b); PNIPAAM bottlebrush (c); and PNIPAAM bottlebrush polymers with scratches.

PNIPAAM is thermo-responsive, due to this property, PNIPAAM can also be used as cell transfer materials, as shown in Figure 5.8: when the temperature is below the LCST of PNIPAAM bottlebrush polymers, PNIPAAM is water soluble and the surface is hydrophilic, therefore cells can not attach to the surface easily, when the temperature increases above its LCST, PNIPAAM becomes insoluble in water, and the surface is more hydrophobic, at the results, cells prefer to absorb onto polymer surfaces. When the system is cooled down below its LCST again, part of absorbed cells will release back into solution since the polymer surface becomes hydrophilic.

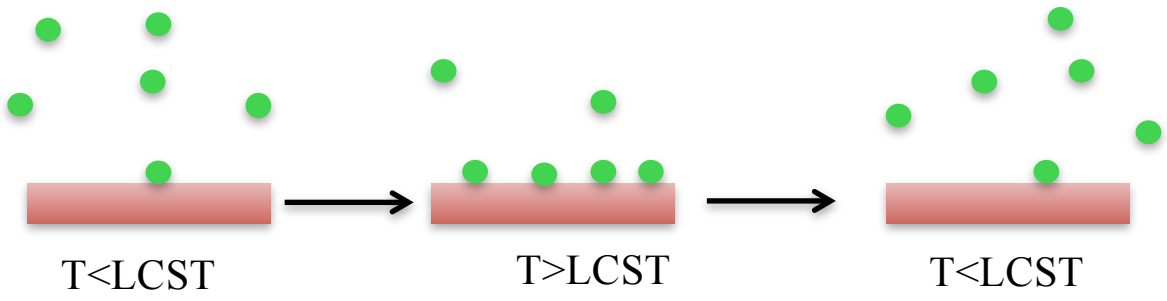

Figure 5.8 Scheme of cell resistant ability of PNIPAAM thin films at different temperatures.

To test above hypothesis, cell solutions were incubated with PNIPAAM substrates at R.T. and 36 °C, and cell numbers on polymer films were counted by fluorescent microcopy. The results are shown in Figure 5.9, although compared to PS control group, PNIPAAM bottlebrush polymer can not absorbed the same amount cells at higher temperature, the release of cells from polymer surfaces into solution was still observed when temperature decreased back to R.T.

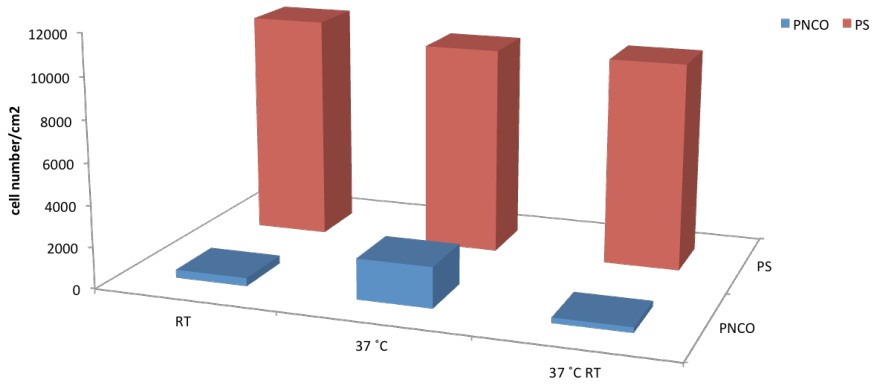

Figure 5.9 Calculated cell absorption onto PNIPAAM thin films at different temperatures.

More characterization of PNIPAAM bottlebrush polymers are needed to get better understand of their anti-fouling abilities. Further studies on the effect of side-chain length, grafting density on cell resistant ability will be conducted to explore other potential applications of PNIPAAM bottlebrush polymers.

5.5 Outlook

Both polymer-coated nanoparticles (brushy nanoparticles) and polymer brushes are well studied, and both of them have diverse applications: such as oil-recovery,[14-16] anti-foulings,[17,18] drug-delivery,[19,20] medical imaging[21,22] et al. However, there are problems or disadvantages for these two non-all polymer materials. For polymer-coated

nanoparticles, ideally, the nanoparticle core determines the size and shape of the particle and a dense polymer brush layer dictates surface properties and mediates interactions with the environment (e.g., solvent, other particles). In practice, achieving polymer-coated nanoparticles with controlled molecular characteristics is limited by low coupling efficiencies of polymers to nanoparticles[1–3], poor displacement of solubilizing ligands from nanoparticle surfaces[4], and poor control over polymerization reactions mediated by chain transfer agents (CTAs) at the nanoparticle surface[5]. It is also hard to calculate the real grafting density, since there may be only partially functionalized and contain adsorbed rather than covalently attached polymers. Additionally, polymer-coated nanoparticles are often insoluble or aggregate strongly even in good solvents for the polymer brush layer[3,6], preventing characterization by standard analytical techniques and potentially incomplete coverage of the insoluble nanoparticle core. For polymer brushes grafted substrates, precisely control of grafting density, brush length is difficult, and the initiation of polymerization from or onto substrates need inert conditions in most cases, which limit the application of polymer brushes onto super large area, like a ship hull.

Bottlebrush polymer exhibits similar architecture to both polymer coated nanoparticles or polymer brush grafted surfaces. (Figure 5.1). Bottlebrush polymer sprovide an alternative route to brushy nanoparticles or polymer brushes. Instead of coupling polymers and nanoparticles or substrates, all-polymer approach can be used to preparation bottlebrush polymers with well controlled core size (backbone length) and shape and the length, grafting density, and composition of polymer brush chains.

In my dissertation, the characterization of conformation at both surface and in solution, solubility, and phase behavior of bottlebrush polymers were illustrated. In recent

small-angle neutron scattering (SANS) studies, we found that the conformation of PS bottlebrushes changed from spherical to rod-like with increasing backbone length.[14] We also investigated the solubility, phase behavior, and solution conformation of poly(N-isopropylacrylamide) (PNIPAAM) bottlebrush polymers and found that PNIPAAM bottlebrush polymers exhibited a lower-critical solution temperature dependent on side-chain length and end-group functionality[12]. PNIPAAM bottlebrush polymers also formed a lyotropic liquid crystal phase above the LCST, for side-chain lengths larger than 9 kg/mol. Bottlebrush polymers prefer to segregate onto surfaces. However, the studies and understanding of bottlebrush polymers are not as much as that to polymer coated nanocomposites or polymer brushes, bottlebrush polymers as great candidate to polymer coated nanoparticles polymer brushes in more application fields are expected.

5.6 Bibliography

1 Li, X., Prukop, S. L., Biswal, S. L. & Verduzco, R. Surface Properties of Bottlebrush Polymer Thin Films. *Macromolecules*, doi:10.1021/ma301046n (2012).

2 Li, X. *et al.* Thermoresponsive PNIPAAM bottlebrush polymers with tailored side-chain length and end-group structure. *Soft Matter* **10**, 2008-2015, doi:10.1039/C3SM52614C (2014).

3 ShamsiJazeyi, H., Miller, C. A., Wong, M. S., Tour, J. M. & Verduzco, R. Polymer-coated nanoparticles for enhanced oil recovery. *J. Appl. Polym. Sci.*, n/a-n/a, doi:10.1002/app.40576 (2014).

4 Li, Y., Zou, J., Das, B. P., Tsianou, M. & Cheng, C. Well-Defined Amphiphilic Double-Brush Copolymers and Their Performance as Emulsion Surfactants. *Macromolecules* **45**, 4623-4629, doi:10.1021/ma300565j (2012).

5 Xue, C. *et al.* Protein Adsorption on Poly(N-isopropylacrylamide) Brushes: Dependence on Grafting Density and Chain Collapse. *Langmuir* **27**, 8810-8818, doi:10.1021/la2001909 (2011).

6 Cunliffe, D., de las Heras Alarcón, C., Peters, V., Smith, J. R. & Alexander, C. Thermoresponsive Surface-Grafted Poly(N−isopropylacrylamide) Copolymers: Effect of Phase Transitions on Protein and Bacterial Attachment. *Langmuir* **19**, 2888-2899, doi:10.1021/la026358l (2003).

7 Yu, Q. *et al.* Protein Adsorption and Cell Adhesion/Detachment Behavior on Dual-Responsive Silicon Surfaces Modified with Poly(N-isopropylacrylamide)-block-polystyrene Copolymer. *Langmuir* **26**, 8582-8588, doi:10.1021/la904663m (2010).

8 Sanford, M. S., Love, J. A. & Grubbs, R. H. A Versatile Precursor for the Synthesis of New Ruthenium Olefin Metathesis Catalysts. *Organometallics* **20**, 5314-5318, doi:10.1021/om010599r (2001).

9 France, M. B., Alty, L. T. & Earl, T. M. Synthesis of a 7-Oxanorbornene Monomer: A Two-Step Sequence Preparation for the Organic Laboratory. *J. Chem. Educ.* **76**, 659, doi:10.1021/ed076p659 (1999).

10 Maillard, D. *et al.* Mechanical Properties of Thin Glassy Polymer Films Filled with Spherical Polymer-Grafted Nanoparticles. *Nano Lett.* **12**, 3909-3914, doi:10.1021/nl301792g (2012).

11 Schaller, K., Fox, S., Bruhn, D., Noah, K. & Bala, G. Characterization of surfactin from Bacillus subtilis for application as an agent for enhanced oil recovery. *Appl. Biochem. Biotechnol.* **115**, 827-836, doi:10.1385/abab:115:1-3:0827 (2004).

12 Li, X., Boek, E., Maitland, G. C. & Trusler, J. P. M. Interfacial Tension of (Brines + CO2): (0.864 NaCl + 0.136 KCl) at Temperatures between (298 and 448) K, Pressures between (2 and 50) MPa, and Total Molalities of (1 to 5) mol¬∑kg‚Äì1. *J. Chem. Eng. Data* **57**, 1078-1088, doi:10.1021/je201062r (2012).

13 Garbin, V., Crocker, J. C. & Stebe, K. J. Forced Desorption of Nanoparticles from an Oil‚ÄìWater Interface. *Langmuir* **28**, 1663-1667, doi:10.1021/la202954c (2011).

14 Xue, B., Gao, L., Hou, Y., Liu, Z. & Jiang, L. Temperature Controlled Water/Oil Wettability of a Surface Fabricated by a Block Copolymer: Application as a Dual Water/Oil On–Off Switch. *Adv. Mater. (Weinheim, Ger.)* **25**, 273-277, doi:10.1002/adma.201202799 (2013).

15 Saleh, N. *et al.* Oil-in-Water Emulsions Stabilized by Highly Charged Polyelectrolyte-Grafted Silica Nanoparticles†. *Langmuir* **21**, 9873-9878, doi:10.1021/la050654r (2005).

16 Walther, A., Hoffmann, M. & Müller, A. H. E. Emulsion Polymerization Using Janus Particles as Stabilizers. *Angew. Chem.* **120**, 723-726, doi:10.1002/ange.200703224 (2008).

17 Lee, H. *et al.* Antibiofouling Polymer-Coated Superparamagnetic Iron Oxide Nanoparticles as Potential Magnetic Resonance Contrast Agents for in Vivo Cancer Imaging. *J. Am. Chem. Soc.* **128**, 7383-7389, doi:10.1021/ja061529k (2006).

18 Chen, T., Ferris, R., Zhang, J., Ducker, R. & Zauscher, S. Stimulus-responsive polymer brushes on surfaces: Transduction mechanisms and applications. *Prog. Polym. Sci.* **35**, 94-112 (2010).

19 Louguet, S. *et al.* Thermoresponsive polymer brush-functionalized magnetic manganite nanoparticles for remotely triggered drug release. *Polymer Chemistry* **3**,

1408-1417, doi:10.1039/C2PY20089A (2012).
20 Sahoo, B. *et al.* Thermal and pH Responsive Polymer-Tethered Multifunctional Magnetic Nanoparticles for Targeted Delivery of Anticancer Drug. *ACS Appl. Mater. Interfaces* **5**, 3884-3893, doi:10.1021/am400572b (2013).
21 Kim, D., Park, S., Lee, J. H., Jeong, Y. Y. & Jon, S. Antibiofouling Polymer-Coated Gold Nanoparticles as a Contrast Agent for in Vivo X-ray Computed Tomography Imaging. *J. Am. Chem. Soc.* **129**, 7661-7665, doi:10.1021/ja071471p (2007).
22 Zhang, F. *et al.* Polymer-Coated Nanoparticles: A Universal Tool for Biolabelling Experiments. *Small* **7**, 3113-3127, doi:10.1002/smll.201100608 (2011).